CHARACTERISATION OF SUPERFICIAL INHIBITORY INTERNEURONS IN ZEBRAFISH OPTIC TECTUM

Abbas, Fatima

Awarding institution:
King's College London

CHARACTERISATION OF SUPERFICIAL INHIBITORY INTERNEURONS IN ZEBRAFISH OPTIC TECTUM

Fatima Abbas

This thesis is submitted for the degree of Doctor of Philosophy

May 2016

Department of Developmental Neurobiology

King's College London

TABLE OF CONTENTS

FIGURES

Chapter 1: Introduction

Chapter 2: Materials and Methods

Chapter 3: Characterisation of SINs

Chapter 4: Tuning of DS SINs relative to other DS populations in the retinotectal circuit

Chapter 5: The role of SIN mediated inhibition in tectal circuitry

Chapter 6: Discussion

TABLES

Chapter 2: Materials and Methods

Chapter 3: Characterisation of SINs

Chapter 4: Tuning of DS SINs relative to other DS populations in the retinotectal circuit

ABSTRACT

Information on the direction of movement of objects in the visual field is vital for visually guided behaviours including prey capture and predator avoidance. The optic tectum is important for producing such visually guided behaviours in zebrafish. Understanding the functional properties of subtypes of neurons within this tectal circuit is vital to understanding the processing responsible. Superficial inhibitory interneurons (SINs) are located in the superficial optic tectum and have laminar arborisations; ablation of these neurons has been shown to perturb prey capture behaviour. In this thesis, the receptive field properties of SINs in the zebrafish optic tectum were characterised. A subset of SINs were found to be direction selective, forming three different direction selective (DS) populations with preferred directions mirroring those of DS retinal ganglion cell (DSGC) inputs to the tectum. Furthermore, the spatial frequency (SF) and temporal frequency (TF) tuning properties of SINs were also characterised, finding that these neurons are selective for smaller moving objects. Comparing SIN DS responses to those of DSGC and tectal neuron populations, SINs have much narrower DS tuning. This narrow DS tuning was insensitive to injection of GABA-A receptor antagonists into the tectum, indicating that GABA-A receptor mediated inhibition is not involved. The role of GABAergic inhibition in generating the properties of DS populations in the tectum was also probed using drug injections, finding that both DS tectal neurons and DSGC properties were not significantly altered when GABA signalling is perturbed. This characterisation of SIN function has identified a narrowly tuned inhibitory interneuron in the tectal circuit, exhibiting band pass filtering for small moving objects. This functional characterisation of SIN receptive field properties indicates a possible role of these SINs in a size selective circuit, possibly relating to prey capture behaviours.

ACKNOWLEDGEMENTS

The list of people whom I'd like to thank for helping me through this PhD is far too long to include in this thesis, but I hope to at least cover a few here. My decision to pursue a PhD is the result of having a great teacher, Dr Martin Meyer. Without the opportunity to carry out my MSc research project in his lab I wouldn't have found the interest I have in visual neurobiology, nor would I have met great scientists, mentors and friends here at the Department for Developmental Neurobiology. Thank you Martin for providing me with so many opportunities, for supporting my development as a researcher and giving me this priceless experience.

Of course, I also want to thank the Meyer lab members, past and present Sarah Hammond, who provided me with so much help and advice. Alison Walker, an ideal role model for a PhD student like myself to follow: hard working and always positive. Paul Hunter, who has dealt with my Matlab/confocal/zebrafish frustrations for over four years with the patience of a saint! As well as dealing with my lack of ability to talk sports, sorry Paul. Nikolas Nikolaou, a fountain of knowledge and fantastic researcher. Tom Ryan, for science talk and general banter. A big thank you to Andrew Lowe: without the analysis software Andrew wrote, none of this work would have been possible.

My time at the Centre for Developmental Neurobiology has been a learning curve, but also provided me with the opportunity to meet wonderful people and brilliant scientists. Everyone has been kind, supportive, and helpful. I would like to mention a few people in particular: Ian Thompson and Esther Bell who provided great mentorship and feedback throughout this PhD. Mark Evans, who set the bar very high for how a successful PhD student should be. Elisa Galliano and Ruth Taylor for coffee breaks and general sanity saving conversation!

A few friends of notable mention: Fatima Ali, Helena Ledmyr, Keir Edmonds, Spot Allen, Fatema Zehra, Zohra Khaku, Ruman Hasan. Thanks all for dealing with the grumpiness and occasional rant!

Finally, I would like to thank my parents for their understanding, patience and belief in my ability. Without them, this PhD would not have been possible and I would like to dedicate this thesis to them. Thank you Mama and Baba, sincerely. The rest of my family, of course, a great source of support, so thank you for understanding when I've had to work weekends or miss family events, Yasin, Taha, Maryam, Batool, May, Ahmed, Eva and of course my wonderful nephews Yunes and Zain.

ABBREVIATIONS

A	anterior
AC	Amacrine cells
AF	arborisation field
AMPA	α-Amino-3-hydroxy-5-methyl-4- isoxazolepropionic acid
A-P	anterior-posterior axis
CV	1- Circular variance
D	Dorsal
ΔF	Relative signal intensity changes (ΔF = (F- baseline), where F = raw fluorescence
ΔF/F	Normalised signal change (ΔF/F = (F- baseline)/baseline))
ddH2O	distilled water
dLGN	Dorsal lateral geniculate nucleus
dpf	days post fertilisation
DS	direction selective
DSGC	direction selective retinal ganglion cell
DSI	direction selectivity index
FWHM	Full width half maximum
GABA	γ-Aminobutyric acid
GABAR-A	γ-Aminobutyric acid receptor A
GABAR-B	γ-Aminobutyric acid receptor B
GABA-R	γ-Aminobutyric acid receptor
GCL	Ganglion cell layer
GECI	genetically encoded calcium indicator
GFP	green fluorescent protein
Hz	Hertz
INL	Inner nuclear layer
IPL	Inner plexiform layer
L	lateral
LEDs	Local edge detectors
LMP	low melting point
M	medial
mitfa	microphthalmia-associated transcription factor a (A.K.A. nacre)
n	number
NBQX	2,3-dihydroxy-6-nitro-7-sulfamoyl-benzo[f]quinoxaline-2,3-dione
nMLF	nucleus of the medial longitudinal fasciculus
NMDA-R	N-methyl-D-aspartate receptor
OMS	Object motion sensing
ONL	Outer nuclear layer

OPL	Outer plexiform layer
OS	orientation selective
OSI	orientation selectivity index
OT	optic tectum
P	posterior
PAC	Polyaxonal amacrine cell
PBS	phosphate buffered saline
PBST	triton-X in phosphate buffered saline
PC	Pyramidal cells
PD	Preferred direction
PFA	Paraformaldehyde
PSD95	Post-synaptic density 95
PTU	n-phenylthiourea
PV	Parvalbumin expressing neurons
PVL	Periventricular layer
PVN	Periventricular neuron
RF	receptive field
RGC	retinal ganglion cell
ROI	region of interest
RT	room temperature
SAC	stratum album centrale
SC	superior colliculus
SD	standard deviation
SEM	standard error of mean
SF	Spatial frequency
SFGS	stratum fibrosum et griseum superficiale
SIN	superficial interneuron
SO	stratum opticum
SOMs	Somatostatin expressing neurons
SPV	stratum periventricularis
SyGCaMP3	synaptophysin GCaMP3
SyGFP	synaptophysin GFP
TF	Temporal frequency
UAS	Upstream Activation Sequence
V1	Visual cortex
VIP	Vasoactive intestinal protein expressing neurons
wt	Wildtype

1 INTRODUCTION

1.1 Visual information: a survival advantage

A key factor for deciding the survival of an organism is its ability to respond to changes in its environment with prompt and appropriate behaviours. Throughout evolution, organisms have gained survival advantage by evolving different mechanisms to detect changes in the environment; the key senses of gustation, olfaction, proprioception, vision, and hearing all confer such advantages. Within systems neuroscience there is a growing momentum towards understanding the circuitry involved in the perception of external changes, but also understanding how this information is processed to lead to different behaviours in response to these changes. Since 1898 and the Golgi-staining study of the avian retina (Ramón y Cajal, 1898) the visual system has been an avidly studied sensory system. Landmark studies, including that of Hubel and Wiesel (Hubel and Wiesel, 1959) of neurons within the visual system with receptive field (RF) properties including direction and orientation tuning, has driven neuroscientists towards understanding the circuitry responsible for such functional properties.

Visual information is used to determine several important survival behaviours. Predator avoidance and prey capture are two prime examples of rapid behavioural choices using primarily visual information. A key question is: How does the brain integrate the basic units of visual information from the external world such as changes in contrast, orientation and size to extract more descriptive and survival related perceptions, such as direction of movement, background motion, prey or predator? Understanding the processing leading to these distinctions first involves understanding what processing visual information undergoes.

In this introduction, I will focus on the organisation and function of neurons in the vertebrate visual system, outlining current understanding of both mammalian and non-mammalian visual neurobiology. Excitatory cells are numerous within the visual system, however, there is growing evidence demonstrating that the diverse response properties of neurons in the visual system are generated through interneurons, with a prime example being the functionally diverse amacrine cells (ACs) in the retina, many of which are inhibitory (reviewed in Masland, 2012). Throughout the visual system, inhibitory neurons are responsible for extraction of features from the visual field and the characterisation of the function of these inhibitory neurons will provide key insights into the processing of visual information in these circuits.

1.2 Processing of visual information in vertebrates

The visual system transmits information through parallel channels from the photoreceptors in the retina, to the higher processing areas including dorsal lateral geniculate nucleus, superior colliculus and visual cortex in mammals or optic tectum in fish, amphibians and chicken (Figure 1.1). Whilst the anatomy varies between species, a central concept is that increasingly complex visual features are extracted at each synapse of the visual system, the mammalian cortex representing the most 'complex' extracted information. By understanding how the neurons within each area interact, we can begin to understand how the processing at each level of the visual system occurs. In the retina, such processing results in the extraction of information of visual features, including direction or orientation of motion, edges, and colour.

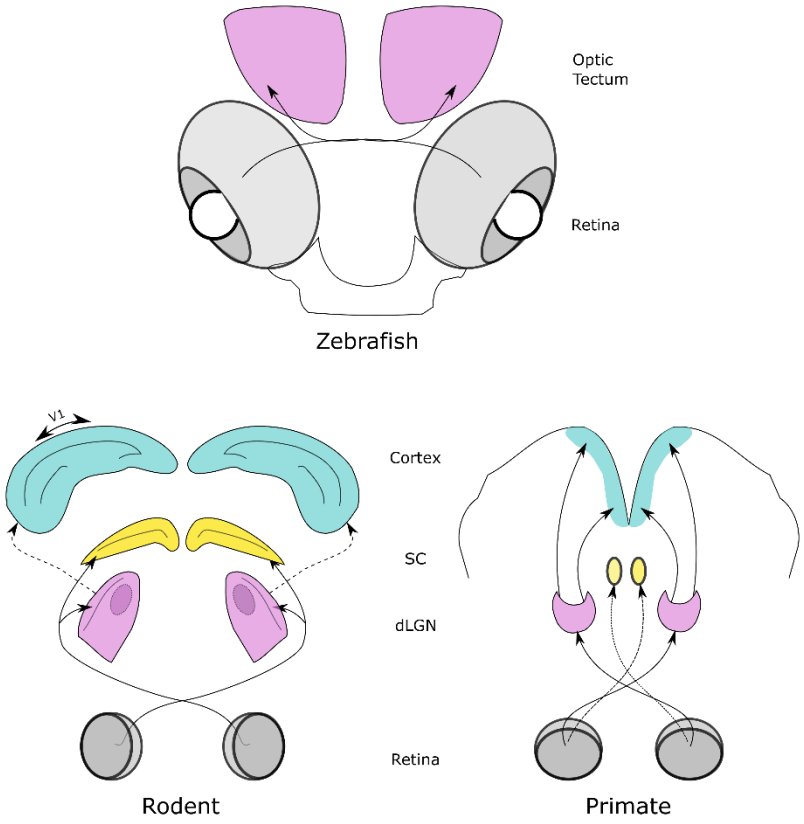

Figure 1-1 Comparison of organisation of visual systems of vertebrates

Illustrative diagrams of visual systems of zebrafish, rodents, and primates, indicating the differences in organisation. The largest retinorecipient area of zebrafish brains is the optic tectum, however in mammals, this is the dorsal lateral geniculate nucleus (dLGN), followed by superior colliculus (SC). Mammals also receive thalamic inputs to visual cortex (V1)

1.2.1 A parallel flow of information in the retina

Whilst many considered the retina to be responsible for very basic processing, it is becoming increasingly clear that it carries out complex computations (discussed in Gollisch and Meister, 2010). Information extracted from the environment becomes increasingly descriptive as information flows through the retina. Thus, the information projected to other visual areas via retinal ganglion cells (RGCs) is not merely a pixel representation of light levels, but a detailed summary of extracted features at each point in visual space.

The retina is a relatively small structure compared to other brain areas, such as cortex, despite this small size, the retina carries out a surprising amount of processing. It is a multi-laminar structure with precise organisation; separating out into plexiform and nuclear layers (Figure 1.2). Dendrites and axons form specific arborisations in the plexiform layers, and somata are arranged in mosaics within the nuclear layers. The plexiform layers also form fine structures, with cells arborizing in very specific layers such as the inner plexiform layer (IPL). There is little variation in gross retinal structure between organisms, surprisingly throughout evolution the underlying structure remained largely the same, with only differences in the numbers of neuronal subtypes differing between species.

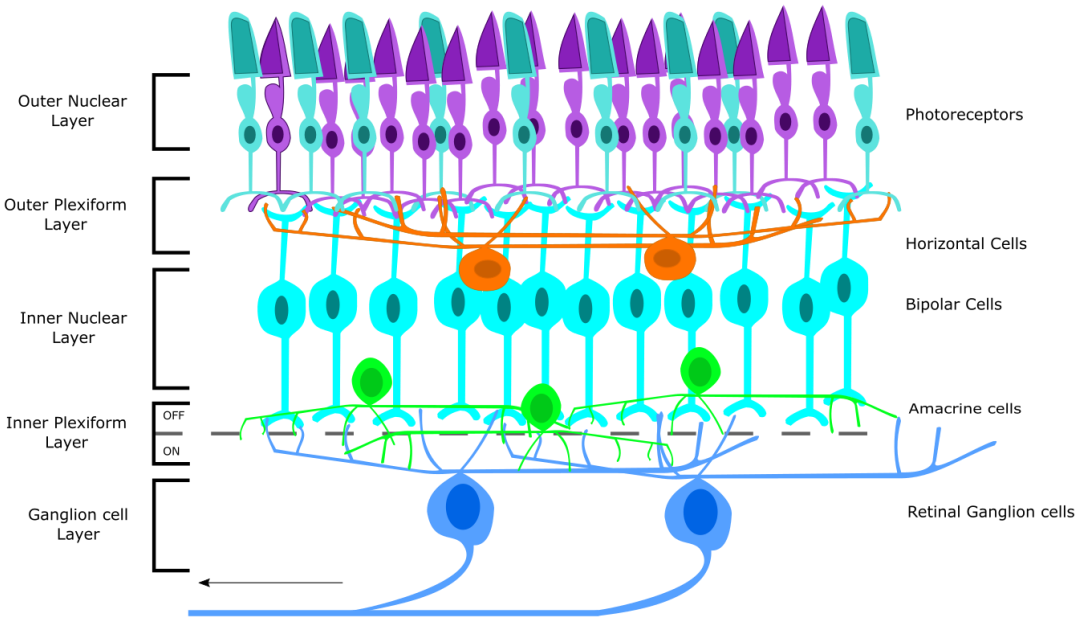

Figure 1-2 Structure of the vertebrate retina

The retina is formed of several layers of neurons and arborisations, organised into nuclear and plexiform layers. Photoreceptors provide information on wavelengths and levels of light; this information is relayed and processed by bipolar, horizontal, and amacrine cells to the sole output of the retina, the retinal ganglion cells.

1.2.1.1 *Photoreceptors provide information on colour and light intensity*

Basic processing first arises in the retina with the specialisation of different photoreceptor subtypes for different wavelengths of light; different cone opsins confer different light wavelength sensitivities within each cone photoreceptor. In zebrafish retina, there are four cone subtypes to detect different wavelengths of light; red and green in the double cone pairs, blue in long single cones and UV in short single cones (Branchek, 1984; Hisatomi et al., 1996; Nawrocki et al., 1985). One primary difference between zebrafish photoreceptors and that of other animals is the presence of two 'green' opsins within a single cone receptor; otherwise, each cone only expresses a single opsin. Mammalian cone subtypes vary, most mammals are dichromatic, with only 'red' and 'green' cones, but higher mammals including macaques and primates developed a 'blue' cone (for review see Jacobs, 2009). Rods are specialised for low light levels and far outnumber cones in the retina, with approximately 20 times the number of cones in mammals. Photoreceptors are arranged in a mosaic, with equal spacing between neurons within a subtype, ensuring equal sampling of visual space.

1.2.1.2 *Horizontal cells: a gain control mechanism for the retina*

Photoreceptors synapse with two main types of neuron in the outer plexiform layer (OPL) the horizontal cells and bipolar cells. Horizontal cells are the first inhibitory cell in the visual system. In primates there are two types of horizontal cell (Boycott et al., 1987; Röhrenbeck et al., 1989), however mice and rats only have one (Peichl and González-Soriano, 1994), whilst in zebrafish three have been observed (Connaughton et al., 2004). These cells feedback onto rods and cones, controlling the levels of their outputs. These cells sample from a wide range of rods and cones, finding the local average illumination and inhibiting the activity of photoreceptors to bring this response down to a level within the retina's working range. This acts as gain control for the retina by preventing saturation. Whilst this inhibition does not play an active role in the extraction of feature information, it is still important for survival, allowing adaptation to different levels of illumination within a visual scene, preventing saturation where extreme differences in levels of illumination occur.

Contrast adaptation is a decreased sensitivity to temporal contrast after increases in variance of light. This is adaptation is mediated primarily by a decrease in excitatory synaptic transmission from bipolar cells to RGCs, however in a study using both calcium imaging and electrophysiology in zebrafish retina it was also found to be facilitated by depression of inhibitory feedback onto bipolar cell terminals from amacrine cells (Nikolaev et al., 2013).

1.2.1.3 *Parallel channels arise at the bipolar cell synapse*

Multiple cone bipolar cells sample from the same pool of cone photoreceptors, contacting specific patterns of cones to incorporate different types of information from their pool of cone inputs. Photoreceptors hyperpolarize in response to light activation, releasing less glutamate. Glutamate release can cause either hyperpolarisation or depolarisation in post-synaptic bipolar cells depending on the glutamate receptor expression in the bipolar cell dendrites. Metabotropic glutamate receptors are responsible for the ON response, (Morgans et al., 2009), whilst Ionotropic glutamate receptors depolarize the cells and thus generate OFF bipolar responses. This difference in receptor expression is what creates the divergence of ON- or OFF- responsive bipolar cells from the photoreceptor inputs (DeVries, 2000; Lindstrom et al., 2014; Puller et al., 2013). At the first synapse of the retinal circuit photoreceptor outputs are segregated into either ON and OFF responses, this is reflected in the arborisations of bipolar neurons in different lamina within the IPL. ON and OFF bipolar cells are present in equal numbers in the retina, but can be further subdivided depending on temporal properties of responses. These subdivisions relate to the length or frequency of input the cones provide to their bipolar synaptic partners; either transient or sustained ON/OFF (DeVries, 2000). These differences in the temporal properties of responses of bipolar cells are due to the differences in recovery times of receptor channels from desensitisation.

Within the OPL bipolar cells incorporate information from multiple photoreceptors and gain control mediated by horizontal cells, providing this information to the next layer of neurons in the IPL. The information passed on by bipolar cells divides into 12 channels of different types of visual information, corresponding to the 12 different bipolar cell types in mouse (Ghosh et al., 2004; Wässle et al., 2009). In zebrafish, 17 bipolar cell subtypes have been identified (Connaughton et al., 2004). Here in the IPL, the amacrine cells (ACs) and retinal ganglion cells (RGCs) form synapses with bipolar cell dendrites, incorporating information from multiple bipolar cells to generate even more diverse and complex channels of information from the visual scene.

Low light sensitive rod outputs follow a less direct pathway to ganglion cells. Multiple rod photoreceptors converge onto rod bipolar cells. The ratio of rod photoreceptors to a bipolar cell far outnumbers than seen with cone bipolar cells. This is largely to increase sensitivity to light. These rod bipolar cells converge onto the cone circuitry via an amacrine

cell (AII) that forms synapses onto cone bipolar axon terminals with RGCs (Strettoi et al., 1994).

1.2.1.4 *Ganglion cells receive bipolar inputs predominantly through amacrine cell synapses*

RGCs are the only neuronal outputs from the retina to visual areas of the brain. Receptive field properties of these ganglion cells are generated through the selective sampling of inputs from bipolar cells, as well as amacrine cell influences. Furthermore, synapses between bipolar cells and ganglion cells are modulated by amacrine cells. Amacrine cells outnumber all other cell types in the retina, except photoreceptors. This large number is indicative of their crucial role in the shaping of the retina's responses to light. Diameters of RGC dendritic arbors range between 200-1000µm, and yet many functional subtypes of RGC respond to stimuli much smaller than their receptive fields. These sub-receptive field responses are due to the influence of amacrine cell inputs onto the ganglion cells, many of which have arbors less than 100µm in diameter.

The functional importance of amacrine cells is evident from the sheer diversity of subtypes present in the retina. Amacrine cells are the most numerous in cell subtypes, with about 30-50 subtypes currently known (Macneil et al., 1999), and seven in zebrafish identified by morphology alone (Connaughton et al., 2004). These neurons express a diverse range of neurotransmitters, but the majority are GABAergic. Another fascinating feature of amacrine cells is their ability to produce excitatory outputs onto other neurons through GAP junctions, despite expression of inhibitory neurotransmitters. A key feature of amacrine cells is a lack of distinct dendritic or axonal arbors. These arbors can both receive excitatory glutamatergic inputs and release inhibitory GABAergic outputs to the same bipolar cell synapses. Amacrine also carry out 'vertical integration'; their arbors can span several layers of the IPL, integrating information from many different cell types.

With such a diverse range of subtypes and neurotransmitters it is unsurprising that these cells have been implicated in the computation of complex features such as direction selectivity (DS), motion detection, size selectivity, and centre surround inhibition. For instance: The AII amacrine cell is involved in the integration of rod information into the cone circuit (Strettoi et al., 1994), and the VGluT3-expressing AC (Lee et al., 2014) which mediates small object motion sensitivity in W3-RGCs (Zhang et al., 2012) via a non-linear spatial

integration of information from neurons with smaller receptive fields (approximately 50 bipolar cells).

The computation of direction of object motion in the visual field has been under investigation since direction-selective ganglion cells (DSGCs) were found to respond strongly to stimuli moving in a preferred direction, with much weaker responses to visual stimuli moving in the opposite direction. The first attempt to understand this mechanism in RGCs presented spatially separated static stimuli with apparent motion in either in preferred or null directions, finding that objects presented in the preferred direction produced excitatory inputs onto the neuron, and those in null direction received inhibitory inputs (Barlow and Levick, 1965).

Thus, over the next four decades, the roles of both inhibition and excitation in the computation of direction selectivity have been intensively studied. Through dual patch clamp recordings, starburst amacrine cells (SACs) were pinpointed as the source of inhibition onto DSGCs (Fried et al., 2002), providing inhibition when visual stimuli are presented in the null direction of motion. This was reinforced by evidence that immunotoxin mediated SAC ablation removes DS responses from DSGCs (Yoshida et al., 2001).

SACs are radially symmetric interneurons, exhibiting both GABA (inhibitory) and acetylcholine (ACh, excitatory) release (O'Malley and Masland, 1989). Strikingly, individual SAC dendrites are capable of independent computations, producing large calcium transients when visual stimuli move in a centrifugal direction along the direction of the arbour, i.e. from soma to dendrite, rather than dendrite to soma (Euler et al., 2002). This means radially segregated dendrites can respond to different directions of motion, and this direction opposes the preferred direction of the DSGC onto which the dendrite synapses. Furthermore, SACs dendrites favourably form synapses onto DSGCs with preferred directions opposing the direction of dendrite growth, creating a bias of synapse number (Briggman et al., 2011). The spatial segregation of SAC inhibition onto DSGCs means that inhibition is temporally offset during motion in preferred direction, delaying inhibition until after excitation inputs have commenced, thus too late to prevent excitation of the RGC.

Previous work pharmacologically blocking GABA mediated inhibition abolished DS responses of RGCs (Wyatt and Day, 1976), but the sites of this GABA receptor antagonism were unknown, and potentially perturbed inhibition elsewhere in the circuit. Similarly, pharmacological blocking of cholinergic signalling in retina whilst presenting drifting gratings abolishes direction selectivity in DSGCs (Grzywacz et al., 1998). Both results raise questions regarding the specific roles of excitation and inhibition. The generally accepted model for

generation of DS in RGCs relies upon a greater level of inhibition from SACs elicited by visual motion in the null direction.

Recent work identified that this model is not strictly accurate; demonstrating that inhibition from SACs is merely part of the mechanism. By recording the responses of posterior motion selective DSGCs in retinas from a conditional knock out mouse in which Vgat, a GABA vesicular transporter is lost only in SACs, Pei et al., (2015) showed that DSGCs retain direction selective properties despite a lack of inhibitory inputs. However, whilst the DSGCs remain direction selective, their DSI values are much lower than those seen in wild type retina. This suggests that SAC mediated inhibition increases DS tuning. Pei et al (2015) also demonstrate through the selective blocking of cholinergic receptors, that ACh excitatory inputs to the DSGCs are direction selective. These results suggest a mechanism requiring two aspects, greater inhibition on null side via SAC GABA release, paired with a directionally tuned excitatory input from the same neurons (Figure 1.3).

Thus, amacrine cells are a prime example of an inhibitory interneuron mediating the extraction of different features of visual information. The integration of inputs from these different amacrine cells producing the diverse and complex receptive field properties in RGCs.

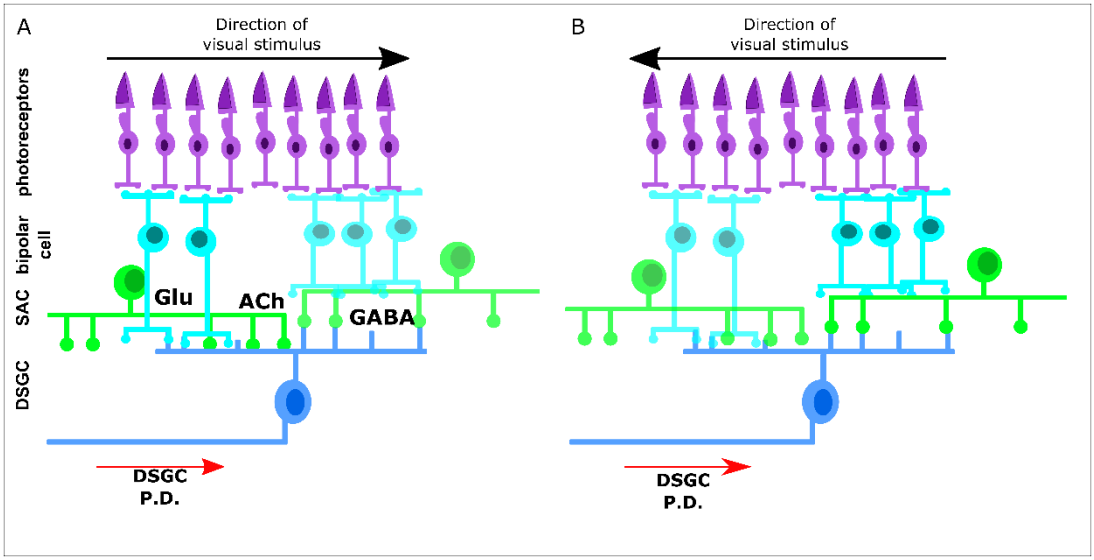

Figure 1-3 Overview of the circuitry involved in generation of direction selective responses in DSGCs

Direction selectivity in DSGCs is mediated through multiple mechanisms. Excitatory inputs from starburst amacrine cells (green) tuned to preferred direction, complemented by GABAergic inhibition tuned to null motion, as well as inputs from bipolar cells, all contribute towards DS tuning in retinal ganglion cells in the retina.

1.2.2 RGCs project feature specific information out from the retina

Precisely organised inputs onto RGCs confer their receptive field properties, with amacrine cells providing transformations generating complex receptive field properties. There are approximately 20 different subtypes of RGCs known in mammalian retina (for review see Sanes and Masland, 2014) and approximately 15 in zebrafish (Mangrum et al., 2002; Robles et al., 2013, 2014). Structural to functional correlations provide a simple way to classify these neurons, for example, the location of RGC dendritic arborisations in the IPL can divide RGCs into either ON, OFF or ON-OFF RGCs (Famiglietti and Kolb, 1976). Similarly, even tiling of neurons across the retina can also be used an indicator of a functional RGC subtype.

One such functional subtype has centre surround inhibition, identified in one of the earliest functional characterisations of visually responsive neurons; these neurons have differential receptive fields, and are known as midget cells in primates. Activation of the central area of the cell's receptive field will activate the neuron's firing, however if this stimulus also activates the surround area of the receptive field this creates a suppression of firing of the neuron (Hubel and Wiesel, 1959). This receptive field organisation is mediated by small field amacrine cells, receiving inputs from bipolar cells with receptive fields in the 'surround' of the ganglion cells' neuron (Kolb and Marshak, 2003). In primates, unlike other mammals, there is a significant increase in the number of midget cells in the fovea. In terms of representation in the retina, these neurons are ~70% of the total neuronal population, and produce a large foveal spatial resolution through a 1:1 relationship of cone to ganglion cell connections, through a special midget bipolar cell (Perry et al., 1984).

1.2.2.1 *Looming response:*

One important feature of movement on the visual scene is that of 'looming' objects, characterised by an increase in an object's size on the visual field. Identification of looming stimuli is key to identifying self–movement towards an object, or the identification of objects moving closer to an animal. Looming sensitive neurons have been described in several animals (Gabbiani et al., 1999; Hatsopoulos et al., 1995; Yilmaz and Meister, 2013).

Alpha RGCs are a subtype of RGC in mouse, analogous to Y-cells in cat, parasol cells in primate and brisk transient neurons in rabbit, all associated with looming detection. They can be separated into three functional subtypes, ON sustained, OFF sustained and OFF transient RGCs. The OFF transient RGCs are also known as approach sensitive RGCs (Münch et al., 2009) as they respond well when a stimulus increases in size. This is comparable to the visual stimulus approaching the animal.

1.2.2.2 *Local edge detectors and object motion sensing ganglion cells:*

Object motion is the ability to detect movement of an object across an area of the visual field, but not movement of whole visual field. It specifically detects movement on the visual field that is not due to shifts generated by eye or animal movement. To make this distinction, the neuron must be able to differentiate between differential and global motion. This detection of motion should also independent of direction. Local edge detectors (LEDs) and object motion sensing (OMS) ganglion cells carry out similar tasks, responding to similar stimuli.

LEDs were found in a range of organisms including frog, guinea pig, cat and primate (Berson et al., 1998; Maturana et al., 1960; Rodieck and Watanabe, 1993; Xu et al., 2005; Zeck et al., 2005). First characterised in mouse and rabbit, this neuron was found to comprise approximately 15% of RGCs in the rabbit retina (Levick, 1967). LEDs are most responsive to moving stimuli that fall directly within the receptive field centre, which is very small for these neurons, as their arbors span only 100µm of the IPL. LEDs are highly tuned to differential motion between the receptive field centre and the surround, but are also insensitive to the pattern of this moving stimulus. These neurons respond with sustained firing when either dark or light moving spots cross the centre of their receptive fields, but are unresponsive with full field stimuli (van Wyk et al., 2006). This lack of response with full field stimulation is due to the strong inhibitory surround. In mouse the analogous neurons are known as W3B-RGCs (Zhang et al., 2012). Movement occurs simultaneously across both the centre and surround of the neuron's receptive fields when fixational eye movements occur, thus this differential motion detection provides a mechanism to determine when motion in visual field is not self-generated. LEDs share many properties with OMS neurons. This intersectionality of receptive field properties is characteristic of neurons in the visual system, with complexity of preferred stimuli identified, and responses of neurons depending on visual stimuli used during experiments, including contrast, spatial and temporal frequency.

Recent work has identified the circuitry involved in generating such response properties in OMS ganglion cells. It was found that a combination of many ON and OFF bipolar neurons providing excitation to the W3-RGCs, a source of inhibition to the amacrine cells excitation from wide-field amacrine cells –VG3-ACs, that produces the OMS properties of W3-ganglion cells (Kim et al., 2015).

1.2.2.3 *Orientation Selectivity:*

Orientation selectivity (OS) is a type of feature selectivity found vertebrate retinas, present in primate (Passaglia et al., 2002), mouse, rabbit (Levick, 1967), cat and zebrafish (Lowe et al., 2013; Nikolaou et al., 2012). Orientation selective RGCs respond maximally to objects orientated along an axis, and minimally to objects along the orthogonal to this preferred axis. These neurons usually have much sharper tuning than seen in DSGCs. In rabbit, only two orientations of motion are detected, horizontal and vertical. However, in zebrafish retina at least four orientations are represented (Lowe et al., 2013). The mechanism generating OS is thought to rely upon presynaptic GABAergic inhibition from amacrine cells and the modulation of bipolar cell outputs (Venkataramani and Taylor, 2010) . Recently, a wide-field polyaxonal amacrine cell (PAC) has been identified in rabbit retina and was proposed to be responsible for generating orientation selectivity in specific OS RGC subtypes (Murphy-Baum and Taylor, 2015).

1.2.2.4 *Direction selective neurons are present in all vertebrates*

One of the most studied feature selective RGCs is the direction selective RGCs (DSGCs). DSGCs have been identified in mouse, zebrafish and rabbit (Lipetz and Hill, 1970; Maturana et al., 1960; Nikolaou et al., 2012; Ott et al., 2007; Oyster and Barlow, 1967), but to date have not been identified in primate retina (see Field and Chichilnisky, 2007). DSGCs can be ON (Yonehara et al., 2009), OFF (Kim et al., 2008) and ON-OFF (Huberman et al., 2009; Kay et al., 2011). The mechanism by which direction selectivity is generated involves a combination of DS tuned excitatory inputs, and SAC derived GABA inhibition to null direction motion, as described earlier in this chapter.

In rabbit, four ON-OFF DSGCs were identified. These neurons respond to directional movement, rather than a particular stationary pattern of stimuli. They respond to four cardinal directions of motion: upward, downward, backward and forward relative to the animal (Huberman et al., 2009; Oyster and Barlow, 1967; Rivlin-Etzion et al., 2011). They show no preference for the contrast of the moving stimulus, and respond to movement of sizes much smaller than their receptive fields. ON-OFF DSGCs are bi-stratified, with dendritic trees in both ON and OFF lamina of the IPL, their arbors aligned tightly with those of SACs (Amthor et al., 1984; Badea and Nathans, 2004). Within the ON-OFF DSGC populations, each cardinal DSGC population forms a separate mosaic on the visual field (DeVries and Baylor, 1997).

ON-DSGCs have been identified in rabbit and mouse (Yonehara et al., 2009). These are monostratified in the ON layer of the IPL, and consequently only respond to light moving edges and spots, and not to dark. ON-DSGCs respond to slower movement than ON-OFF DSGCs. These neurons project to accessory optic system (AOS) which is involved in the optokinetic reflex; the AOS is responsible for eye movements that reduce movement of the visual scene across the retina caused by movement of the animal. There are three different directionally tuned ON-DSGCs, sensitive to upward, downward and forward motion relative to the animal (Dhande et al., 2013).

In zebrafish, direction selectivity is centred on the same three axes found in ON-DSGCs, responding to upward, downward and forward motion relative to the fish (Nikolaou et al., 2012). These DS populations had previously been identified in Goldfish tectum (Maximov et al., 2005).

The J-RGC projects to the SC, and is an upward responding OFF-DSGC, unsurprisingly OFF-bipolar cells arborize in the same lamina as these OFF-DSGCs. J-RGCs have an asymmetric arborisation which is thought to contribute to their direction selectivity; the vector of the dendritic arborisation matches that of the preferred direction of motion (Kim et al., 2008).

1.2.3 Several brain areas receive retinotopic maps of information via RGCs

The output of the retina is a retinotopic map, populated with 'streams' of different forms of information from the visual scene, including direction of motion, contrast, looming, local and global motion, as well as colour. This retinotopic map forms layers of input into retinorecipient areas including superior colliculus or optic tectum. There are approximately 20 brain regions that receive RGC inputs in mammals (Ling et al., 1998). In zebrafish, there are 10 RGC arborisation fields (Figure 1.5B), the largest of which is the optic tectum (arborisation field 10, AF-10) (Burrill and Easter, 1994).

1.2.3.1 *Dorsal Lateral Geniculate Nucleus:*

In mammals, information from the retina projects to dorsal lateral geniculate nucleus (dLGN) via RGCs, which then relays this information to the cortex. The dLGN was originally thought to only be a relay between retina and cortex; however, recent evidence indicates that this is not the case. The dLGN receives cortical feedback (Olsen et al., 2012), which has been implicated in processing within the circuit, and interneurons have been identified. The majority of neurons in the dLGN are 'relay neurons' (~75%) projecting information to the cortex, with the remaining 25% being composed of interneurons (Sherman and Guillery,

2001). Neurons in the dLGN have a diverse range of response properties, including direction selectivity (Marshel et al., 2012), orientation selectivity (Zhao et al., 2013) and ON or OFF centre neurons (Grubb and Thompson, 2003) .

In neurons of the dLGN direction selectivity relies upon inputs from DSGCs that terminate in the superficial dLGN (Huberman et al., 2009; Kim et al., 2008). Similarly, orientation selectivity in the dLGN is independent of cortical feedback, but rather a consequence of inputs to these neurons (Zhao et al., 2013). A particularly interesting GABAergic interneuron was identified in cat dLGN, these neurons have dendrites that function independently to both the axon, and other dendrites (Hamos et al., 1985), much like Amacrine cells, and are likely to be involved in gain control of relay neurons (Sherman, 2004).

1.2.3.2 *Optic Tectum/Superior colliculus produces goal directed behaviour from retinal inputs*

The superior colliculus (SC), or optic tectum (OT) in non-mammalian vertebrates, is responsible for body and gaze orientating behaviours . In mouse and rat, the superficial SC is one of the largest areas of ganglion cell innervation, and the largest retinorecipient area in organisms such as zebrafish and Xenopus. It is here in the optic tectum that goal directed behaviours including phototaxis (Chen and Engert, 2014), prey capture (Budick and O'Malley, 2000; Gahtan et al., 2005; Smear et al., 2007) and predator avoidance (Bass and Gerlai, 2008; Gerlai et al., 2009) are initiated in zebrafish. In higher mammals such as primates, it is also implicated in saccades and spatial attention (Carello and Krauzlis, 2004).

The structure of this brain area is multi-laminar, the number of layers varying by species. Innervation from RGCs is retino-topically arranged, forming primarily in the superficial SC (Hofbauer and Dräger, 1985). Other sensory maps form in deeper lamina, including those relating to motor movements (Deeg et al., 2009). For instance in Xenopus, mechanosensory inputs form in deeper layers of the tectum, whilst RGC inputs are in superficial laminae (Hiramoto and Cline, 2009). These sensory maps align in retinotopic space, with visual auditory or somatic information from a particular area surrounding the organism represented in a similar area of SC.

Whilst the retina has been the subject of extensive work to discern the circuitry, the tectum and superior colliculus lack such a high level of description of cell subtypes, connectivity and synaptic connectivity. Establishing the circuitry of the tectum is vital, using such techniques such as serial EM reconstruction, and combinations of genetic cell subtype labelling and electrophysiology. Morphological studies of tectal cell subtypes have been carried out,

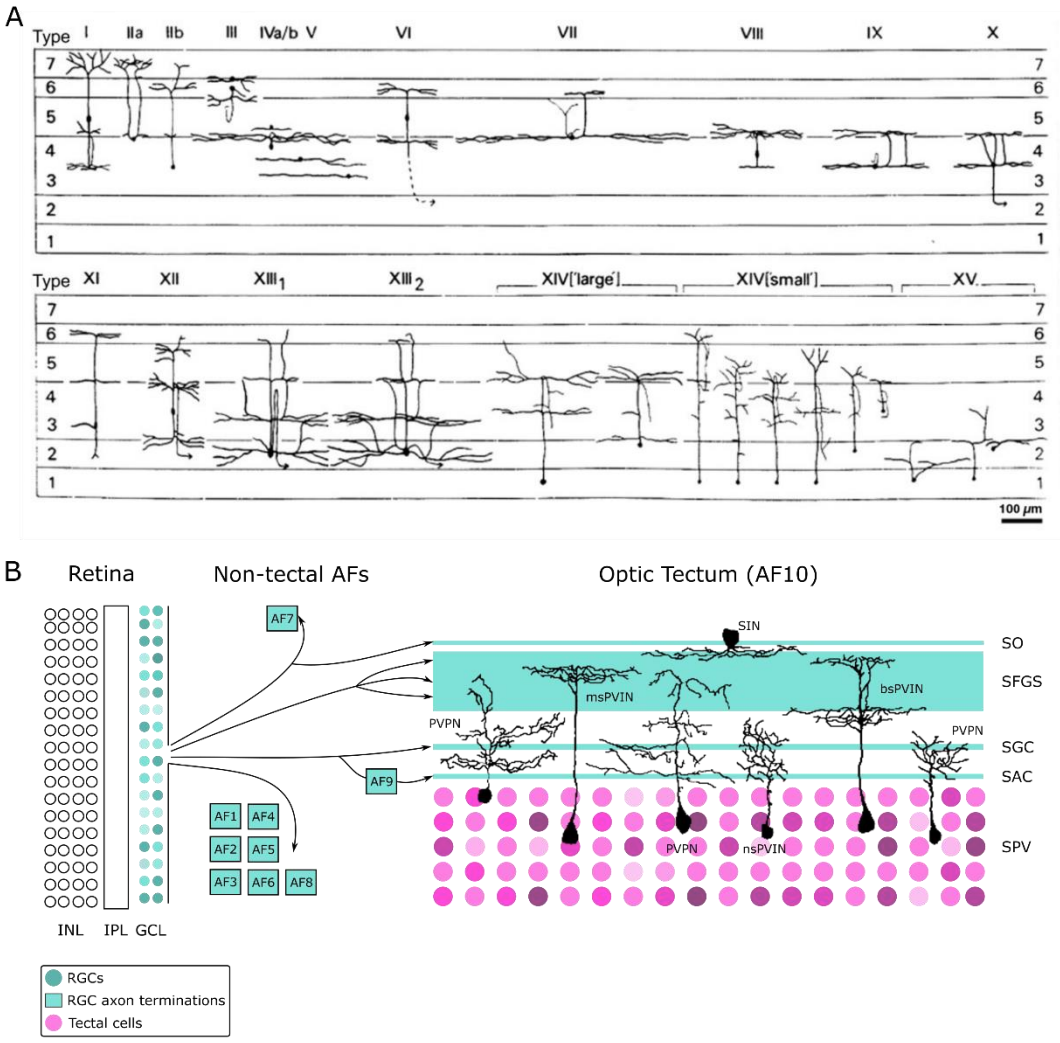

Figure 1-4 Tectal cell types and morphologies in Goldfish and Zebrafish

A. Figure of morphologies of the 14 neurons identified in Goldfish (from Meek and Schellart, 1978) B. The organisation of retinal ganglion cell (RGC) outputs in zebrafish. There are 10 visual arborisation fields in the brain of larval zebrafish, the largest of which is the optic tectum (AF10). RGC axons terminate in different lamina of the optic tectum, with the majority arborizing in SFGS. The seven identified tectal cell morphologies are shown in their relative tectal laminae. Adapted from (Nevin et al., 2010)

however, finding approximately 8 morphological subtypes, whilst in goldfish over 14 subtypes were identified (Figure 1.4 adapted from (Meek and Schellart, 1978; Nevin et al., 2010).

Unlike LGN or cortex, there has been relatively little work identifying the receptive field properties of specific neuronal subtypes in SC. Golgi studies identified several different morphological subtypes, including several interneurons such as horizontal cells, marginal cells, and stellate cells (Figure 1.5, adapted from Langer and Lund, 1974). Of particular interest are the horizontal cells, which were thought to provide long distance lateral inhibition within collicular layers (Langer and Lund, 1974). From characterisations of

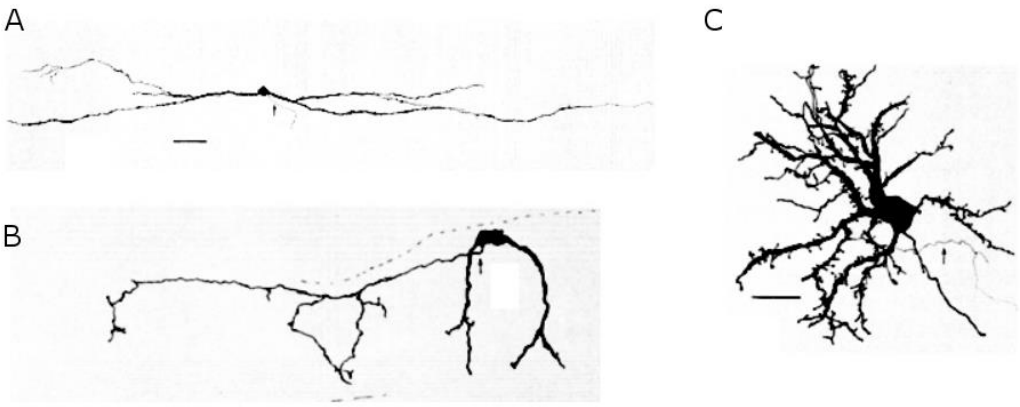

Figure 1-5 Morphologies of selected interneurons of the Superior Colliculus

Adapted from (Langer and Lund, 1974), examples of the morphologies of interneurons found in the superior colliculus of rat. A. horizontal cell, B. marginal cell C. stellate cells.

horizontal cell receptive fields it was found that these neurons have compact circular receptive fields that do not match the size of their arborisations (Wang et al., 2010).

Functional studies in the superior colliculus identified orientation selective (Cynader and Berman, 1972; Girman and Lund, 2007), direction selective (Cynader and Berman, 1972; Mooney et al., 1985), and size selective neurons with size preferences varying between species (Prévost et al., 2007). GABA expression is dispersed throughout the entire SC (reviewed in Mize, 1992), with no apparent bias to any particular lamina, however interneurons with morphologies matching those of horizontal cells were found to express GABA in superficial superior colliculus (Endo et al., 2003). The inhibitory nature and the wide horizontal dendritic field indicates that these neurons are likely to contribute to the generation of feature selectivity in neurons within the SC.

Early electrophysiological studies of tectal neurons indicated that tectal neurons exhibit diverse stimulus selectivity, with ON and ON-OFF subtypes, some exhibiting tonic activity, as well differences in responses to moving spots versus stationary spots in the RF. Tectal neurons also had more complex compound receptive fields, comprised of two or more regions in the visual field that elicited responses separated by regions of unresponsiveness (Sajovic and Levinthal, 1982a, 1982b).

Population studies of neurons in the periventricular layer (PVL) of the optic tectum of zebrafish identified an emergent functional population of DS tectal neurons in addition to the three found in RGCs, sensitive to backward motion relative to the fish (90°, seen in Hunter et al., 2013). This direction of motion is not present in DSGC inputs to the tectum, indicating that the tectal circuit carries out a computation using its inputs in order to

generate this emergent DS population. A calcium imaging study in adult zebrafish identified both orientation and direction selective neurons in the tectum (Kassing et al., 2013), helping to confirm results identifying populations of DS tectal neurons in larval zebrafish, as well as four OS populations of tectal neuron along the cardinal axes of the larvae (Hunter et al., 2013).

It is likely that within these four populations there are several different morphological and functional subclasses of DS neuron. Further refinement of these populations according to such properties as neurotransmitter expression, projection or interneuron, size selectivity, or excitatory vs inhibitory could be useful for characterisation of the computations within the tectal circuit. Furthermore, visually responsive neurons respond to many different features: full field or narrow field movement, contrast differences, sinusoidal gratings, edge movement, looming stimuli. Ideally, experiments would utilise a barrage of stimuli to characterise DS or OS neuronal populations in the tectum, probing all these properties to produce a comprehensive functional description as seen in a recent characterisation of mouse ganglion cell subtypes (Baden et al., 2016).

An example of a functional and morphological description of tectal neurons is work in which two GABAergic DS subtypes in the larval zebrafish tectum were characterised using GCaMP3 expression under Oh-3:Gal4 and Oh-4:Gal4 promoters (Gabriel et al., 2012). These neurons preferred directions of rostro-caudal or caudal-rostral movement (equivalent to motion at 30° and 270°) consistent with two populations seen in tectal neuron population data (Hunter et al., 2013), as well as DSGC inputs to tectum (Nikolaou et al., 2012). These neurons have striking bi-stratified arborisations, with the topmost arbour localising predominantly with DSGC axons. These neurons receive excitatory inputs during motion in preferred direction, and inhibitory inputs to motion in null direction. This supports the idea that DS is not computed within the tectum, but inherited from DS inputs from the retina. The authors proposed two theories on where this null direction inhibition arises from, wither a superficial inhibitory interneuron (SIN), or inhibition from other tectal neurons through their dendritic arborisations in the deeper tectal lamina (Gabriel et al., 2012).

SINs are the only morphological subtype of tectal neuron with somata located just above RGC inputs in the superficial layers of the optic tectum. SINs have radial arborisations surrounding their soma, a morphology much like the SACs in the retina, suggesting they too may be responsible for feature selectivity. These neurons can be labelled by an enhancer trap line, *s1156tGal4* (Scott and Baier, 2009). SINs labelled by this line co-labelled for GABA expression, indicating that these neurons are inhibitory. Further, changes in SIN GCaMP

fluorescence in response to visual stimuli indicated these cells are respond to whole field flashes of light, but not small moving bars (Del Bene et al., 2010). This initial characterisation of SINs was a step towards understanding these neurons, but lacked the experimental design to make useful conclusions on the role of SINs in the tectal circuit. The stimuli used did not probe such important properties as direction selectivity, and critically the analysis used to determine the SIN properties was not effective for dissecting out the functional diversity within the SINs, simply masking the superficial-most third of the neuropil and using net fluorescence changes across this entire area as the functional description of these neurons.

Further experiments using an alternative transgenic line to label these neurons, found that SINs are size selective (Preuss et al., 2014). This size selectivity may be inherited from size selective RGC inputs identified in the same study. Preuss et al (2014) suggest that SINs are involved in the decision making process between prey capture and predator avoidance based on their size preferences. Whilst this paper provides a better description of SINs, it too neglects to characterise the full receptive field properties of these neurons. The experiments provide motion along the anterior to posterior or posterior to anterior axis. Motion sensitive neurons respond sub-optimally to moving stimuli at non-preferred directions, and this may alter the responses to size seen regarding in the SINs.

Zebrafish Optic tectum is largest but not the site of ganglion cell arborisation. There are nine non-tectal arborisation fields in zebrafish brain (Burrill and Easter, 1994). Recent work has identified that the important function of prey capture may be mediated not through the tectum, as previously described, but through AF7 (Semmelhack et al., 2014). They identified RGC axons responsive to small moving dots equivalent in size to prey that they identified as innervating both AF7 and the superficial tectum, SO. Through ablation of AF7, they saw a reduced level of prey capture in larvae. Similarly, they labelled neurons in the AF7 layer to identify potential projection neurons, identifying two subsets, one that projected to tectum, and a second that projected to nucleus of the medial longitudinal fasciculus (nMLF) indicating a role in generating prey capture swims (Thiele et al., 2014).

1.2.3.3 *In visual cortex, inhibitory neurons shape response properties:*

In mammals, visual cortex (also referred to as striate cortex, or V1), is involved in perception and contextual processing of visual information (Albright and Stoner, 2002). V1 is a structure with six lamina, consisting of several morphological subtypes of neuron with specific functions, layer IV receives the majority of input from LGN. As with most visual areas of the

brain, the cortex receives a retinotopic map of inputs (Schuett et al., 2002; Wagor et al., 1980). Neurons in visual cortex exhibit many different receptive field properties including direction selectivity (De Valois et al., 1982), orientation selectivity (Hubel and Wiesel, 1962), contrast sensitivity (Glickfeld et al., 2013), and spatial frequency tuning (Issa et al., 2000).

Inhibitory neurons are involved in the shaping of response properties of individual neurons in cortex (Isaacson and Scanziani, 2011), and these inhibitory neurons have diverse functional and morphological specialisations (Markram et al., 2004). Specifically, inhibitory interneurons have been implicated in the generation of orientation selectivity of cortical neurons, where tuned OS inputs from dLGN are refined with local inhibition in the cortex to orthogonal orientations (Bonds, 1989; Pfleger and Bonds, 1995; Shapley et al., 2003). Immunological labelling of inhibitory neurons in the cortex identified three main subtypes: vasoactive intestinal protein expressing neurons (VIP+), somatostatin-expressing neurons (SOM+) and parvalbumin expressing (PV+) neurons (Xu et al., 2010). In V1, these inhibitory neurons have broader orientation tuning than neighbouring excitatory neurons (Kerlin et al., 2010).

SOM+ interneurons are a located in layer II/III of the visual cortex. These SOMs exhibit tuning preference for large objects, with no surround suppression (Adesnik et al., 2012), and receive inputs from pyramidal cells (PCs) with tuning preferences for smaller objects. SOMs provide inhibition to neighbouring PCs (Wang et al., 2004) and PV+ inhibitory neurons (Cottam et al., 2013). SOMs mediate surround inhibition in excitatory neurons in layer II/III by summating excitatory activity from smaller inputs, using this to provide inhibition to the rest of the circuit (Adesnik et al., 2012). SINs in the optic tectum and SOMs in the cortex, share many similarities, both neurons exhibit size selectivity and provide inhibition to the rest of the circuit (see Barker and Baier, 2013).

1.3 Thesis Aims

This thesis aims to contribute to a description of the visual system circuitry by generating a description of the function of one subtype of tectal neuron, the SIN. From work carried out in the retina, as well as visual cortex, it is clear that there is a theme running throughout the visual system of inhibitory interneurons processing visual information before relaying this to projection neurons. Inhibition has a key role in refining and extracting complex information from a combination of different inputs. The importance of inhibition for shaping of receptive

field properties is most evident when looking at the role of such interneurons as the amacrine cells in the retina, as well as inhibitory neurons in the visual cortex (see review by Isaacson and Scanziani, 2011).

Traditionally visual physiology has been studied in mammals such as primates (Bredfeldt and Ringach, 2010; Ringach et al., 2002; Wurtz and Albano, 1980), cat (Priebe and Ferster, 2005; Somers et al., 1995) and more recently mouse (Gonchar et al., 2007; Niell, 2011; Piscopo et al., 2013). Previous work on non-mammalian visual physiology involved a range of techniques, including electrophysiology, whole population calcium imaging, and single cell patching (Baden et al., 2014; Niell and Smith, 2005; Sajovic and Levinthal, 1982a; Scott and Baier, 2009; Stuermer, 1988). More recently a greater shift towards using these smaller vertebrates has been largely due to the ease with which these organisms are bred, the rise in ease with which they can be genetically manipulated, and their significantly smaller sizes, making them much easier to image using the latest microscopy techniques (Feierstein et al., 2014).

The small scale of larval zebrafish makes them ideal for imaging, as well as the short development time needed for their visual systems to reach full maturity (7dpf). The zebrafish visual system is easily accessible, without the need for invasive surgery to access for microscopy, and can be imaged due to the translucency of the larval zebrafish body (Feierstein et al., 2014; Muto et al., 2013; Orger et al., 2008). This allows long-term functional imaging without the need for invasive techniques. Not only this, but visually guided behaviours are well studied in zebrafish (Bass and Gerlai, 2008; Bianco and Engert, 2015; Bianco et al., 2011; Budick and O'Malley, 2000; Chen and Engert, 2014; Gahtan et al., 2005; Muto and Kawakami, 2013; Orger et al., 2008; Portugues and Engert, 2009).

While the optic tectum in zebrafish is relatively less characterised than the circuitry of mammalian superior colliculus, it is very likely that the processing motifs and strategies are conserved. With the relative ease of use of zebrafish larvae as a model organism for addressing visual circuitry, and the lab's experience in using visual stimuli to probe this circuitry in vivo, we aimed to look for similar patterns of the extraction of information through inhibition within the tectum.

This project looks at a particular inhibitory tectal neuron, the SIN, with the aim of identifying the role the inhibition it provides to the circuit. Chapter 3 characterises SIN functional properties, looking specifically at direction, spatial, and temporal tuning. Chapter 4 follows these experiments up by comparing the receptive field properties of these SINs to both the inputs to the tectum (RGCs) and other neurons within the tectum (tectal neurons), using

pharmacology to determine if GABA-A receptor mediated inhibition is required for SIN DS tuning differences when compared to the rest of the DS circuit. Chapter 5 then uses pharmacology and genetically driven ablation to determine what happens to DS populations in absence of these cells and their inhibition.

The information these experiments provide alone are not sufficient to draw conclusions as to the processing involved in the entire circuit, but they do provide a foundation upon which more detailed experiments can be based. By generating functional profiles of each cell subtype within the tectal circuitry, and their connectivity within the circuit, a functional map can be built. From this information we can begin to understand the transformations that occur within a circuit and the processing that is required to utilise visual information to guide behaviour.

In summary, this thesis aims to answer the following questions:

- Does the s1156tGal4 line used in (REF) label all SINs in the optic tectum?
- What are the preferred stimuli of SINs, probing specifically:
    - Direction selectivity and Orientation selectivity
    - Spatial frequency tuning
    - Temporal Frequency tuning
- How do SIN preferred stimuli compare to RGC inputs and Tectal neurons?
- What role does SIN mediated inhibition play in tectal circuit?

2 MATERIALS AND METHODS

2.1 Materials

2.1.1 Plasmids

Insert	Vector Backbone	Vector Source	Fluorescence	Source
UAS:Tdt; UAS:Syp:GFP	pEGFP-N2	Clontech	Red, Green	(Meyer et al., 2005)

Table 2-1 DNA plasmids used for single cell labelling in SINs

2.1.2 Antibodies

Antibody name	Recognises	Dilution used	Supplier
Anti-GFP (chick)	GFP, GCaMP	1:500 (whole mount)	Life Technologies, Grand Island, USA
TO-PRO-3	Nuclear label	1:1000 (whole mount)	
Anti-chick Alexa 488	Primary antibodies raised in chick	1:500 (whole mount)	

Table 2-2 Antibodies used for characterising *s1156tGal4* line

2.1.3 Experimental Solutions

Paraformaldehyde (PFA): 4% PFA in 3% sucrose, 60mM PIPES, 25mM HEPES, 5mM EGTA, 1mM $MgCl_2$

Danieau: 58mM NaCl, 0.7mM KCl, 0.4mM $MgSO_4$, 0.6 mM $Ca(NO_3)_2$, 5.0 mM HEPES (pH 7.6)

2.1.4 Transgenic Lines

Allele	Background	Source	Referred to as:
Et(-1.5hsp70l:Gal4-VP16)s1156t; mitfa$^{w2/w2}$	Gal4 Enhancer trap line labelling SINs, with some sparse expression in RGCs and tectal neurons, crossed with mitfa pigment line	ZIRC	*s1156t:Gal4*
Tg(-17.6isl2b:GAL4-VP16,myl7:EGFP); mitfa$^{w2/w2}$	Gal4 attached to isl2b promoter region, expresses in RGCs	(Ben Fredj et al., 2010)	*Isl2b:Gal4*
Tg(elavl3:GCaMP5G)a4598 mitfa$^{w2/w2}$	Elavl promoter driving GCaMP5 expression in mitfa background		*HuC:GCaMP5*
UAS:GCaMP5; mitfa$^{w2/w2}$	UAS:GCaMP5 line crossed with mitfa pigment mutant	Gift from E. Dreosti, UCL	
UAS:KillerRed; mitfa$^{w2/w2}$	UAS:KillerRed line crossed with mitfa pigment mutant	Gift from F. del Bene, Institute Curie, Paris	
mitfa$^{w2/w2}$	Homozygous mutants for nacre w2 mutation	From Robert Kelsh, University of Bath	

Table 2-3 Table of transgenic lines used in experiments, sources, alleles, background

2.1.5 Pharmacological agents

Chemical	Action	Final concentration	Diluent	Supplier	Cat. Num.
Ethyl 3-aminobenzoate methanesulfate (MS-222)	anaesthetic	0.04%	ddH2O	Sigma-Aldrich, St. Louis, MO	A5040
SR 95531 hydrobromide (Gabazine)	Selective, competitive $GABA_A$ receptor antagonist.	10µM	Danieau	Tocris Bioscience, Bristol, UK	1262
APV	NMDA receptor antagonist	50µM	Danieau	Sigma-Aldrich	A5282
NBQX	AMPA receptor antagonist	10µM	Danieau	Tocris Bioscience, Bristol, UK	0373
(R)- Baclofen	selective $GABA_B$ agonist	10µM	Danieau	Tocris Bioscience, Bristol, UK	0796
CGP 54626 hydrochloride	Selective $GABA_B$ receptor antagonist	10µM	Danieau	Tocris Bioscience, Bristol, UK	1088

Table 2-4 Table of pharmacological agents used

2.1.6 Chemicals

Chemical	Diluent	Final concentration	Supplier	Cat. Num.
PBS (Phosphate Buffered Saline)	ddH_2O	NaCl 0.137mol, KCl 0.003mol, Na_2HPO_4 0.008mol, KH_2PO_4 0.0015mol	Oxoid Ltd.	BR0014
Triton-X100	PBS	1% in PBS	Sigma-Aldrich	X100
Blocking reagent	PBS	0.25% in PBS	Roche, Nutley, NJ	11096176001 ROCHE
Trypsin	PBS	0.4% in PBS	Sigma-Aldrich	T2600000
Agarose, low gelling temperature	danieau	1% or 2%	Sigma-Aldrich	A9414
N-phenylthiourea, PTU	ddH20	0.0045%	Sigma-Aldrich	P7629

Table 2-5 Table of chemicals used, diluents, concentrations and supplier catalogue numbers

2.2 Methods

2.2.1 Zebrafish

All work was approved by the local Animal Care and Use Committee, King's College London, and was performed in accordance with the Animals (Experimental Procedures) Act, 1986, under license from the United Kingdom Home Office.

Functional imaging experiments were carried out on zebrafish in the nacre mutant background. These larvae have reduced skin pigmentation due to a loss of neural crest derived melanophores (Lister et al., 1999), but retain the pigmented epithelium in retina which is necessary for normal vision. Larval zebrafish were kept at 28.5°C on a 14h On/10h off light cycle. All larvae were kept in danieau solution.

2.2.2 Mosaic labelling of SIN neurons

s1156t:Gal4 embryos were injected at one- to four-cell stages of development with plasmid DNA diluted to 50ng/µl in danieau solution. Plasmid DNA was prepared using Qiagen miniprep kits (Qiagen). Injected larvae were maintained at 28.5°C in danieau solution with PTU to prevent pigmentation from developing. These were then immobilised in 1% low melting point agarose (Sigma-Aldrich, UK) on a microscope slide, and imaged with a confocal microscope equipped with spectral detection scan head and the W Plan-Apochromatic 20x/1.0 DIC M27 75mm (Carl Zeiss) objective.

2.2.3 Immunocytochemistry

To determine numbers of SINs labelled by the s1156t:Gal4 line crossed with UAS:GCaMP5, a nuclear stain (TO-PRO-3, Life Technologies) was used to label all cell nuclei in the transgenic line. An anti-GFP antibody (Life Technologies) was used to detect GCaMP expression.

Seven-day-old (7dpf) larvae were anaesthetised in MS-222 and fixed in 4% PFA in PBS at 7dpf overnight at 4°C. Following fixation, the larvae were washed thoroughly in phosphate buffered solution (PBS) several times. Fixed larvae were then permeabilized in 0.25% trypsin (in PBS, Roche) for 30mins on ice, washed again in PBS several times, before blocking for several hours at room temperature in 0.4% blocking reagent in PBS-T (Roche, Nutley, NJ). Incubation with primary antibodies diluted (1:500) in PBS-T (1%) took 48 hours at 4°C. After incubation the larvae were washed thoroughly again in 1% PBS-T before blocking for several hours in 0.4% blocking reagent diluted in PBS-T at room temperature. Larvae were then

incubated in secondary antibody diluted (1:500) in 0.4% blocking reagent in PBS-T overnight at 4°C, with TO-PRO-3 nuclear staining (1:1000, Life Technologies).

To determine the proportion of SINs labelled by the s1156t:Gal4 line, the number of GFP-positive cells in s1156t:Gal4;UAS:GCaMP5 was expressed as a percentage of the number of nuclei labelled with TO-PRO-3 within the tectal neuropil. SINs are the only identified cell type in the neuropil; TO-PRO-3 labelled nuclei within the neuropil are therefor likely to be SIN neurons.

2.2.4 Live Calcium Imaging

All imaging was carried out using an LSM 710 confocal microscope equipped with a spectral detection scan head and a W Plan-Apochromat 20x/1.0 DIC M27 75mm (Carl Zeiss) objective. GCaMP imaging was carried out using an Argon 488nm multi-line laser at low power (~5%) to prevent photo bleaching and minimal pinhole (~1 Airy Unit (AU)) to ensure signal is recorded only from the desired cells and axons within the imaging plane. All experiments were recorded as 12-bit time series to ensure large dynamic range recording of signal changes.

SINs were recorded at 4Hz and 256x256 pixels (170.04 µm x 17.04 µm, pixel size: 0.664 μm^2). To image RGC axonal responses, experiments were recorded at 4.1 Hz, with an image size of 256x256 pixels (105.9 µm x 105.9 µm, pixel size: 0.42 μm^2). The average presynaptic bouton in zebrafish RGCs is ~0.8µm in diameter (Meyer et al., 2005). RGC experiments with multiple sections of RGC axons sampled per larvae were carried out 2µm apart to ensure no boutons were sampled twice. Tectal neuron experiments were carried recorded at a rate of 3Hz, with an image size of 256x256 pixels (207.03 µm x 207.03 µm pixel size 0.812 μm^2).

Larvae were screened using a confocal microscope with minimal laser power and exposure for expression of GECIs (GCaMP5 in SINs or SyGCaMP3 in RGC axons) prior to experiments. Larvae were mounted dorsal side up on a custom slide in 2% low-melting point agarose (Sigma, UK) made in danieau solution. This was sufficient to immobilise the larvae whilst imaging without the need for anaesthesia. The agarose was removed from in front of the right eye facing the projector screen to allow an unobstructed view.

Larvae were imaged while in a custom made imaging chamber with diffusive filter 3026 (Rosco Inc., Hollywood, CA) fitted to one side as a projection screen. This was filled with danieau and the larva was placed on a platform within this chamber at 30mm from the screen (Figure 2.1). The DLP pico projector (Optomota) was calibrated regularly to ensure luminance was maintained across experiments. The projected image covered

approximately 97° x 63° degrees of visual field. Stimuli were at a luminance of 25% and 175% (corresponding to eight cd/m^2 – 56cd/m^2) of the mean grey luminance of the background (32 cd/m^2). These were controlled by specially written Matlab (Mathworks) and LabVIEW code and driven by ViSaGe (Cambridge research systems, UK) stimulus presenter. Neuronal responses in the contralateral (left) tectum were simultaneously imaged with the confocal microscope. Time and duration of stimuli were captured using a TTL trigger sent from ViSaGe and detected by ZEN software.

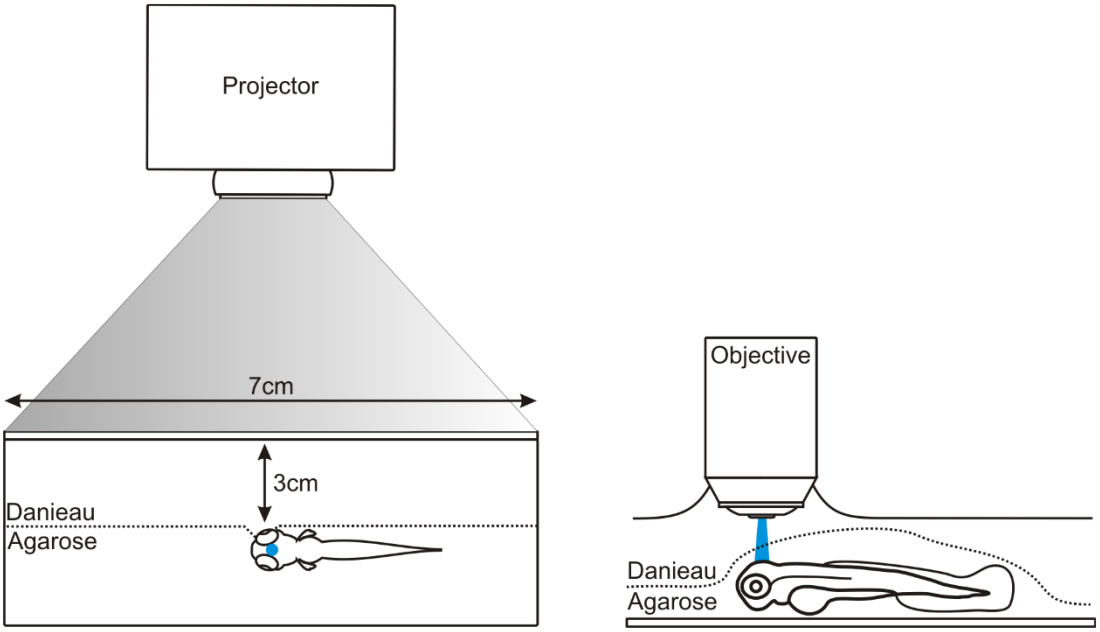

Figure 2-1 Experimental set up for visual stimulation of larval zebrafish whilst imaging neuronal activity in vivo

The functional responses of neurons in the visual system were assessed in response to visual stimulation. Larval zebrafish mounted in 2% low melting point agarose were immersed in danieau in a custom made imaging chamber. The larva is positioned 3cm from a screen with a diffusive filter, upon which visual stimuli are presented. The contralateral eye to the tectal hemisphere being imaged faces the screen.

2.2.5 Orientation/Direction experiments

For orientation experiments, sinusoidal gratings drifting in 12 different directions were presented in a pseudo random order. The direction of motion was orthogonal to the long axis of the gratings. The sinusoidal gratings had a fade time of at least 3 seconds; this allowed gratings to fade in or out to mean grey before and after the epoch to ensure that fluorescence signal from previous epochs had decayed before the next epoch is presented. A spatial frequency of 0.05 cycles/° was used, with a temporal frequency of 1 cycle/second for all orientation experiments- stimulus parameters known from previous experiments to elicit reliable responses from neurons in the tectum (Nikolaou et al., 2012). A randomly placed blank epoch, in which a mean grey background is displayed on the projector screen, was also included to aid in baseline fluorescence calculation; this was a minimum of 2 seconds.

2.2.6 Spatial Frequency experiments

For spatial frequency (SF) experiments, sinusoidal gratings were played at the direction producing the greatest response during the preceding orientation experiment (manually detected from raw fluorescence values obtained during the preceding orientation experiment), and a temporal frequency of 1 cycles/second. Initial experiments used a range of spatial frequencies from 0.014 to 1 cycles/°, but after analysis of initial experiments, the range was lowered to SFs from 0.014 to 0.5 cycles/°. Seven SFs within this range were presented in a pseudo-random order, with spatial frequencies equally spaced along a logarithmic scale, and a blank epoch of median grey to determine baseline. The fade time was 3 seconds to ensure decay of GECI signal between epochs.

2.2.7 Temporal frequency experiments

For temporal frequency experiments, the same direction of drifting sinusoidal gratings were played at a spatial frequency of 0.05 cycles/°. The temporal frequency was sampled equally spaced along a logarithmic scale at seven TFs from 0.15 to 1.5 cycles/second, delivered in a pseudo random order with minimum 3-second fade time.

2.2.8 Pharmacological Experiments

Tg (Isl2b:Gal4;UAS:SyGCaMP3), Et (s1156t:Gal4;UAS:GCaMP5), or Elavl:GCaMP5 fish were imaged using the same settings as described above for orientation experiments. Two orientation tuning experiments were carried out prior to drug injection as a control. Following these controls, immediately prior to imaging, the tectal neuropil contralateral to the eye facing the visual stimuli was injected using an Intracel Picospritzer III (injection settings: 10 PSI, ~15 second pulse) with freshly prepared drug diluted in danieau. The borosilicate needle was cut with a large tip, to dispense a volume of approximately 5.4nl, to facilitate flow. Immediately following this injection, another orientation experiment was carried out on approximately the same cell/RGC axon plane, judged by markers including blood vessels within the neuropil, melanophores in skin around tectum and eyes. A repeat experiment was carried out to ensure the drugs had ample time to diffuse and act. Time series of each orientation experiment were discarded if drift induced by removal from danieau or drug injection had occurred. To control for the injection procedure, danieau solution alone was injected.

2.2.9 Killer Red ablation experiments

Et (s1156t:Gal4;UAS:KillerRed);Elavl:GCaMP5 fish were functionally imaged at 6dpf. Imaging was carried out on three planes through the tectum, one central to the neuropil, and one either side of this by a 7µm step to ensure a large coverage of the dorsal-ventral axis of the tectum. As the average cell body of a tectal cell is approximately 7µm (Sajovic and Levinthal, 1982b), this ensures we did not sample the same neurons more than once. A single orientation experiment was carried out on each plane. Following imaging, the larvae were mounted onto a slide, and exposed to wide field fluorescence (Zeiss Axioskop, Prior Lumen 200, bulb wavelength at 100% strength, wavelength 540-580 nm) for 45 minutes. Larvae were left to recover overnight before imaging again. At 7dpf, the larvae were imaged again at the same planes, with care being taken to match planes as closely as possible, using blood vessels, skin melanophores and distance from central plane of tectal neuropil.

2.2.10 Analysis

2.2.10.1 *Pre-processing of time series data*

All time series experiments were first corrected by realigning using a rigid body algorithm (spm8, http://www.fil.ion.ucl.ac.uk/spm/) to remove artefacts from movement of the larvae

or drift during recording. Median filtering of a kernel size of one voxel was used to remove dark and shot noise. Spatial smoothing with a 2D Gaussian kernel of two voxels to improve signal to noise. Low frequency baseline drifts were corrected using a cubic spline algorithm extrapolating between knots averaged from 5 seconds of interepoch-interval data. Signal intensity changes were calculated at each voxel, and integral responses during the epochs calculated to produce a response value for each experiment epoch. To ensure analysis took into account the properties of the calcium indicators used, probe decay time was included into the pre-processing analysis parameters.

Direction and Orientation selective indices (DSI and OSI (see equation 2-6 below), Niell & Stryker, 2008) were calculated based on fitted von-Mises profiles (Swindale, 1998). DSI and OSI are calculated using responses at preferred angle (R_{pref}), null direction (R_{null}), preferred orientation (R_{pref_ori}), and the orthogonal to this orientation (90° from preferred orientation, R_{orth}).

$$DSI = (R_{pref} - R_{null})/(R_{pref} + R_{null})$$

$$OSI = (R_{pref\_ori} - R_{orth})/(R_{pref\_ori} + R_{orth})$$

$$1\text{-}CV = V = 1 - |R|$$

Equation 2-6: Equations for calculating DSI and OSI, 1-C.V. of cell/neuron responses

An estimate of goodness of fit of the von-Mises curve, R^2, was also calculated. Generally, direction selective responses were determined based on stringent criteria; Direction selective: **DSI > 0.5, OSI <0.5, R^2 > 0.7**; Orientation selective: **DSI < 0.5, OSI >0.5, R^2 > 0.7**. The fitting to integral responses also provides the preferred direction of motion from the centre of the fitted curve.

2.2.10.2 *SIN analysis*

ROIs were limited to GCaMP signal exclusively from SIN cell somas. The mean responses within these ROIs were used to create response profiles for each SIN. For DS experiments, responses to the visual stimuli across all 12 epochs were used to determine the direction selectivity, with a 13th epoch consisting of median grey background.

To classify SINs as either DS or OS, we used the following criteria: **DSI >0.5, OSI<0.5 or CV >0.4, R^2 >0.7**. The 1- Circular variance metric was added to determine if neurons exhibit symmetric tuning, where zero indicates responses to all orientations/directions and one indicates responses to only one direction (Batschelet, 1981). The DSI and OSI metrics can suffer from over-fitting with low signal to noise data as well as limited fitting points that

increases contamination between metrics, thus creating situations where a cell may have both high DSI and high OSI simultaneously (see also Mazurek, Kager, & Van Hooser, 2014).

SINs often exhibited both high DSI and OSI values, and the addition of 1-C.V. allowed us to identify those neurons that were DS. Mean responses were calculated from all the responding voxels within an ROI to ensure that these values were representative of the responses of that neuron.

To derive the number of subtypes of DS or OS SINs, average DS fitted angles were calculated for each SIN soma and plotted on a cumulative histogram summarizing the incidence of cells over binned preferred angles (0–360°). Multiple von-Mesis curves were fitted to cumulative histograms using a multidimensional constrained nonlinear minimization approach, with peak-centre, height, concentration as free dimensions. The bandwidth of the curves was used to define the preferred angle bounds between which the cells within these populations lie. Polar plots were generated of the mean responses of cell's within each of these populations to all 12 angles presented during experiments, with S.D.s also plotted. The bandwidth of each cell's responses was also calculated, this was defined as the full width at the half maximum of the cell's responses to epochs.

SF and TF experiments were analysed in a similar manner, with time lapse images realigned, and ROIs used to determine mean responses across all voxels within a cell soma. Using the integral response plots, we then plot normalised response curves for each population.

2.2.10.3 *Comparative experiments*

Original experiments probing DS populations in RGCs were carried out using synaptically localised GCaMP3, and experiments characterising DS tectal neurons used bulk loaded Oregon-Green BAPTA-1 AM, a fluorescent calcium indicator. To ensure comparisons between SIN and tectal neuron or RGC response profiles are only due to properties of the cells themselves rather than the optical reporters used, the Isl2b:Gal4 promoter line was crossed with a UAS:GCaMP5 line to express cytoplasmic GCaMP5 in RGC axons, and the elavl:GCaMP5 line was used to look at tectal neuron response properties.

Orientation experiments were carried out to determine the DS and OS populations within the RGCs and tectal neurons. Time series experiments were carried out using identical parameters to those used to characterise the SIN properties. DS population differences and individual differences were then compared. Using modified criteria where R^2 threshold was dropped slightly to 0.6, data from all larvae were grouped into a pre-drug and post drug, or

pre- and post-ablation conditions. A slightly lower R^2 threshold was used to ensure that any voxels that became marginally less well fitted after drug application were still included in results after the criteria were applied. All data was analysed using ΔF and responses were normalised to the maximum response size to allow comparison of voxels with different levels of GCaMP expression.

Cumulative histograms of voxel preferred directions were compared between conditions, as well as data on DSI values, bandwidth of responses (using FWHM) and preferred angles. This was used for both SIN drug injection experiments as well as tectal neuron drug injection experiments.

3 CHARACTERISATION OF SINS

3.1 Introduction

At larval stages of development zebrafish larvae exhibit a repertoire of visually-driven behaviours such as prey capture (Bianco and Engert, 2015; Bianco et al., 2011; Patterson et al., 2013) and predator avoidance (Douglass et al., 2008) and are increasingly being used to study the circuitry that underlie these behaviours. Furthermore, because of their small size and transparency they are particularly amenable to imaging-based approaches to study neural circuit structure and function. Zebrafish are also very amenable to genetic manipulation, making them ideal for using genetically-encoded reporters of neural activity, such as GCaMPs to study neural circuitry (Feierstein et al., 2014).

To date most studies have used population functional imaging to describe visually responsive neurons (see Hunter et al., 2013; Nikolaou et al., 2012, for example). While useful for functional categorisation of neuronal subtypes, such population-based approaches cannot be used to describe other aspects of visual circuitry such as the morphology of the individual circuit components. Previous work utilising electrophysiology to characterise the functional properties of tectal neurons did not usually characterise a genetically defined subtype (see Gabriel et al., 2012 for one exception). Furthermore, most studies only focus on one aspect of stimulus selectivity, such as direction (Nikolaou et al., 2012) or size (Preuss et al. 2014, however see Sajovic and Levinthal, 1982b and Bianco and Engert 2015). We know from studies in other organisms that response properties of visually driven neurons are rarely this simple, as they often demonstrate selectivity for multiple attributes of a visual stimulus. (Niell and Stryker, 2008).

In order to gain more insight into tectal circuitry a more detailed description of the individual cell types within the tectum is necessary. This includes neuronal morphologies receptive field characteristics and neurotransmitter identity. Receptive field characterisation provides insight into what visual features might activate a given cell type (and hence what behaviours they might be involved in) while morphology and neurotransmitter identity provides clues as to how a cell type interacts within other components of the circuitry within which it is embedded.

A better functional description of individual cell types in the tectum requires the means to label the same subtypes of neuron in the tectum repeatedly. Previous work has characterised tectal neuron properties using electrophysiology, but these recordings were

often of randomly selected neurons and may not have targeted less common neuron types (Sajovic and Levinthal, 1982a, 1983; Vanegas et al., 1974). The s1156t:Gal4 line (Scott and Baier, 2009) provides the ability to label a subtype of neuron in the tectum, the superficial inhibitory interneuron (SIN). These neurons are set apart from other tectal neurons by their location; whilst the majority of neurons in the tectum are located at a deeper tectal location, within the periventricular layer, SINs have somata located superficially under the skin of the tectum.

I first characterised the numbers of SINs labelled with the *s1156tGal4* transgenic line to determine if the entire SIN population was labelled, or only a subset. Then, in order to describe SIN receptive field properties, this line was crossed with a UAS:GCaMP5 line, to express the genetically encoded calcium indicator (GECI) in SINs. Changes in GCaMP5 fluorescence were imaged on a confocal microscope whilst a drifting sinusoidal grating stimulus was simultaneously presented to the contralateral eye. By systematically changing the direction, spatial and temporal frequency of the stimulus the direction, spatial and temporal frequency tuning properties SINs were described.

The findings presented here suggest that the *s1156tGal4* line labels only a small subset of SINs. Consistent with previous findings I show that this subset contains three different direction selective populations whose preferred directions match those of the direction-selective RGCs that target the tectum (Hunter et al., 2013). However, data presented here demonstrates that the tuning bandwidth of SINs is significantly narrower than that seen in the RGCs. Furthermore, I demonstrate that direction-selective SINs are also selective for high spatial frequencies suggesting that the SIN neurons might only be engaged under specific stimulus conditions such as those that might be encountered during visually guided behaviours reliant upon size discrimination in visual field, such as prey capture, or shoaling.

3.2 Results

3.2.1 The *s1156tGal4* line labels a subset of SINs in the optic tectum

To label SINs the previously published *s1156tGal4* enhancer trap line was used (Scott and Baier, 2009). To determine the extent of SIN labelling in the s1156t:Gal4 line, it was crossed with a transgenic UAS:GCaMP5 line. Double transgenic larvae were fixed at 7dpf and antibody labelled with anti-GFP (to label GCaMP5-expressing SINs) and a nuclear stain (TO-PRO-3, Life Technologies) to visualise cells within the tectal neuropil (SINs are the only identified cell type in the neuropil, TO-PRO-3 labelled nuclei within the neuropil are therefore likely to be SIN neurons). This allowed us to determine the total number of neurons in the superficial neuropil layer in the tectum, and the number of SINs labelled by the *s1156tGal4* line. We found that the labelling in this line is not specific to SINs (Figure 3.1). In the example shown tectal cells within the periventricular layer are also labelled (indicated by yellow arrow), as well as retinal ganglion cell axons.

The data also shows that the line does not label the entire population of SINs, with a mean number of 26 SINs per tectal hemisphere (n = 4 tecta, in 3 larvae), which represents only 10% of all the cell bodies labelled by TO-PRO-3 in the superficial tectal neuropil.

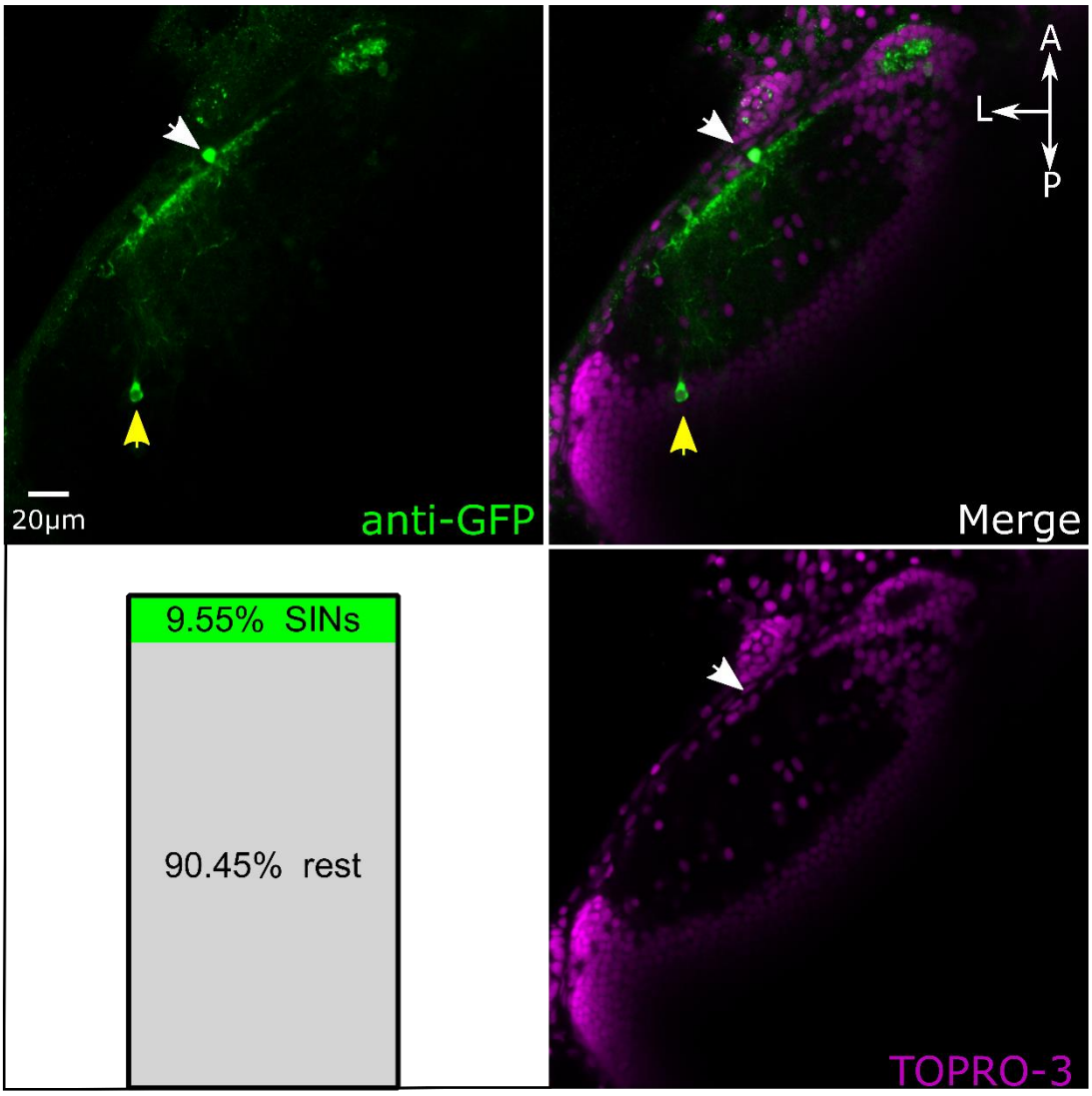

	SINS	Total cells in SO
Average	25.8(±2.287)	270.5(±18.59)

Figure 3-1 Quantification of the labelling of SINs in the s1156tGal4 line

The number of SINs labelled in double transgenic larvae (n=4 tecta) was quantified by expressing the number of SINs labelled by GCaMP5 (green) as a percentage of total numbers of SINs labelled by the nuclear stain TO-PRO-3 (magenta). Scale bar is 20µm. Table average numbers of cells labelled per tectum, ±S.D.

3.2.2 SINs produce robust somatic responses to moving stimuli

To characterise the receptive field properties of SIN neurons the s1156t:Gal4 line was crossed with the UAS-GCaMP5 transgenic line and confocal imaging of SIN somata was used to monitor responses to the drifting grating stimulus. Not all SINs responded to the stimulus. This suggests that the SINs may be functionally diverse or that the visual stimulus did not intersect the receptive fields of all labelled cells. From the data collected, I found the overwhelming majority of visually responsive SINs labelled in this line to be direction selective. Of all 190 visually responsive cells imaged, only eight were orientation selective (Figure 3.2) and 177 were DS. Consequently, I concentrated on characterising the more abundant DS SINs.

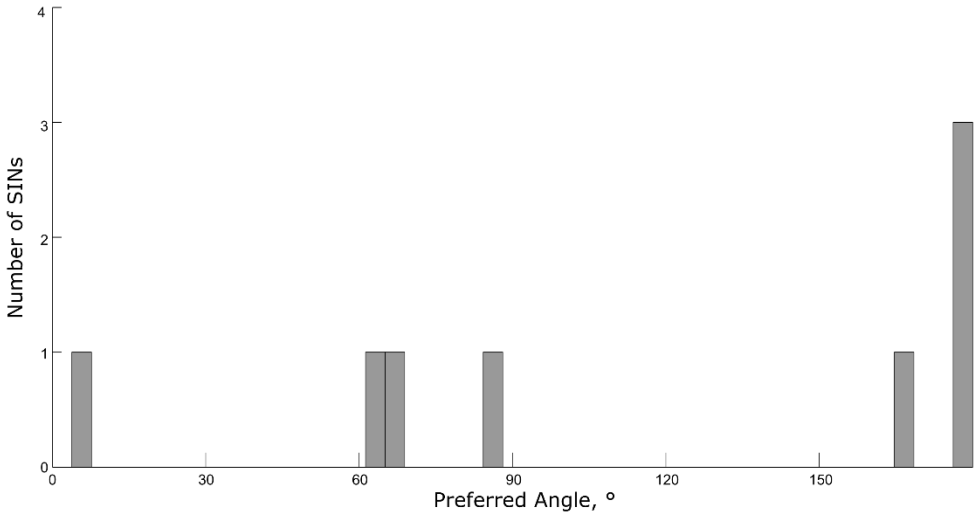

Figure 3-2 Histogram of preferred angles of Orientation selective SINs

n = 8 cells

DS SINs produced robust somatic changes in fluorescence in response to certain directions of moving grating stimuli (Figure 3.3A and B). For each SIN neuron, I determined the preferred angle of motion (see Methods). The polar plot (Figure 3.3C) shows that for this SIN the direction producing the largest integral response is between 120-150°, which relative to the fish corresponds to motion in the ventral/caudal direction with the preferred angle being 140° (Figure 3.3C). This example cell is also highly direction selective, with a DSI value of 0.95 where the maximum possible value is a DSI of 1.0.

Figure 3-3 Response properties of an example direction selective SIN

A. Raw fluorescence changes of a SIN in response to direction tuning experiment stimuli, arrows indicate direction of moving sinusoidal gratings, white dashed line indicates skin covering the tectum, scale bar is 25µm. B. ΔF responses of the same example SIN during the entire experiment. Duration of epochs are indicated by shaded area of graph. Direction of moving stimulus is indicated by red arrow, with null epoch. C. Polar plot indicating the preferred angle of the cell, and DSI value as calculated from responses during the experiment

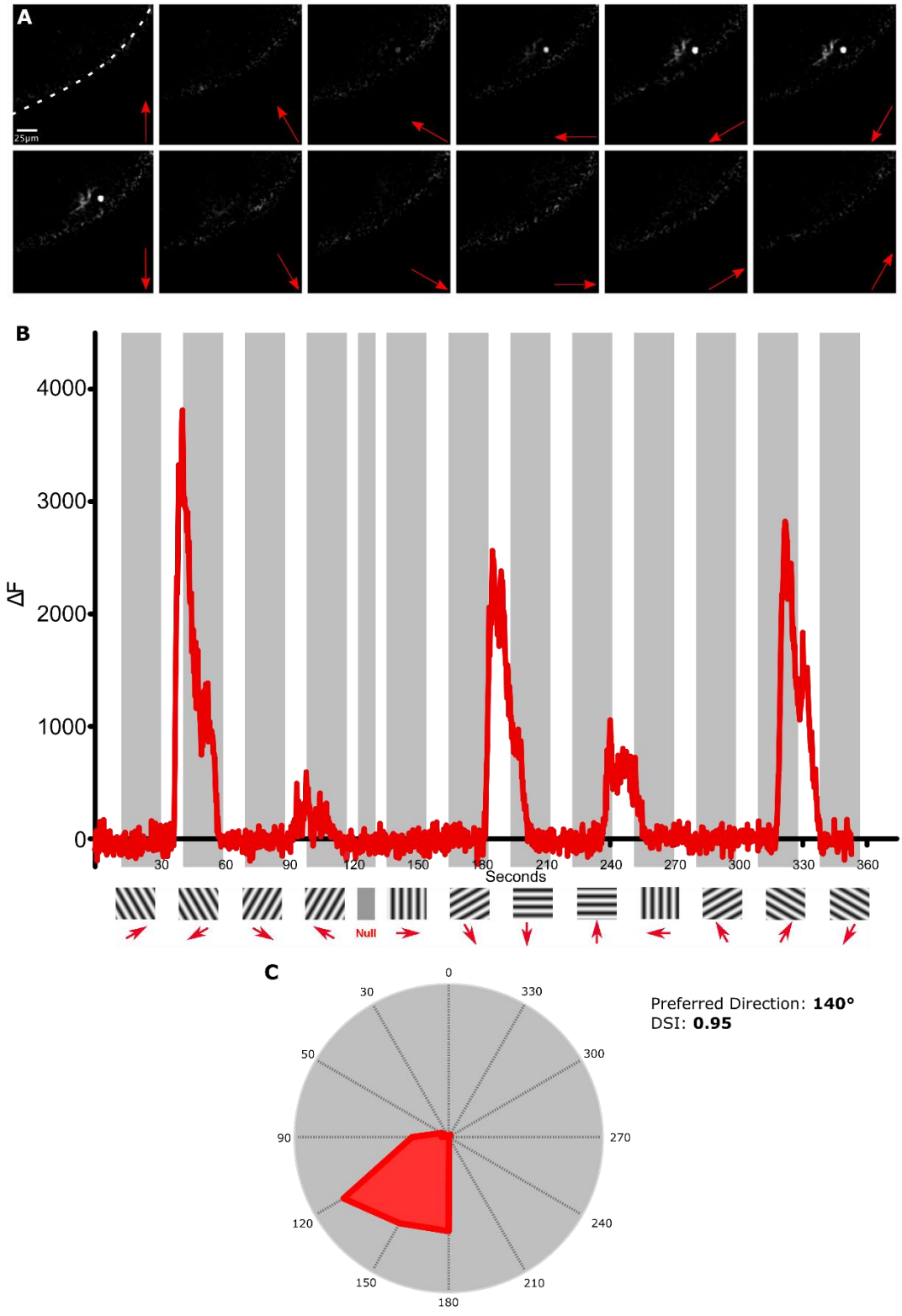

The average DSI value across all DS-SINs was 0.856 (n= 177, S.D. ± 0.1060). From the plot of the DSI values of every DS SIN imaged we can see that many of the SINs imaged had DSI values on the higher end of the DSI scale (Figure 3.4A with error bars indicating ±S.D.). Using the full-width half maximum of the integral responses, I found that DS SINs had a mean tuning bandwidth of 92° (n=177, S.D. 9.233, Figure 3.4B, with error bars indicating ±S.D.).

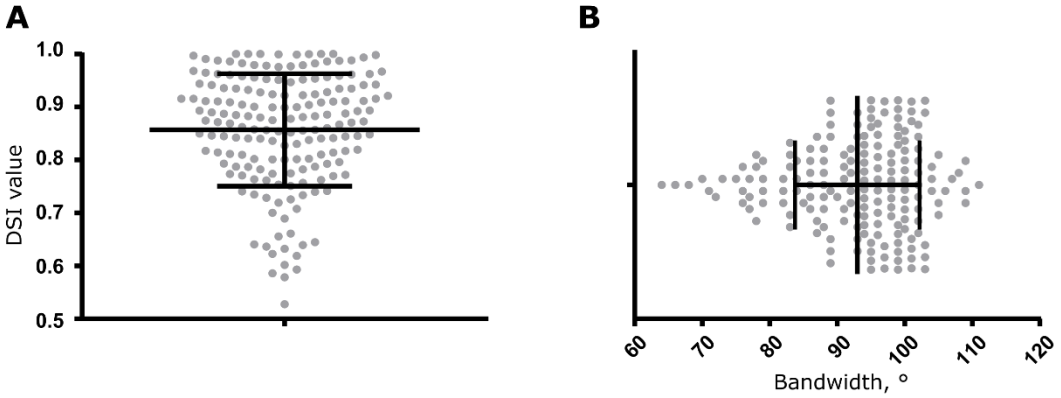

Figure 3-4 DSI values and Bandwidths of all DS SINs imaged

A. DSI values of all DS SINs imaged (n=177, S.D. ± 0.1060, error bars indicate S.D.), all values are >0.5 due to criteria applied for classifying neurons as direction selective. B. FWHM bandwidths (°) of all DS SINs imaged (n=177, S.D. ± 9.233°, error bars indicate S.D.)

3.2.3 The *s1156tGal4* line contains three populations of direction-selective SINs

By plotting the preferred directions of all the responding SINs as a histogram, I aimed to identify from the distribution of preferred directions subtypes of direction-selective SINs. Fitting von-Mises curves to the population histogram revealed three normally-distributed, non-overlapping populations with population peaks centred at 9°, 157°, and 264° (Figure 3.5, upward, downward and forward motion relative to larva, respectively). These populations are similar in preferred directions to those seen in DSGCs and DS tectal neurons.

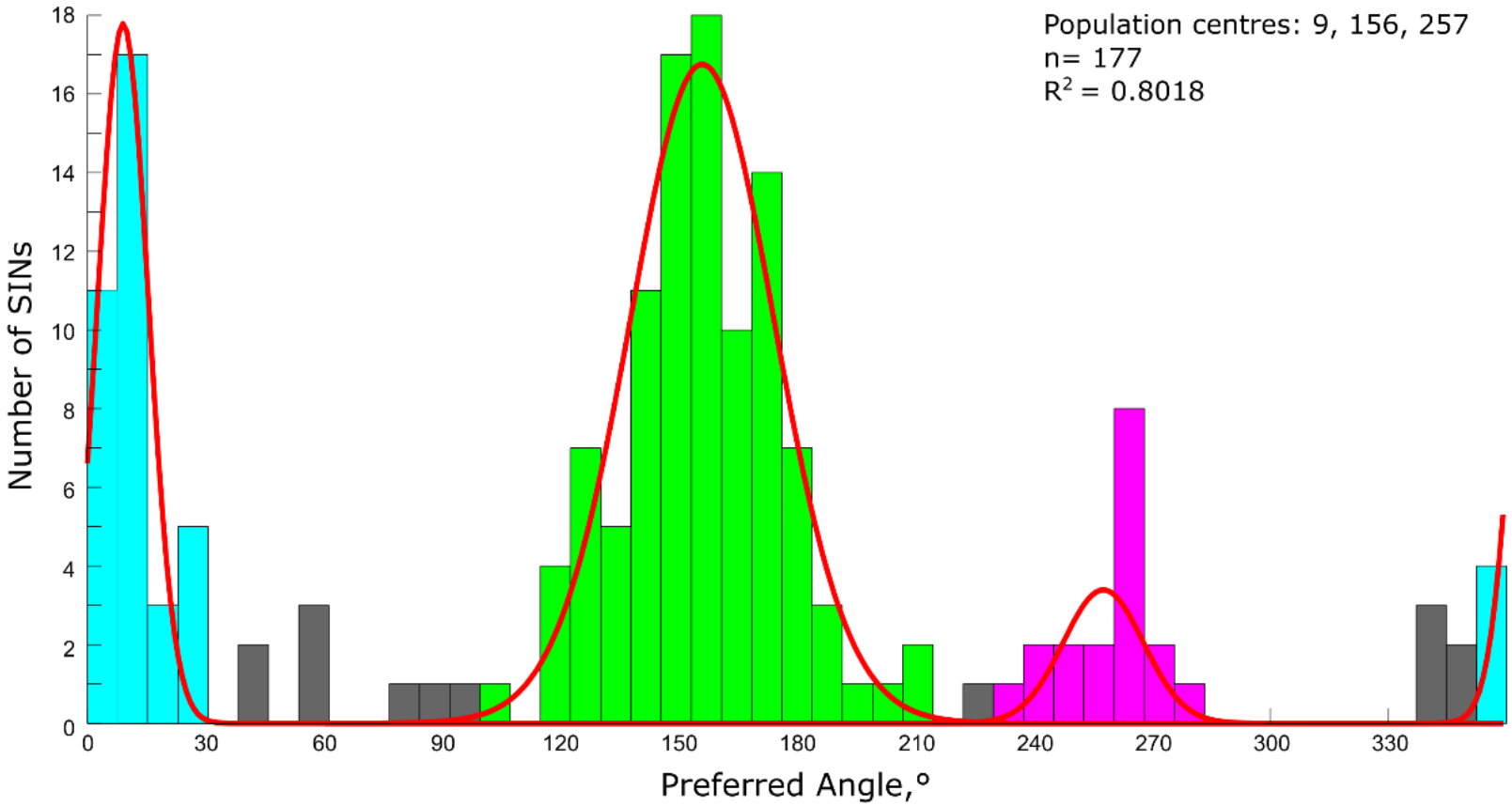

Figure 3-5 Histogram of preferred directions of all DS SINs identified

Population centres of 9°, 156° and 257°, corresponding to upward, downward and forward motion, respectively. Coloured bars indicate neurons within the same subpopulation, n= 177 SINs, R^2 = 0.8018

3.2.4 Tuning properties of direction-selective SIN subtypes

In the above section where DSI and tuning bandwidth of DS SINs were analysed, DS SINs were treated as a single population. The finding that there are three subtypes of DS SIN, separable by preferred angle, raises the question of whether there are subtype-specific differences in DSI and tuning bandwidth. Comparing between the three DS SIN populations we see there are indeed differences in DSI values (Figure 3.6A); the upward population has a mean DSI of 0.91 (SEM ±0.016, n = 23), downward selective population has a mean DSI of 0.86 (SEM ±0.01, n=82) and forward population mean DSI of 0.78 (SEM±0.05, n=9). The differences in DSI between the populations are significantly different between all populations (Figure 3.6A, One-way ANOVA with post-hoc Tukey's multiple comparisons test overall p = 0.0011, up vs down adjusted p =0.0332, up vs forward adjusted p = 0.0010, down vs forward adjusted p = 0.0421).

The upwardly tuned SINs, with a population preferred angle of 9° have a mean tuning bandwidth of 97.26° (SD ±6.36, n = 23), downward-selective SINs with a population preferred angle of 157° have a mean tuning bandwidth of 95° (SD ±6.732, n=83) and forward-selective SINS with a population preferred angle of 264° have a mean tuning bandwidth of 84° (SD ±10.68, n =10). Comparing bandwidths between SIN populations, we see significant differences between the means of all populations (One-way ANOVA with post-hoc Tukey's multiple comparisons test, overall p <0.0001, up vs down adjusted p =0.3360, up vs forward adjusted p<0.0001, down vs forward adjusted p < 0.0001).

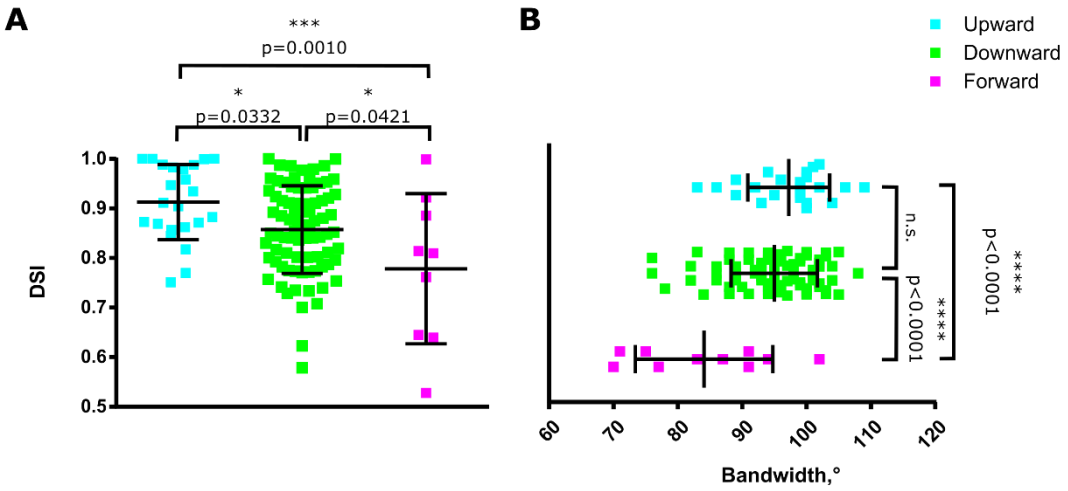

Figure 3-6 Comparisons of DSI and bandwidth values of DS SINs from each population

For each population, upward n = 23 cells, downward n = 82 cells, forward n = 9. A. DSI values of neurons from each DS population, bars indicate mean ± S.D., with statistical significance between populations indicated B. FWHM bandwidths of individual DS SINs split according to populations, bars indicate mean ± S.D., statistical significance between populations indicated. Comparisons using One-way ANOVA and Tukey's multiple comparisons tests

The tuning of each population can be summarised by generating normalized population responses of each DS population, and calculating FWHM based on these responses (Figure 3.7A, FWHM is dashed line). We see that the upward motion sensitive population is much more narrowly tuned than the forward motion sensitive population, and slightly narrower than downward motion sensitive SIN responses (FWHM values of 69°, 83°, 125° for upward, downward and forward populations respectively). This difference in tuning bandwidth between the vertically tuned DS SINs and forward tuned DS SINs is also easily discernible when comparing polar plots of mean integral responses for each population (Figure 3.7B, dashed lines indicate ±2 S.D. of mean population responses).

Comparing the three measures (Table 3-1) the outcomes of comparisons of DSI, and FWHM of population mean normalized responses seems to contradict that of the bandwidths of individual neurons within each population. In general, the upward population is more tuned than the other two DS SIN populations, and the forward responsive population is much broader in its tuning to preferred direction. This agrees with previous data on DSGC responses; however, this data was collected using a synaptically localised GCaMP3.

	Measure			
Comparison	**DSI (p value)**	**Bandwidth (p value)**	**FWHM of population normalized response**	**Conclusion:**
Upward vs. Downward	** (up>down)	n.s. (up=down)	69° vs 83° (+14°) (down>up)	Upward more tuned
Upward vs. Forward	* (up>forward)	** (up>forward)	69° vs 125° (+56°) (forward>up)	Upward more tuned
Downward vs. Forward	n.s.	*** (down>forward)	83° vs 125° (+42°) (forward>down)	Conflicting

Table 3-1 Table comparing differences between three measures used to compare DS tuning of SINs in each population

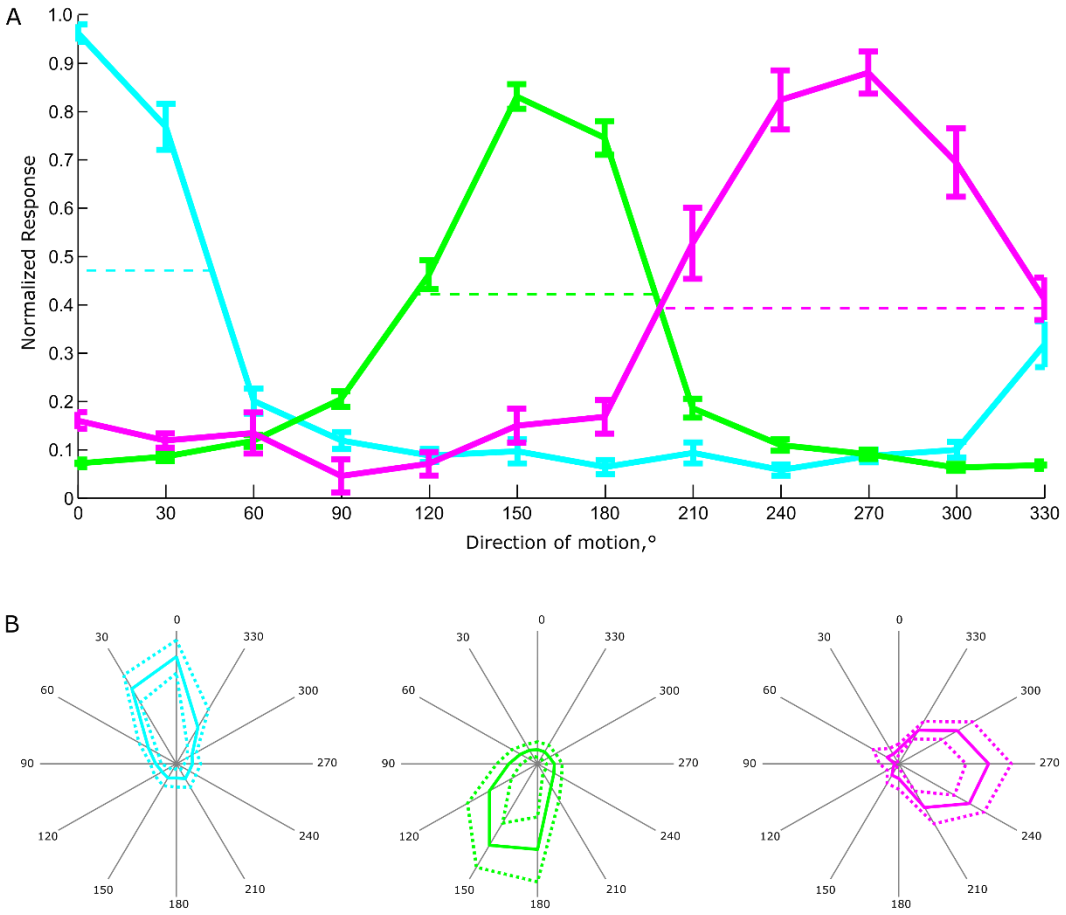

Figure 3-7 Relative differences in tuning to preferred directions of three DS SIN populations

A. Plot of mean normalized population responses to directions of motion presented in experiments, FWHM of responses indicated by dashed lines. B. Polar plots of mean responses of each population, showing distinctly different tuning bandwidths, for reference, 0° corresponds to upwards motion relative to larva, with 90° corresponding to backwards motion.

3.2.5 Spatial frequency tuning of DS SINs

In order to characterise the spatial frequency tuning profiles of DS SINs, gratings of various spatial frequencies were presented. The direction of the grating was matched to the preferred direction of the SIN imaged. This was estimated from the largest response seen during an orientation-tuning experiment that preceded every spatial frequency tuning experiment (see Figure 3.2 B). Initial SF experiments used seven sizes of sinusoidal gratings between 0.014 to 1.5 cycles/° to probe the spatial frequency properties of these neurons. After these initial experiments, we found the range of stimulus sizes covered was too broad and neurons would not respond to stimuli smaller than 0.25 cycles/°. Thus, subsequent experiments covered a smaller range sinusoidal grating sizes (0.5 – 0.014 cycles/°). The largest spatial frequency of stimulus presented was constrained by the dimensions of the display screen used.

Figure 3.8 A shows the result of a spatial frequency tuning experiment performed on a SIN neuron tuned to motion in the downward direction. This clearly demonstrates responses that are selective for certain spatial frequencies.

Figures 3.9 A-C show normalised responses from spatial frequency tuning experiments for each subtype of DS-SIN. These experiments reveal that SINs tuned to upward and downward motion exhibit band-pass filtering (Figure 3.9 A-B), responding to spatial frequencies between approximately 0.2 and 0.014 cycles/°. The two populations appear to have similar spatial frequency tuning profiles, with maximal responses usually between 0.03 and 0.08 cycles/°. This size of stimulus equates to roughly 6.25-16.7° of visual space. However, the upward responding population respond to slightly higher spatial frequencies, equivalent to smaller sizes of stimulus, seen in the rightward shift of plotted integral responses. For the population tuned to forward motion I was only able to perform a spatial and temporal frequency tuning experiment on one neuron. Thus, it is difficult to draw any definitive conclusions about the spatial-frequency tuning properties of this subtype. The tuning curve for this cell indicated that this population may prefer much larger stimuli than was possible to probe using our projector set up (Figure 3.9C).

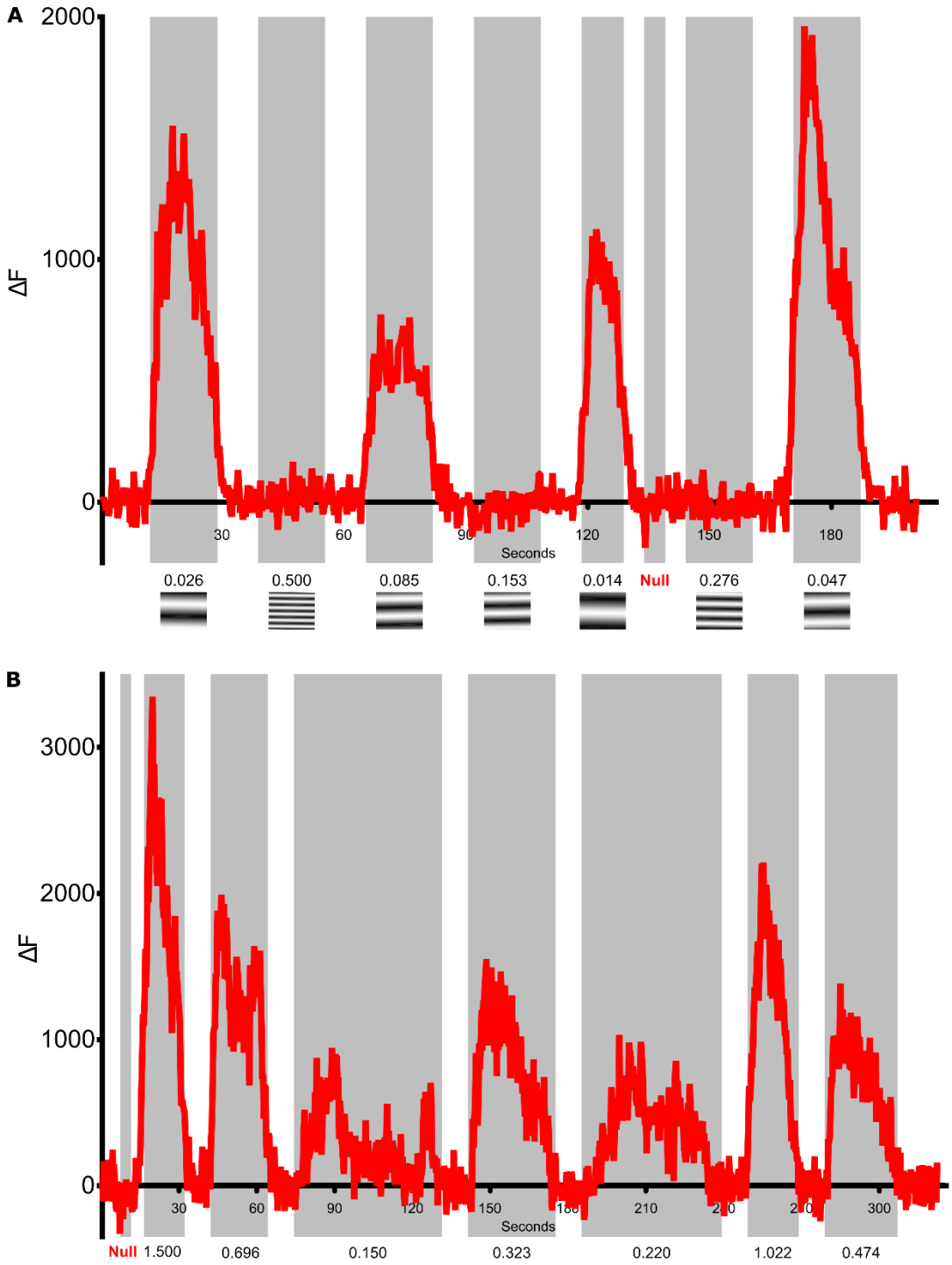

Figure 3-8 Raw responses from example cell to spatial frequency and temporal frequency tuning experiments.

A. Raw responses of example DS SIN from Figure 3.2 to spatial frequency tuning experiment, grey shaded areas on axes indicate duration of epochs with illustrative indications of relative sizes of each spatial frequency (not to scale). B. Raw responses of previous example cell to temporal frequency tuning experiment, grey shaded area indicates duration of epoch.

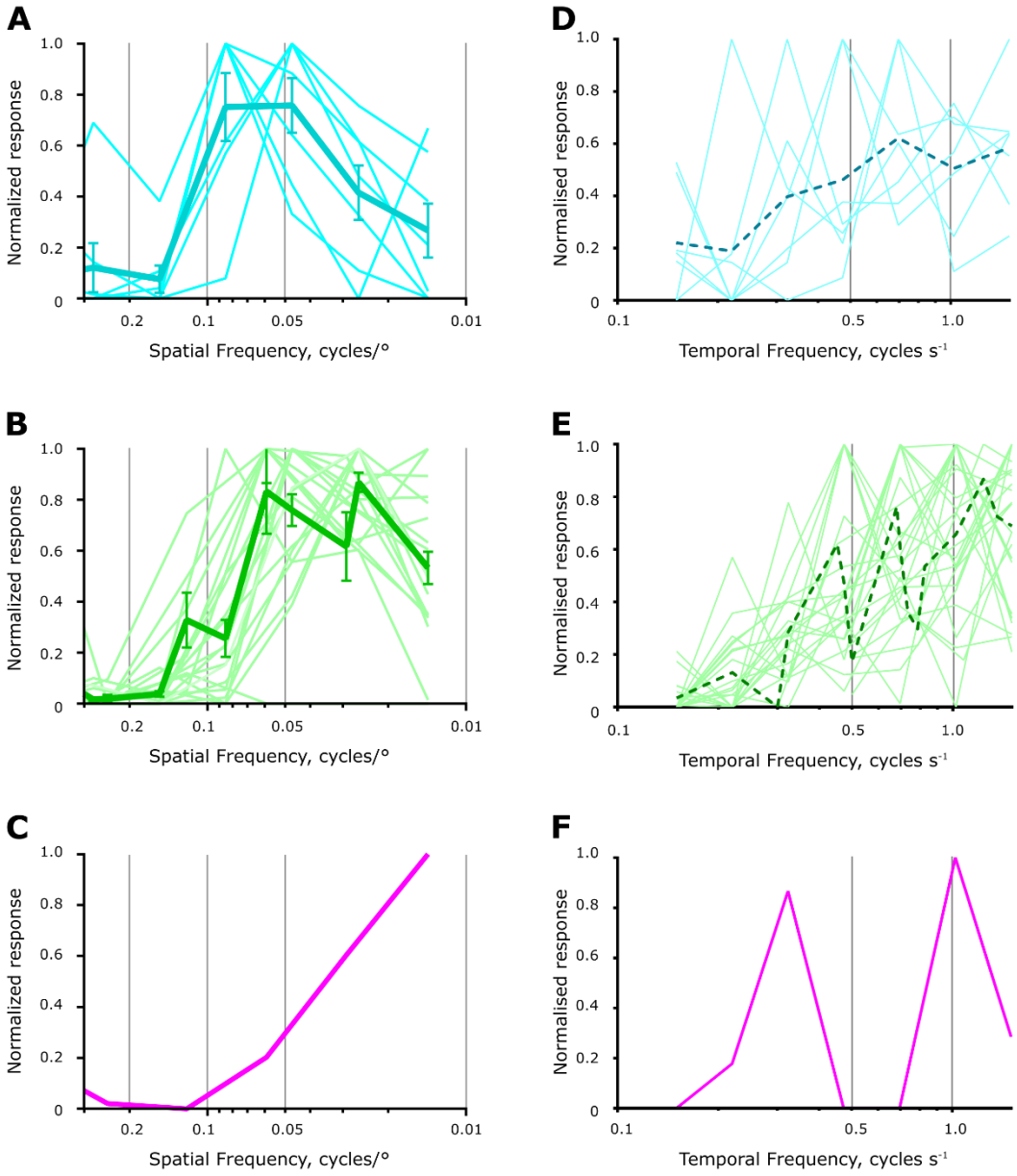

Figure 3-9 DS SIN population spatial and temporal frequency tuning

A-C DS SIN spatial frequency tuning, with normalized responses for neurons within each population plotted, as well as mean responses for entire population (bold plot with error bars, error bars indicate ± S.D.), gratings were presented at preferred angles, with TF of 1.0 cycles s^{-1}. D-F DS SIN temporal frequency tuning, bold dashed lines indicate mean responses of population, presented at preferred angle with SF of 0.05 cycles/°

3.2.6 Temporal frequency (TF) tuning in DS populations of SINs

Using the same direction determined in the DS experiment we then probed the TF tuning of the SINs. From the example cell's raw ΔF plot (Figure 3.8B); temporal frequency produces different amplitudes of calcium increases in response different temporal frequencies of stimuli. From the seven temporal frequencies we presented, we found that SINs do not greatly favour particular speeds of moving stimulus. The general trend of responses indicates that the SINs respond better to higher temporal frequencies, but this is not conclusive from the data (Figure 3.9 D-F).

3.3 Discussion

This quantification of the labelling of SINs in the *s1156tGal4* line shows that this line labels approximately 10% of SINs in the tectum, a fraction of those found in the superficial tectum. However, the data presented here shows that even within the small fraction of SINs labelled in the st1156tGal4 line there is functional heterogeneity- some SINs were orientation selective, others were non responsive to a drifting grating stimulus while many were direction-selective. It is not clear what exactly is being labelled in this line. It may be that the st1156tGal4 line is selective for a few subtypes of SIN and that these are labelled completely in the transgenic line. If this is the case then the full functional diversity of SINs is not captured in this study because we are simply not labelling all subtypes. Alternatively, the st1156tGal4 line may target all subtypes equally but because of mosaicism only a few cells are being sampled. In this case, the subtypes described here may reflect the full diversity of the SIN population. It would be informative to use as many alternative strategies as possible to label SINs so that the full repertoire of subtypes can be captured.

I found a very small number of orientation selective SINs, which is in line with previously published data (Hunter et al., 2013), but I found a strong bias towards DS SINs in the *s1156tGal4* line. Within this subset of DS SINs we determined that there are three DS populations, with population angle centres corresponding to upward (9°) downward (156°) and forward (257°) motion relative to the larvae. These preferred directions of DS SINs match those of DSGCs described elsewhere (Nikolaou et al 2012) indicating that DS SINs receive direct inputs from DSGC axons.

Labelling with OG-B seems to detect different populations of DS SINs (sensitive to backward and upward motion -population centres of 21° and 126°) whilst missing others (the downward and forward DS populations, see Hunter et al., 2013). It is possible that with the bulk labelling calcium transients from SINs are masked by fluorescence in the neuropil, or in the skin, resulting in fewer SINs being detected. Similarly, data from OG-B experiments were using bar stimuli, rather than the sinusoidal gratings used here, this grating stimulus may elicit higher responses in a more diverse range of SINs than bars. Preliminary data comparing individual SIN responses to experiments using bars and gratings did not find a difference in preferred angles or DSI values.

A striking difference between DS SINs and DSGCS is the differences in the relative abundance of directionally tuned DS subtypes. DS SINs responsive to upward and downward directions of motion are labelled more frequently by the s1156tGal4 line than that forward

motion responsive SINs, which is almost completely the opposite to levels of representation of the three directions seen in DSRGCs, which has much greater numbers of forward tuned neurons than upward and downward motion tuned. A key question is whether this difference in representation is real, and thus is because the tectum does not filter information on forward motion from the retina, or is this due to poor labelling of SINs in this enhancer trap line.

Most characterisations of functional properties of tectal neurons focus on only one aspect of visual stimulus, such as size tuning or present a basic stimulus such as small boxes moving along the A-P axis. Our approach, in which preferred direction was used to probe spatial and temporal frequency tuning, is a more comprehensive approach to probing receptive field properties. Visually responsive neurons are often selective for more than one aspect of visual stimulus, and response properties can be different depending on stimuli used (Pearson and Kerschensteiner, 2015; Tikidji-Hamburyan et al., 2015). Thus in addition to direction-selectivity I also examined spatial and temporal frequency tuning of SINs.

I found that all three DS SIN populations showed a preference for moving stimuli roughly equivalent to 6.5° to 16.7° of visual space. In context, these SINs are probably equivalent to 'small' size selective SINs -responding to stimuli between to 2-8° in size (Preuss et al., 2014). Previous studies have found similar sizes of stimulus elicits prey capture (~13.5° moving at ~30°/s) (Bianco et al., 2011), similar to the size of a paramecium (15° moving at 50°/s), the chosen prey of larval zebrafish, when in close proximity to a larva. Because of the extremely low frequency of forward motion sensitive SINs, we only encountered one neuron to carry out spatial frequency experiments on, thus more experiments would be necessary to describe their spatial and temporal frequency properties with sufficient detail.

The disparity in sizes eliciting prey capture behaviours is problematic. In fact, previous work found that moving dark stimuli between the sizes of 1-5° elicit prey capture behaviour; with larger 10° spots eliciting predator avoidance movements at a similar success rate (Bianco et al., 2011). These experiments did not maintain a constant distance of visual stimulus as the stimuli were projected to unrestrained larvae. The distances of objects eliciting successful prey capture responses were on average 1.55mm (±0.66mm) away, but ranged between 0.5 - 3.5mm. The distance of the visual stimulus from the larva could greatly affect the perceived size of the object. The same authors later published what seems like contradictory results in which large (13.2°) dark fast (30°/s) moving spots elicited prey capture behaviour more successfully than small (3.2°) (Bianco and Engert, 2015), these experiments used stimuli at a fixed distance from the larvae (7mm). Moreover, screen

distance from larva used to determine size selectivity in Preuss et al., (2014) was 20mm, where stimuli between 2-8° in size were labelled “small”, and 16-64° were deemed “large”.

This disparity between sizes seen to elicit prey capture is an ideal example of how comparing size selectivity of neurons between experiments is particularly difficult; it indicates that the perception of size is dependent on the absolute size (Douglas et al., 1988). The distance of the presented stimulus and size of stimulus combined provides information on the size of an object to the organism. A large object in the distance will have the same size on the visual field as a smaller object in very close proximity to the animal. As a result, studies on prey capture, for instance, may find that size of stimulus eliciting prey capture may vary greatly depending on the distance of the stimulus from the animal, despite using the same calculation to determine the size of the stimulus on the retina.

Using the insights of the sizes eliciting prey capture in Bianco et al (2015), which provides a link between stimulus size and behaviour, we can make links between the DS SIN stimulus size preferences. The change in distance of stimulus from 1mm to 7mm led to an increase in the stimulus size eliciting prey capture behaviours. As the visual stimuli in this thesis were presented on a screen 30mm from the larvae, with maximal response ranges to visual stimuli ranging between the sizes of 6.25° to 16.7° of visual field (depending on DS population), we can conclude that these are roughly equivalent to prey sized objects in the aforementioned studies.

Temporal frequency tuning experiments were less conclusive, but this is supported by previous work which indicates that responses from neurons selective for stimuli of this size are less sensitive to changes in temporal frequency (Bianco et al 2015). Faster TFs were not utilised originally as preliminary experiments indicated they did not generate responses from DSGCs. Increasing the range of TFs presented is necessary in order to probe the TF tuning of SINs fully.

4 TUNING OF DS SINS RELATIVE TO OTHER DS POPULATIONS IN RETINOTECTAL CIRCUIT

4.1 Introduction

The previous chapter describes the characterisation of the functional properties of DS SINs, and indicates that SINs provide the tectal circuit with inhibition at specific directions of movement, with preference for sizes of small moving objects similar in size to stimuli found to elicit prey capture behaviour (Bianco et al., 2015).

From data collected on the tuning of DS SINs, this subset of neurons appears to have narrower tuning around preferred direction than DS tectal and DSGC populations (Hunter et al., 2013; Nikolaou et al., 2012). However, previously published data on DSGC populations were obtained using Isl2b;SyGCaMP3 expressing larvae in which GCaMP was localised to the presynaptic boutons of RGC axons (Nikolaou et al., 2012), and DS tectal data was gathered using bolus loading of Oregon Green 488 BAPTA-1 AM into larval tecta . In this chapter, I wanted to determine whether the narrower tuning bandwidth of DS SINs is a consequence of the different calcium indicators used in each experiment, or other experimental procedures used, such as stimulus type.

To answer this question the differences in DS tuning between SINs, RGC axons and tectal cells were compared by collecting data on DS populations using the same experimental paradigms, analysis criteria and by expressing the same GECI – cytosolic GCaMP5 - in both RGCs and tectal cells. These experiments are detailed in this chapter. Differences in DS populations and their receptive field properties were analysed by comparing the DSI values, FWHM bandwidths of individual DS neuron responses, and FWHM of the mean response of all neurons in the upward, downward and forward DS populations.

These comparisons between DS SINs, and DSGCs showed that DS SINs are indeed more narrowly tuned to preferred directions than RGCs, finding that DS SINs are more tuned to preferred directions than DS tectal cells. These differences were less evident between forward motion selective populations.

Following this, I wanted to explore the possible mechanisms responsible for this narrowing of tuning in SINs relative to DSGCs and DS tectal cells. Two theories were proposed on how this narrowing is achieved. Either the SINs are intrinsically less excitable neurons, leading all neuronal responses to be much smaller, a so-called “ice berg effect”, or SINs receive inhibitory inputs to non-preferred stimuli thus sharpening their tuning to preferred direction

and reducing responses to non-preferred directions. Because the techniques and equipment to probe the excitability of SINs using electrophysiology were not available, I concentrated on using pharmacological manipulations to determine if inhibition had a role in narrowing SIN tuning.

Thus, GABA-A receptor mediated inhibition was blocked using pharmacology whilst probing the direction selective properties of SINs. The data suggests that SIN tuning is not affected by antagonism of GABA-A receptor mediated inhibition by injection of the drug gabazine. There was little to no difference in DSI values, preferred directions, nor the bandwidths of SINs before and after drug injection when compared to controls in which danieau was injected. Leaving open the possibility that DS SINs have an intrinsic mechanism to reduce their excitability.

4.2 Results

4.2.1 Comparing DS SINs to DSGCs

To determine if there was a significant difference in how tuned the two types of neurons are to their preferred directions I compared the tuning properties of DS SINs in each of the three populations to their corresponding populations in RGCs. In order to have appropriate numbers for statistical analyses it was necessary to take the DSGC population averages per larva imaged rather than voxel numbers when comparing to SIN data. (Analysis of voxel numbers would have produced an inappropriately large N for statistical analyses, i.e. it may have produced statistical significance even when effect sizes are very small).

Isl2b:Gal4;UAS:GCaMP5 transgenic larvae were imaged at 7dpf and responses to moving sinusoidal grating stimulus were used to determine the properties of DSGCs in the tectal neuropil. Histograms of DSGC voxel preferred angles indicate three populations with preferred angles closely matching those seen in previous work using SyGCaMP3 and moving bar stimuli (Nikolaou et al., 2012), with slight differences in population centres that are in line with variability seen between larvae. DSGC population centres at 24°, 131°, and 256° (equivalent to upward, downward and forward motion relative to larva, Figure 4.1A , R^2 =0.98646, total n=10114 voxels from 26 larvae). Relative proportions of each DS population matched those seen in previous work, the largest DSGC population was the forward motion selective 256°, followed by the downward motion sensitive population at 123° and the smallest population at 26° degrees sensitive to upward motion (7946, 138 and 39 voxels respectively). Thus, using cytosolic expression of GCaMP5 instead of SyGCaMP3 in RGC axons does not significantly alter DSGC populations identified in tectum.

One striking difference between DSGC populations and DS SIN populations is the relative numbers of voxels/neurons in each population. The majority of DSGCs are selective to forward motion (270°), whereas this is by far the smallest population in DS SINs. Similarly, the two other DS populations selective for upward and downward motion are the least abundant populations in DSGCs, whereas, proportionally, these are the most common subtypes in DS SINs (Figure 4-1B). However, it is not clear if these relative proportions are a true reflection of all DS SINS because, as shown in Chapter 3, the *s1156tGal4* line used does not label all SIN neurons.

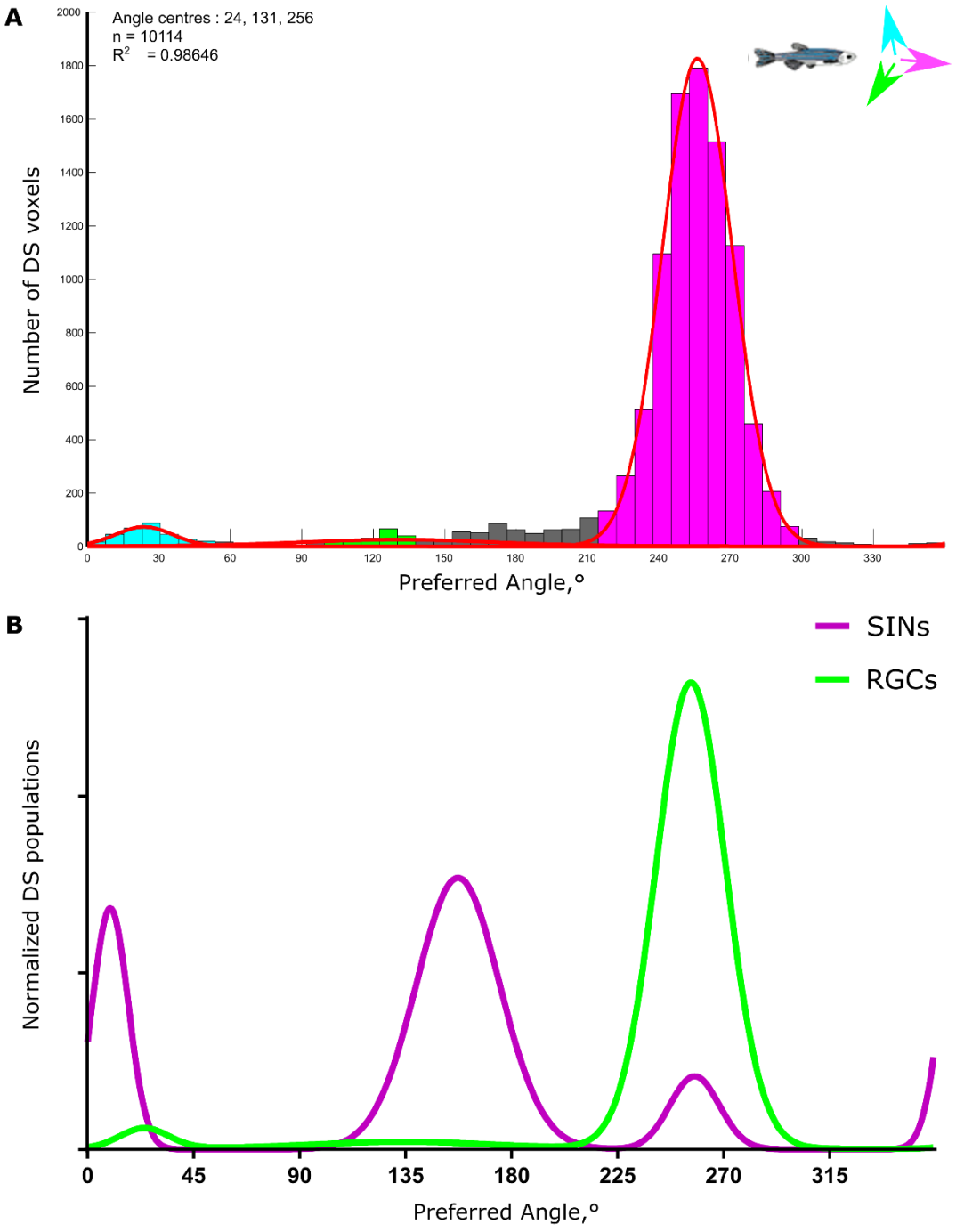

Figure 4-1 DSGC populations found using GCaMP5 are very similar to those obtained using SyGCaMP3 expression

A Histogram of DSGC voxel preferred directions, total n = 10114 voxels in 29 larvae. Three populations with normal distributions are found, with angle centres of 24°, 131° and 256°. B Comparison of DS SIN and DSGC population sizes. DS populations were normalised to total number of DS voxels for RGCs and cells for SINs.

Three measures of the tuning of DS populations were compared: DSI values; FWHM bandwidths of individual neurons; and FWHM of the population mean normalised responses. Plots of the average responses from neurons in each DS population (Figure 4.2 A-C DS SIN responses, A'-C' DSGC responses, mean responses with ±2 S.D. in dashed lines) shows that SINs exhibit much narrower DS tuning than DSGC counterparts. These polar plots show that DSGCs respond to a greater range of non-preferred directions of stimuli than SINs do, indicating that SINs have highly tuned DS properties and generate lower responses to non-preferred directions.

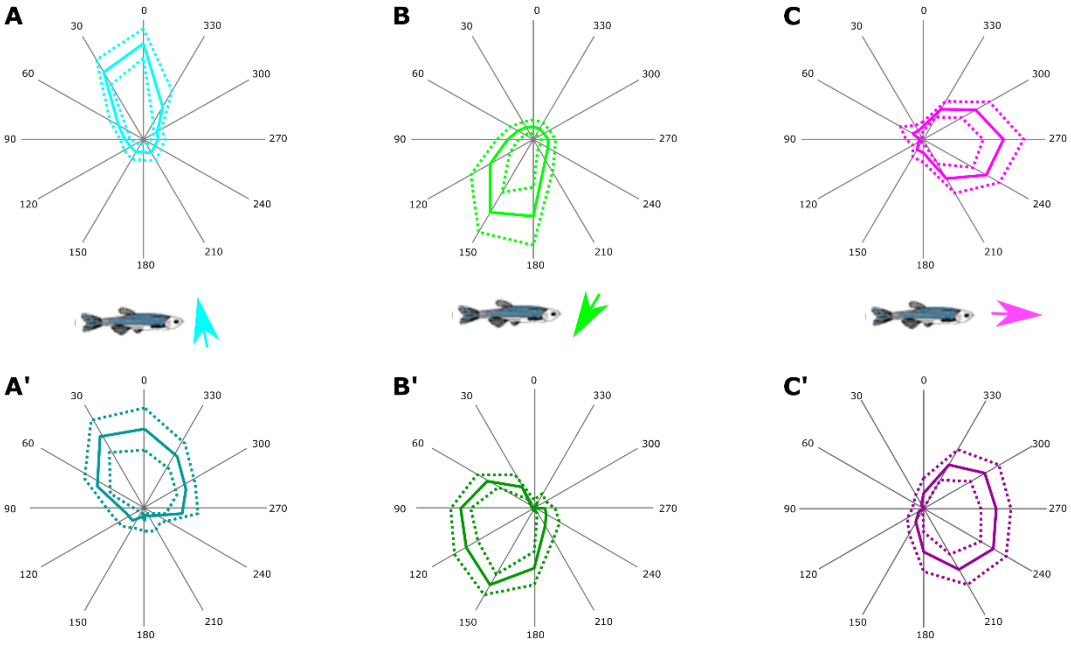

Figure 4-2 Polar plot of mean population responses of DS SINs and DSGCs to each direction of motion presented during experiments

A-C shows each DS SIN population response plot, A'-C' shows respective DSGC response plots. Dashed lines indicate ± S.D. With directions of preferred motion illustrated relative to fish.

DS SINs also have significantly higher DSI values in the two larger populations of upward and downward motion sensitive neurons than in DSGCs (Figure 4.3 A, p <0.0001, and p=0.005 respectively, Unpaired t test with Welch's correction, two tailed). Indeed, the mean DSI value for upward motion detecting RGCs was 0.5994 (±0.1099 S.D., n=11 larvae), compared to that of SINs at 0.9126 (±0.07592 S.D., n=23) and mean DSI value for the downward sensitive population was 0.7207 (± 0.1062 S.D., n=13 larvae) in RGCs and 0.8573 (±0.08842 S.D., n=82) for SINs. The third, forward motion sensitive population was not significantly different in DSI values (mean SINs =0.7782 ± 0.1514 S.D., n= 9, mean RGCs =0.7924, ±0.05596 S.D., n= 26 larvae, p = 0.7900, Unpaired t test with Welch's correction, two tailed).

Comparing the FWHM bandwidths of individual neurons, only SINs in the upward motion sensitive population differ significantly in FWHM bandwidths when compared to RGC counterparts (Figure 4.3 B , p= 0.0011, Unpaired t test with Welch's correction, two tailed). Both forward and downward motion sensitive DS SINs and RGCs had very similar mean FWHM tuning bandwidths (Figure 4.3 B, p=0.8009, RGC n= 11 larvae, SIN n= 23; p=0.2962, RGC n=13 larvae, SIN n = 82 respectively, Unpaired t test with Welch's correction, two tailed).

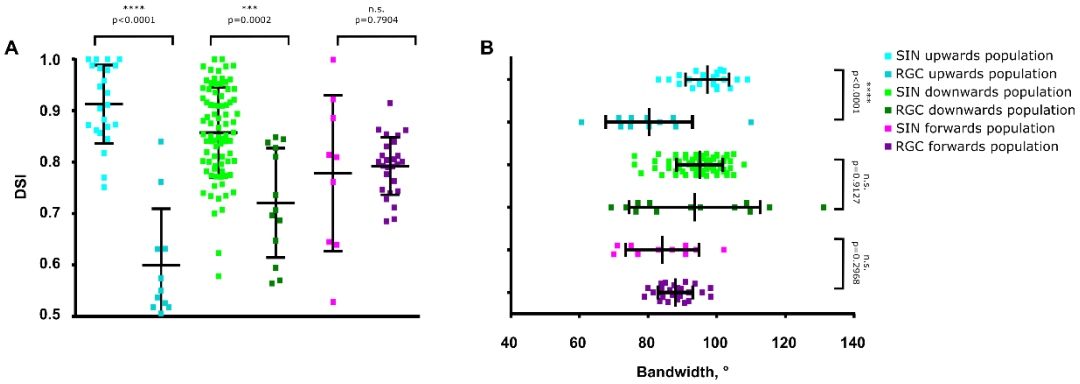

Figure 4-3 Comparisons of DSI values and FWHM bandwidths of each DSGC and DS SIN population

A. DSI values of each DS SIN neuron and mean DSGC DSI value per larva, B. FWHM bandwidths of each DS SIN neuron and mean DSGC bandwidth per larva imaged. Error bars indicate mean ± S.D, two-tailed Unpaired t test with Welch's correction were used for all comparisons. Significance of differences are indicated. DS SINs upward n = 23 cells, downward n = 82 cells, forward n = 9 cells, DS RGC upward n = 11 larvae, downward n = 13 larvae, forward n = 26 larvae.

The third measure used to determine differences in tuning to preferred angles was the FWHM of the mean normalised responses of neurons in each DS population (Figure 4.4- A-C, FWHM indicated with dashed horizontal lines). This comparison gives an indication of the tuning of each DS population as a whole (rather than on the cell-by-cell/fish by fish basis as above). DS SINs responding to upward motion, for instance, have a FWHM of mean normalized responses of 69°, whereas upward motion responding RGCs have a FWHM of

107°, a difference of +38°. The downward selective DS SINs showed much larger differences in FWHM, with RGCs having a FWHM of 155° compared to only 76° in the DS SINs, a difference of +79°. As expected, the forward motion sensitive DSGCs and SINs had larger FWHM values, 125° in SINs and 156° in DSGCs, a difference of 31°.

The population responses to each direction of motion (i.e. each epoch of the stimulus set) were also compared between RGCs and SINs to identify if there were significant differences. Responses to the epochs between SINs and RGCs in the upward and downward motion sensitive populations were significantly different in amplitude (Figure 4.4 A and B, epochs with significant differences indicated, multiple t tests using Holm-Sidak method with alpha=5.000%, error bars indicate S.D., upward RGCs n = 74, upward SINs n=23, downward RGCs n=195, downward SINs n=83).

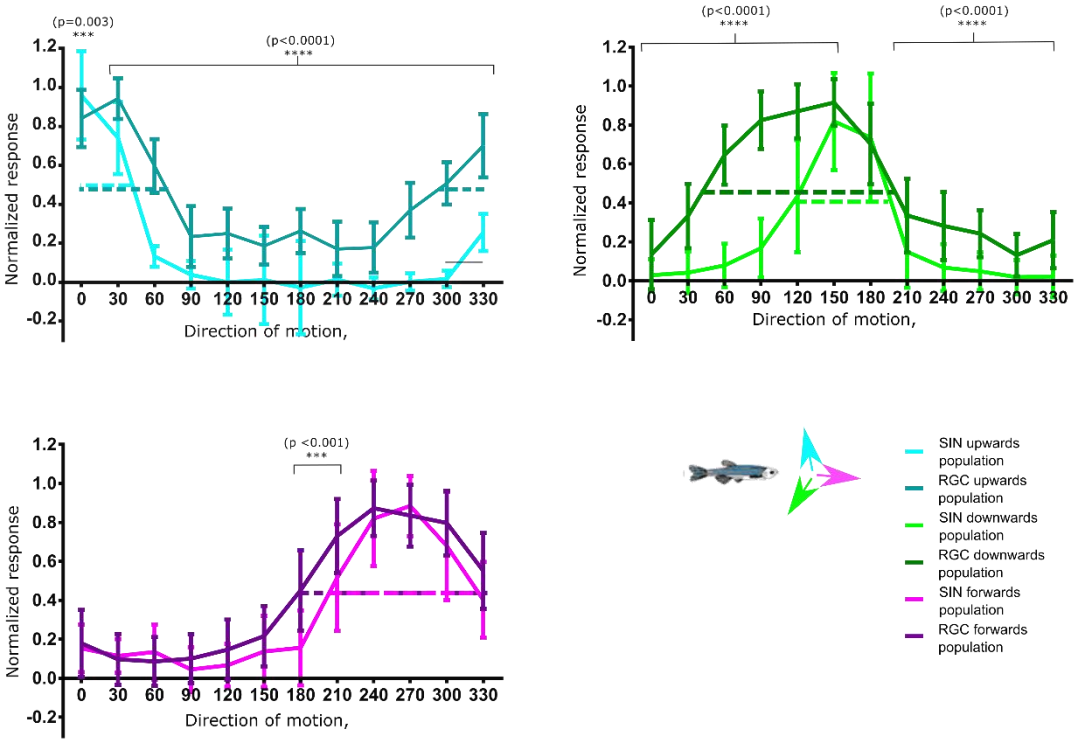

Figure 4-4 Population mean normalized responses of DSGCs and SINs in each of three DS to each direction presented in experiments

Error bars indicate ±S.D., dashed lines indicate FWHM bandwidth for average response of whole population. Significant differences in response sizes indicated by p values above each point as determined by multiple t tests with Holm-Sidak correction.

Summary of tuning bandwidth differences between DSGCs and DS SINs

I compiled an overview of the tuning differences between DS SINs and DSGCs using all three above measures (Table 4-1). When comparing the differences between each of the measures, it appears that the FWHM values generated for each individual cell and voxel does not agree with the DSI values nor the population FWHM. Both DSI values and FWHM of population mean normalised responses appear to agree on the level of tuning of RGCs and SINs, indicating that there is a difference in tuning between RGC inputs and SINs.

Population:	**Measure:**								
	1: mean FWHM, °			2: DSI value			3: FWHM of mean population responses, °		
	SINs	RGCs	Difference (RGC - SIN)	SINs	RGCs	Difference (RGC – SIN)	SINs	RGCs	Difference (RGC - SIN)
Upward	97	80	-17	0.91	0.60	-0.31	69°	107°	+38°
Downward	95	94	-1	0.86	0.72	-0.14	76°	155°	+79°
Forward	84	88	+4	0.78	0.79	+0.01	125°	156°	+31°

Table 4-1 Summary table of differences in measures of tuning to preferred angles between DS SINs and RGCs

Red text indicates differences supporting narrower SIN tuning compared to RGCs.

4.2.2 Comparing DS SINs and DS tectal neurons

Having found that SINs exhibit narrower DS tuning than DSGCs, we then compared SIN tuning to DS tectal cells expressing GCaMP5, to determine if SINs also exhibit narrower tuning than DS tectal cells. As reported previously in Hunter et al., 2013, plotting preferred directions of DS cells onto a histogram produces four coherent populations of DS tectal neurons form (Figure 4.5 A), three have preferred directions almost matching those of RGCs but the fourth tectal population has a preferred direction centred around 90°, equivalent to backward motion relative to the larva (Figure 4-5B). This fourth population is also observed when using pan neuronal GCaMP5 expression.

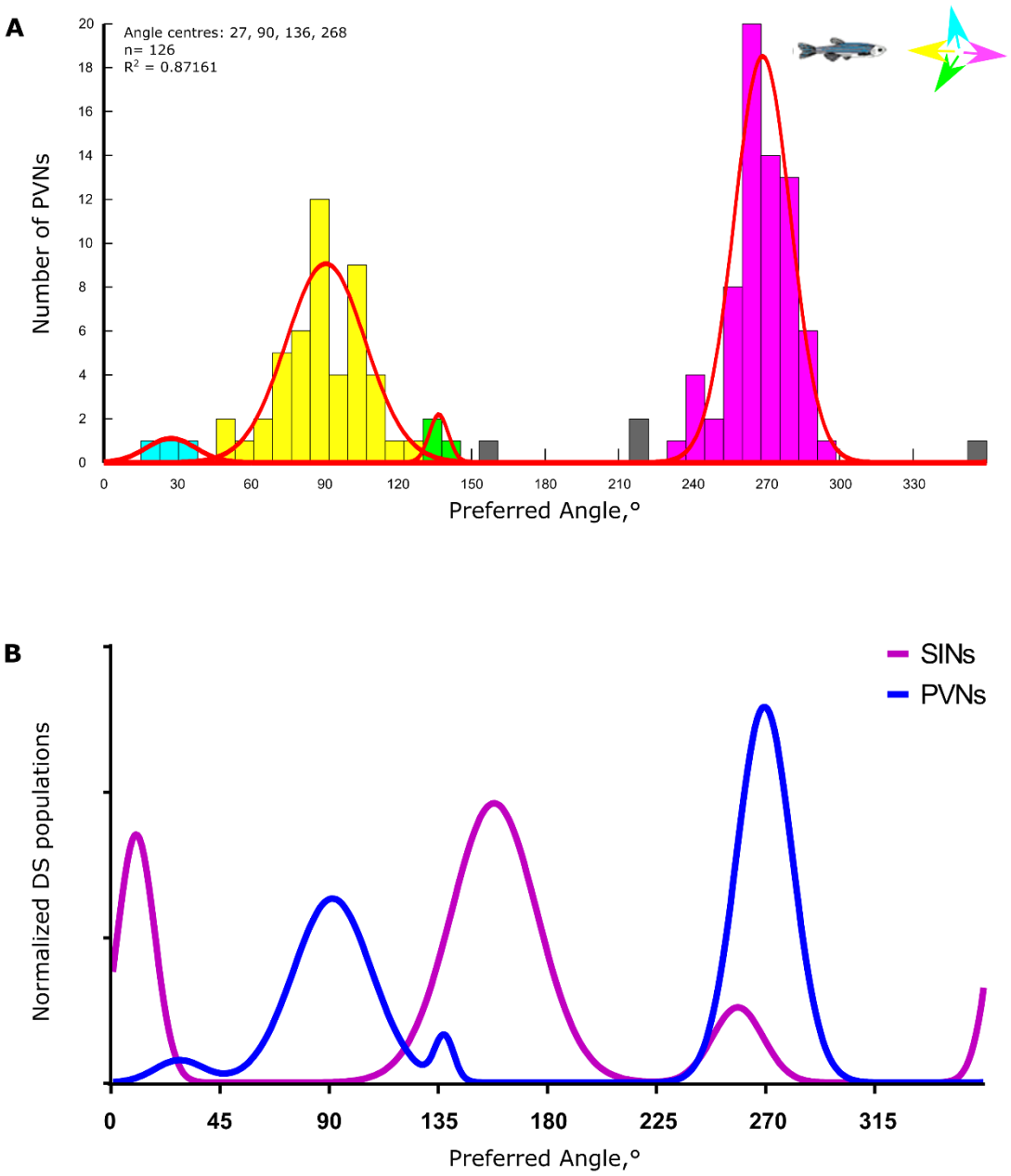

Figure 4-5 DS tectal neuron populations identified using GCaMP5 are very similar to those identified with bulk calcium indicator labelling

A. Histogram of DS PVN voxel preferred directions, total n = 126 tectal neurons. Four populations with normal distributions are present, with angle centres of 27°, 90°, 136° and 268°, R^2 of 0.87161. B. Comparison of DS SIN and DS tectal neuron population sizes. DS populations were normalised to total number of DS neurons

Polar plots of DS SIN and tectal cell responses show the population responses to each direction presented during DS tuning experiments, (Figure 4.6, DS SINs A-C, DS tectal cells A'-C', with D showing responses of the backward motion selective tectal population not present in DS SINs, dashed lines indicate ± S.D.). To quantify the differences in tuning, three measures were compared.

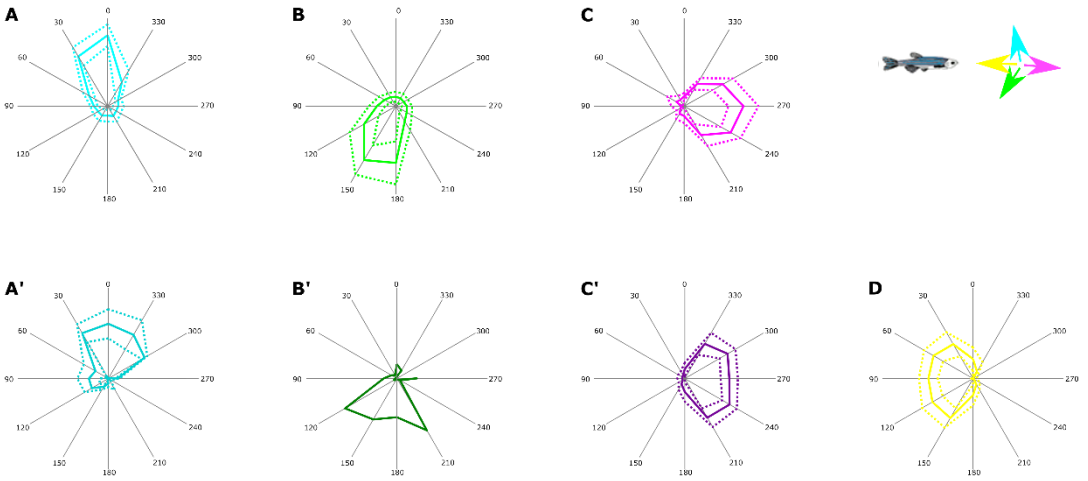

Figure 4-6 Polar plot of mean population responses to each direction of motion presented during experiments

A-C shows each DS SIN population response plot, A'-D' shows respective DS tectal neuron response plots. Dashed lines indicate ± S.D. Plot D' shows mean population responses of backward motion responsive PVNs not found in DS SINs

Comparing the DSI values of neurons within each tectal and SIN population, SINs have higher DSI values compared to tectal cells (Figure 4.7 A). The mean DSI value for SINs in the upward population of SINs is 0.9126 (±0.07592 S.D., n=23) whereas in tectal cells of the same population it is 0.8218 (± 0.02616 S.D., n=2). The mean DSI value for SINs in the downward motion sensitive population is 0.7207 (± 0.1062 S.D., n=13), slightly higher than the only tectal cell within the same population with a DSI value of 0.6958. Due to the relative scarcity of tectal cells in the upward and downward motion responsive populations, the two largest populations of DS SINs, it is impossible to make statistical comparisons. The forward motion responsive SINs (mean DSI 0.7782, ± 0.1514 S.D., n= 9) had broadly similar DSI values to that of tectal cells (mean DSI 0.8520, ± 0.06941 S.D., n=47) of the same DS population, although again the lack of SINs in this population makes statistical tests difficult.

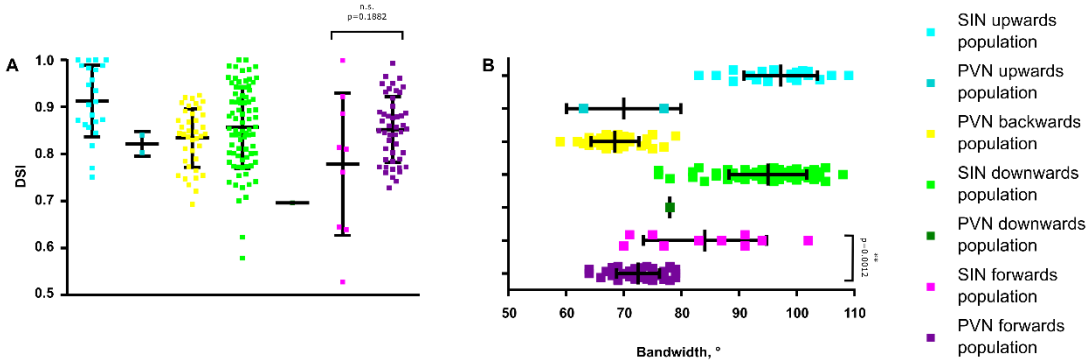

Figure 4-7 Comparisons of DSI values and FWHM bandwidths of each DS SIN and tectal neuron population

A – DSI values of each SIN neuron and mean tectal neuron DSI per larvae. B – FWHM bandwidths of each DS SIN neuron and mean tectal neuron bandwidth per larvae imaged.

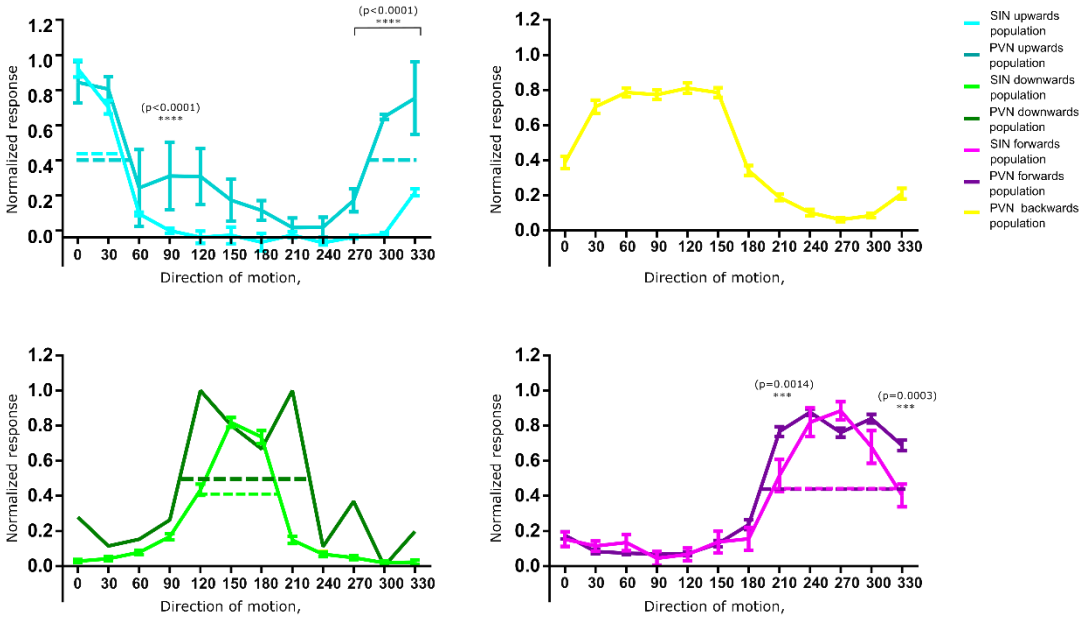

Figure 4-8 Population mean normalized responses of DS SINs and PVNs in each of three DS populations to each direction presented in experiments

A. upward motion sensitive B. emergent DS population in tectal neurons responding to backward motion, C. downward motion sensitive, D. forward motion sensitive neurons. Error bars indicate ±S.D., dashed lines indicate FWHM bandwidth. Significant differences in response sizes indicated by p values above each direction as determined by multiple t tests with Holm-Sidak correction

To compliment DSI as a measure of tuning to preferred angles, the FWHM bandwidths of responses from DS SINs were compared to their counterparts DS populations in tectal cells. As seen with DSGCs, it appears that tectal cells are more narrowly tuned than SINs in all three populations (Figure 4.7 B). This difference does not reflect the differences seen in tuning from polar plots of average responses (Figure 4.8 A-C, A'- C'), which indicates that DS SINs are more narrowly tuned than DS tectal cells.

In an attempt to bring a consensus on whether tectal cells are less tuned to preferred angles, a third measure to quantify tuning to preferred angles was used, FWHM of the mean normalized responses of the population. The FWHM of plots of mean normalized responses of cells, or voxels, within each DS population were calculated. Using this measure, tectal cells have larger FWHM values than SINs in all three DS populations (Figure 4.8 A-C). Upward motion responsive tectal cells had a FWHM of 94°, compared to 69° in the corresponding SIN population, a difference of +25°. Downward responsive tectal cells had a FWHM of 121°, compared to 76° in SINs, a difference of +45°, and the forward responsive tectal cells had a FWHM of 136° compared to 125° in the SINs, a modest difference of +11°. All three indicate that SINs have narrower in response tuning to preferred angle than tectal cells.

Summary of differences between DS SINs and DS tectal neurons

Population	Measure:								
	1: mean FWHM, °			2: DSI value			3: FWHM of mean of normalized responses, °		
	SINs	tectal cells	Difference (tectal - SIN)	SINs	tectal cells	Difference (tectal - SIN)	SINs	tectal cells	Difference (tectal - SIN)
Upward	97	70	-27	0.91	0.82	-0.09	69°	94°	+25°
Downward	95	78	-17	0.86	0.69	-0.17	76°	121°	+45°
Forward	84	72	-12	0.78	0.85	+0.07	125°	136°	+11°

Table 4-2 Summary table of differences in measures of tuning to preferred angles between DS SINs and tectal cells

Red text indicates differences supporting narrower SIN tuning compared to DSGCs

Comparing all three measures used to quantify the level of tuning the SINs and tectal cells had to their preferred angles, the DSI values and the differences between FWHM of the mean population responses both indicate that DS SINs are more tuned to preferred direction than DS tectal cells, with the FWHM bandwidths of individual neurons contradicting this (Table 4-2).

4.2.3 Effect of antagonising GABA-A Receptor mediated inhibition on SIN tuning

To investigate whether the narrow tuning of SIN DS responses is shaped by inhibition, GABA-A receptors were antagonised in the optic tectum by injection of gabazine into the neuropil, and differences in SIN DS properties were measured. Because of the relative scarcity of labelled SINs in the *s1156tGal4* line responses from the same SINs could be compared pre- and post-drug injection with confidence.

To ensure that the injection settings used to disperse drug into the tectum were sufficient to diffuse to the superficial layers of the tectal neuropil and act on SINs, APV and NBQX was injected into the tectum to block excitatory signalling (NMDA and AMPA receptor antagonists). Following injections SINs were not responsive to visual stimuli.

Danieau was injected into the tectal neuropil to determine what effects the injection procedure itself had on DS SIN tuning properties. Preferred direction ($p = 0.1465$, Wilcoxon matched-pairs signed rank test, two tailed, n=13), bandwidths ($p=0.2087$, Wilcoxon matched-pairs signed rank test, two tailed, n=13) and mean normalized integral responses ($p>0.05$ for all points, multiple t tests using Holm-Sidak method with alpha=5.000%, n=13)

are not significantly altered by the process of injection into the tectal neuropil (Figure 4.9 A,B,D). However, there was a significant increase in DSI values between pre and post injection conditions (Figure 4.9 C, p=0.015, Wilcoxon matched-pairs signed rank test, n=13). There was also one case in which a SIN 'flipped' its preferred direction by approximately 180°, it is not clear why this may be the case, it is possible that in this one example a SIN in very close proximity was mistaken for the original neuron post injection.

Because SINs were matched pre- and post-injection, the integral responses to different directions of motion could be compared directly to determine if danieau injection altered the integral response amplitude. Because the downward direction selective population of SINs is the most abundant, only the integral responses from neurons in this population were compared. The mean integral responses pre and post injection were not altered by injection of danieau (Figure 4.9 E, downward direction selective SINs, for all directions p>0.05, multiple t tests using Holm-Sidak method with alpha=5.000%, n=7, population mean integral responses in bold black and bold red, individual neuronal integral responses in lighter shades of grey and red). These data suggest that, for the most part, the injection procedure itself had no effect on SIN tuning or response amplitude.

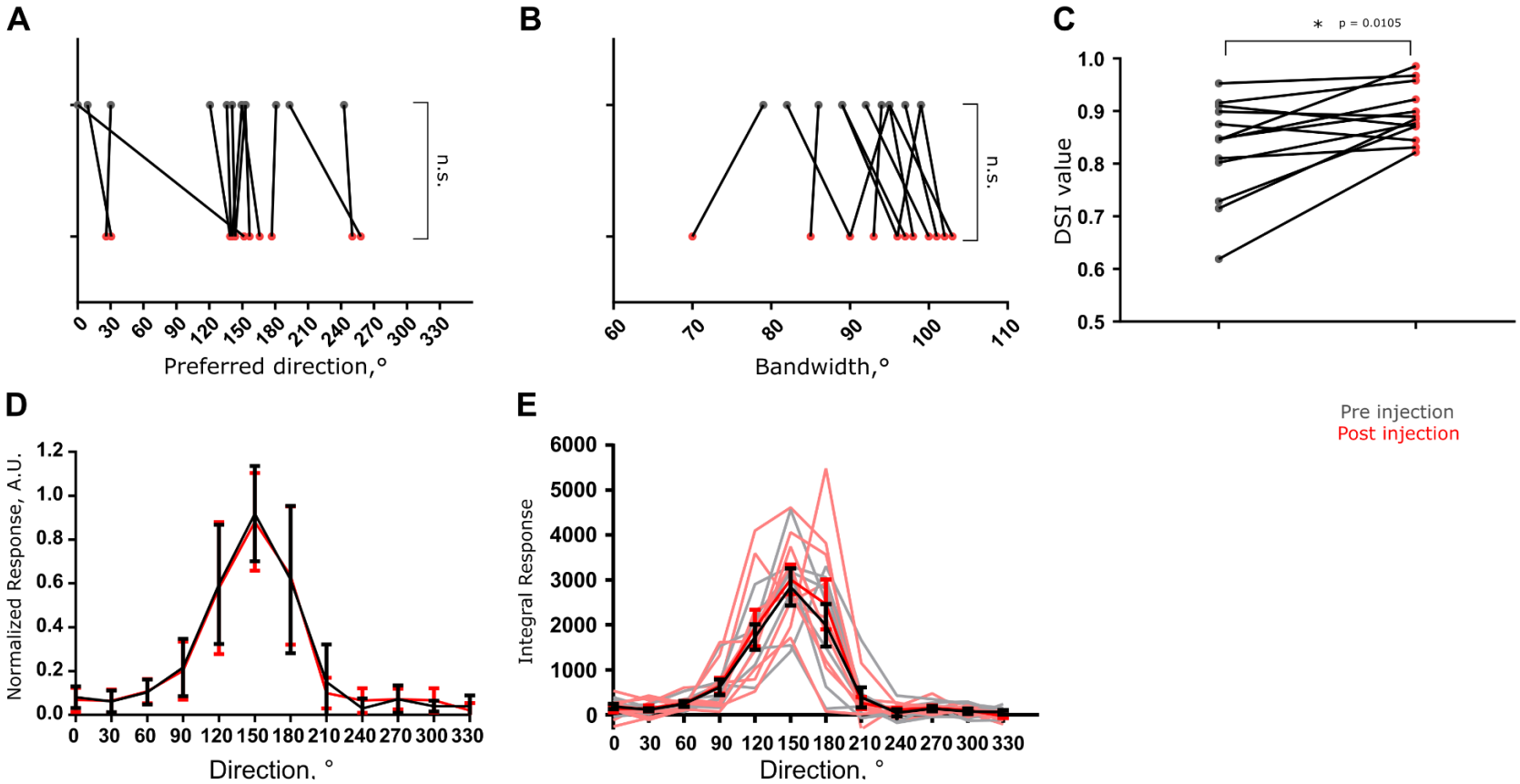

Figure 4-9 Danieau injection into neuropil has no discernible effect on DS SIN properties, except DSI.

Pre- injection indicated in grey, post injection in red. A. SIN preferred directions before and after danieau injection p >0.05 , B. SIN FWHM bandwidths before and after danieau injection, p = , C- SIN DSI values before and after injection of danieau, p = 0.00105, D. no change in normalized responses of SINs in downward motion detecting population before and after danieau injection, error bars indicate ±S.D. p >0.05 all points, multiple t tests using Holm-Sidak method, E. no change in integral responses of SINs selective for downward motion after danieau injection, error bars indicate ±S.D., p >0.05 all points, multiple t tests using Holm-Sidak method

Having identified the unwanted effects of microinjection of volumes into the tectal neuropil, the GABA-A receptor antagonist Gabazine was injected into the tectum and effects on DS SIN tuning properties were recorded. Perturbing GABA-A receptor mediated inhibition did not affect the properties of DS SINs significantly. There was slight variation in preferred angles, though these differences are not significant (Figure 4.10 A, p= 0.7353, Wilcoxon matched-pairs signed rank test, two tailed, n=39), as with control injections, there were four cases of 'flipped' preferred directions in SINs after drug injection.

Differences in bandwidth of DS tuning were also not significant (Figure 4.10 B, p = 0.2155, Wilcoxon matched-pairs signed rank test, two tailed, n=39), as well any changes in DSI values (Figure 4-10 C, p = 0.2357, Wilcoxon matched-pairs signed rank test, two tailed, n=39). Interestingly, there was no significant difference in DSI values after gabazine injection, which appears to contradict the increase of DSI values seen after control injections.

As expected, the majority of SINs observed were of the two more abundant DS populations, responsive to upward and downward motion. Thus, the mean normalized responses of neurons in these populations were compared to determine if the tuning of responses was altered. No significant changes in the mean normalized response plots of either population were found (all p >0.05, multiple t tests using Holm-Sidak method with alpha=5.000%, n=6 for upward population, n=39 for downward population). The raw integral response plots of neurons pre and post drug injection were compared to determine if more subtle changes to the amplitude of SIN responses occurred after gabazine injection. There were no significant differences in SIN responses in the largest population represented the downward DS population, (Figure 4-10 F, p > 0.05, multiple t tests using Holm-Sidak method with alpha=5.000%, n=13), nor the upward DS population (Figure 4.10 E, p > 0.05, multiple t tests using Holm-Sidak method with alpha=5.000%, n=39).

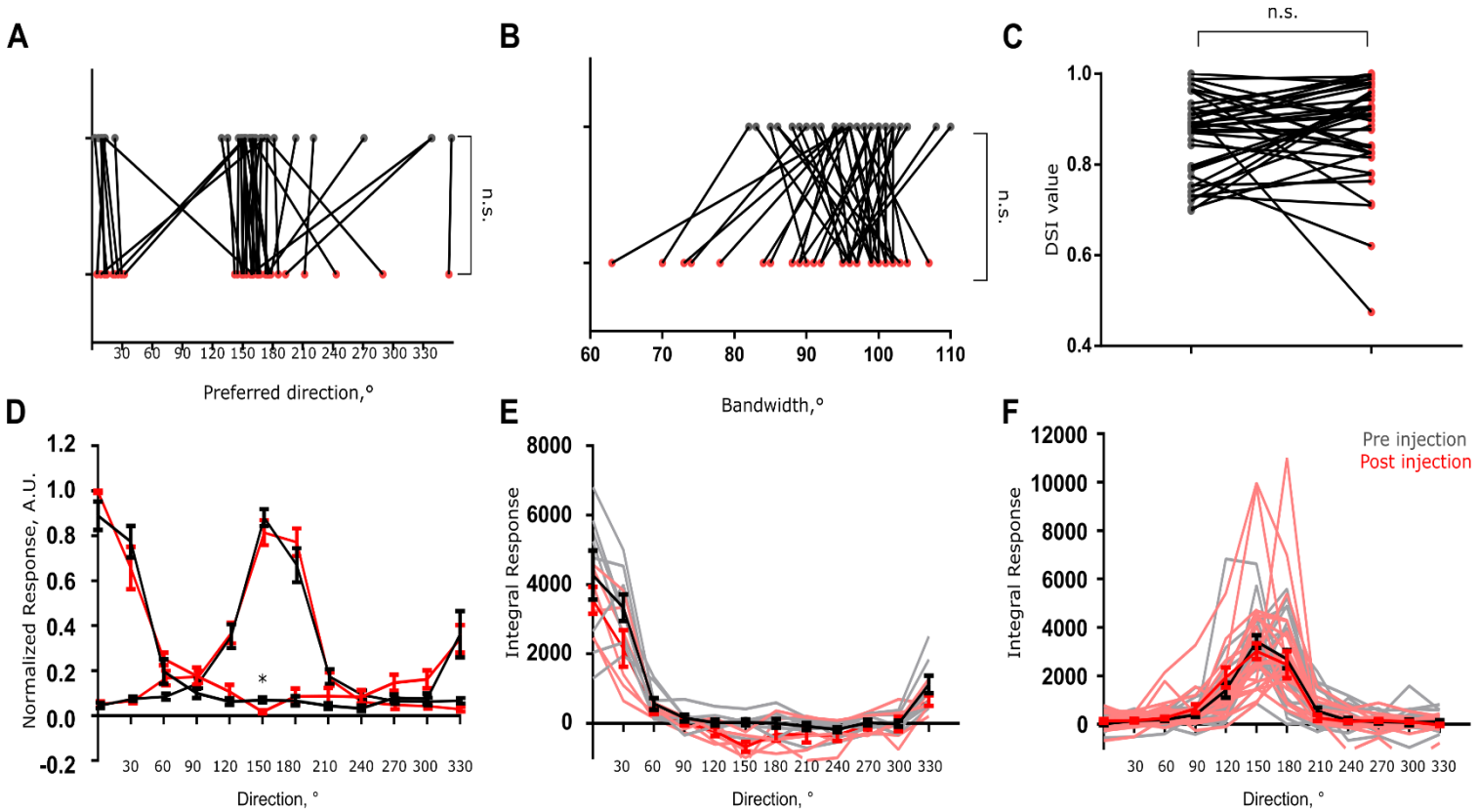

Figure 4-10 Gabazine injection into neuropil has no discernible effect on DS SIN properties.

Pre- injection indicated in grey, post injection in red. A. SIN preferred directions before and after danieau injection p >0.05 , B. SIN FWHM bandwidths before and after danieau injection, p >0.05 , C. SIN DSI values before and after injection of danieau, p = 0.00105, D. no change in normalized responses of SINs in downward motion detecting population before and after danieau injection, error bars indicate ±S.D. p >0.05 multiple t tests using Holm-Sidak method, E. no significant change in integral responses of SINs selective for upward motion after danieau injection, error bars indicate ±S.D. , p > 0.05 all points, multiple t tests using Holm-Sidak method. F. no significant change in integral responses of SINs selective for downward motion after danieau injection, error bars indicate ±S.D. , p >0.05 all points, multiple t tests using Holm-Sidak method

4.3 Discussion

Functional imaging of RGCs and tectal neurons expressing GCaMP5 reproduces DS populations seen in Nikolaou et al., (2012) and Hunter et al., (2013), both studies using different calcium indicators. DS SINs labelled by the *s1156tGal4* line have preferred angles almost matching that of DSGCs, indicating that DS properties of SINs are inherited from RGC inputs. When compared to tectal cells expressing GCaMP, SINs also have very similar DS populations, with the sole exception of the 90° backward motion selective tectal population, a DS emergent population in the tectum. SINs seem to have opposing proportions of neurons in each DS population compared to tectal cells and RGCs, having very few forward motion selective neurons, and larger numbers of upward and downward selective neurons. It is difficult to say whether this difference in DS proportions is the actual representation of directions of DS SINs, or whether this is a consequence of the sparse labelling in the *s1156tGal4* line used to characterise these neurons. The pan-neuronal GCaMP5 line, *HuCGCaMP5*, could have been used to determine if this proportion was due to the selective labelling in the *s1156tGal4* line, however, it was found that SINs are not labelled in this line (data not shown). In *HuCGCaMP5* larvae, obvious cell-sized areas without GCaMP5 expression are present in the superficial tectum, where SINs are normally found. Thus to determine if this SIN data is representative of SINs as a whole would either involve bulk labelling of SINs using Oregon-Green BAPTA-AM, or the use of another transgenic line known to label SINs, such as *Oh:GCaMP6s* (Preuss et al., 2014).

The comparison of DS SINs and DSGCs responses indicates that DS SINs do exhibit narrower tuning of responses and that differences were not due to the type of GECI used to probe these responses, nor any differences in experimental protocol. Similarly, DS tectal cells are less tuned to preferred direction than DS SINs. This indicates that if SINs do indeed receive their input from RGCs then they narrow their tuning relative to their inputs from the retina.

Two different mechanisms were proposed for this narrow tuning, either SINs receive inhibitory inputs tuned to non-preferred angles, thus reducing or preventing responses to non-preferred direction excitatory inputs, or that DS SINs have an intrinsically lowered excitability, thus only responding to higher levels of excitatory inputs i.e. the preferred direction of motion. Determination of excitability of SINs would require the use of electrophysiological recording in vivo whilst presenting stimuli, a technique not readily available in the lab. Thus, efforts were concentrated on using pharmacological manipulation to examine if inhibition causes narrowing of DS SIN tuning compared to putative inputs.

The primary source of this inhibition could have been mediated by ionotropic GABA-A receptors, so this receptor was pharmacologically perturbed whilst SIN DS tuning properties were probed. Injections of Gabazine, a GABA-A receptor antagonist, into larvae expressing GCaMP5 in SINs did not alter any of the properties of DS tuning of these SINs. The exception was four SINs whose preferred angle appeared to 'flip' approximately 180°. Control experiments using danieau injections, however, also generated a 'flipping' of DS preferred angles in one cell. Thus, it is possible that this 'flipping' is caused by the injection of volumes of liquid into the tectum.

Whilst it appears that these results support the theory that the narrower DS tuning of SINs is not mediated via inhibition from other tectal neurons, there are several problems with this experiment. For instance, the use of Gabazine to perturb GABA-A receptor mediated inhibition. A particular problem with blocking of GABA-A signalling is that it is known to induce seizures in neural tissues, producing large waves of excitation. In an attempt to block GABA-A receptor activity whilst maintaining the ability to measure changes to neuronal responses with GECIs preliminary experiments were carried out where concentrations of Gabazine were titrated to the point at seizures were infrequent in larvae. Consequently, it was found that a gabazine concentration of 10μM produced little to no seizure activity in larval tecta. In very few larvae this concentration produced seizures in the tectum when injected, which I assumed was an indication that the concentration of drug was still sufficient to prevent GABA-A mediated inhibition, and that these larvae were slightly more prone to seizures than others were. Several other studies have used this concentration to mediate GABA-A receptor activity blocking in cell culture (Soiza-Reilly et al., 2013). There was no way of quantifying if this concentration of drug was sufficient to prevent GABA-A mediated inhibition in whole animal injections, and several other studies injected Gabazine into tissues at much higher concentrations (Auferkorte et al., 2012; Tabor et al., 2008). Without having the ability to prevent GABAergic signalling without inducing seizures, that the concentration of drug used was insufficient cannot be ruled out.

Ideally, the efficacy of the Gabazine concentration would be tested in a few tectal neurons by electrophysiological recording of inhibitory inputs onto neurons. A distinct absence of inhibition after injection would indicate the concentration was appropriate. An alternative control experiment to indicate if the gabazine concentration was sufficient, would be to observe the effects of Gabazine on a direction or orientation selective neuron in the tectum whose response properties were known to be in part produced by GABA-A mediated inhibition (Grama and Engert, 2012). Several other studies utilised another GABA-A receptor antagonist, Bicuculline, at varying concentrations (Del Bene et al., 2010; Ramdya and Engert,

2008; Sajovic and Levinthal, 1983), this drug however has reported non GABA receptor activity and for this reason was not used in this experiment.

It is possible that the SINs create an 'iceberg' effect with their responses to moving stimuli at non-preferred directions being insufficient to bring SINs to their firing threshold, once above this threshold of activation SINs are activated strongly. This would also not have been reflected in changes in integral responses of SINs after drug injection. Further, the differences in DSI values between SINs and DSGCs and tectal cells may be a result of this intrinsically higher required level of activation. Ideally, recording responses from SINs using electrophysiology whilst presenting visual stimuli would allow the probing of SIN excitability. Similarly, this would indicate if SINs receive inhibitory inputs. The potassium ion conductance of the SINs could be manipulated to alter resting membrane potential, changing the intrinsic excitability of the neuron, thus if SIN tuning changed after manipulation this would indicate this narrow tuning could be via an intrinsic mechanism rather than derived from inputs.

5 THE ROLE OF SIN MEDIATED INHIBITION IN TECTAL CIRCUITRY

5.1 Introduction

Results described in chapters three and four demonstrate several things, firstly that the response the *s1156tGal4* line labels a DS SIN subpopulation. These DS SINs have preferred angles almost matching those seen in RGC inputs to the tectum and exhibit band pass spatial frequency tuning to moving stimuli. Secondly, in chapter Four it was demonstrated that SINs are more narrowly tuned to preferred directions than DSGC inputs and DS tectal neurons, and that this sharpness of DS SIN tuning is not dependent on GABA-A receptor mediated inhibition.

A key question that remains is what the role of direction selective inhibition has in the tectal circuit? Whereas most neurons in the tectum have somata located in the periventricular layer (PVL), medially in the larval brain, SINs have very superficial and laterally located somas, directly above the tectal neuropil, and DS SIN populations almost mirror DSGC populations. In the tectum, information flow occurs from the superficial to the deeper layers of the neuropil, with lateral information processing (Kinoshita et al., 2002). I hypothesised that SINs were superficially localised in order to carry out lateral inhibition to shape the DSGC outputs in the tectal neuropil.

In this chapter, I tested the hypothesis that inhibition shapes the tuning of DSGCs, tectal neurons or both. In order to address this question DS tuning properties in RGCs and tectal neurons were measured before and after pharmacological and genetic perturbation of inhibition in the tectum. Inhibition was perturbed by injection of pharmacological blockers of GABA receptor function into larvae expressing GCaMP5 whilst RGC DS outputs were measured, comparing DS populations, bandwidths, and DSI values before and after addition of drug.

To probe the role of SIN mediated inhibition within the tectal circuitry, GABA inhibition was perturbed in two ways. The first was blanket perturbation of GABA mediated inhibition from all neurons in the tectum through the injection of drugs that modify GABA receptor function the neuropil. These included gabazine (GABA-A receptor antagonist), Baclofen (GABA-B receptor antagonist) and CGP-54626 (GABA-B receptor agonist). By injecting these drugs directly into the tectum of larvae with pan neuronal expression of GCaMP5 (*HuC:GCaMP5)* and observing the changes to DS tuning, the effect of inhibition could be analysed.

As blanket perturbation of inhibition does not provide information on the specific role SIN derived inhibition provides in the circuit a more selective method for perturbing inhibition was used. SINs were ablated in the tectum using the genetically encoded KillerRed protein (Bulina et al., 2006; Teh et al., 2010). Expressing the KillerRed fluorophore under the control of the *s1156tGal4* promoter line in larvae expressing pan-neuronal GCaMP5. This pan neuronal labelling with GCaMP5 allowed us to measure the changes to tectal activity before and after ablation of DS SINs, providing a more accurate representation of the role DS SINs have in processing in the tectal circuitry. Whilst the numbers of SINs labelled with *s156tGal4* is not the complete population of SINs in the tectum, it labels a subpopulation of DS SINs, with the two largest populations responding to upward and downward motion.

Results suggest that SIN-mediated inhibition does not modulate tuning of DSGC in the tectal neuropil, and that the DS response properties of RGCs in tectal neuropil are a result of processing undergone in the retina. Similarly, it was also found that inhibition does not have a role in the generation of DS tectal neuron responses, as both pharmacological and genetic perturbation of inhibition did not significantly alter DS tectal neuron populations and response properties.

5.2 Results

5.2.1 Determining the effect of inhibition on DSGC tuning

The superficial location of SINs indicates that they could be providing pre-synaptic inhibition to RGC axons. To determine if presynaptic inhibition is modulating DSGC outputs in the tectal neuropil, GABA receptor modulating drugs were injected into *Isl2b:Gal4;UAS:SyGCaMP3* expressing larval zebrafish and differences in DS responses pre- and post-drug injections were compared. Several different drugs were used to modify signalling in the tectal neuropil; Gabazine a GABA-A receptor antagonist, CGP-54626 a GABA-B receptor antagonist, baclofen a GABA-B receptor agonist, APV/NBQX a drug combination inhibiting in AMPA/NMDA receptor activity, and a control danieau injection.

GABA-A receptor mediated inhibition is ionotropic, whereas GABA-B receptors are metabotropic, it was predicted that perturbation of GABA-B receptor mediated inhibition would affect RGC response properties if pre-synaptic modulation is involved shaping of their responses in the neuropil, as these are the receptors that are usually found in pre-synaptic terminals.

Danieau injections were carried out as a control to determine the effect injection into the tectal neuropil had on response properties. The mean number of visually responsive voxels per larva did not change significantly after injection (Figure 5.1 A), however the standard deviations indicate that there is a great variability in voxel numbers between larvae. The slopes of the cumulative frequency plots indicate that there is little difference in DS voxel preferred directions (P.D.s) before and after injection. Voxel bandwidths were used as a measure of how tuned DS voxels were to preferred angles, and mean DS voxel bandwidths were unchanged after danieau injection (Figure 5.1 B). Comparing DSI values for voxels in the three DS populations, there is a decrease in upward responsive voxel DSIs, and slight increase in forward responsive DSI values (Figure 5.1 C). The mean normalised responses of DS voxels in each population before and after drug injection to identify any changes in response properties. Normalised responses to the 12 directions of motion presented did not change after drug injection (Figures 5.1 D and E). These results demonstrate that injection of danieau injection alone does not significantly alter response properties of DS voxels, beyond the variability in DS voxels already present between larvae.

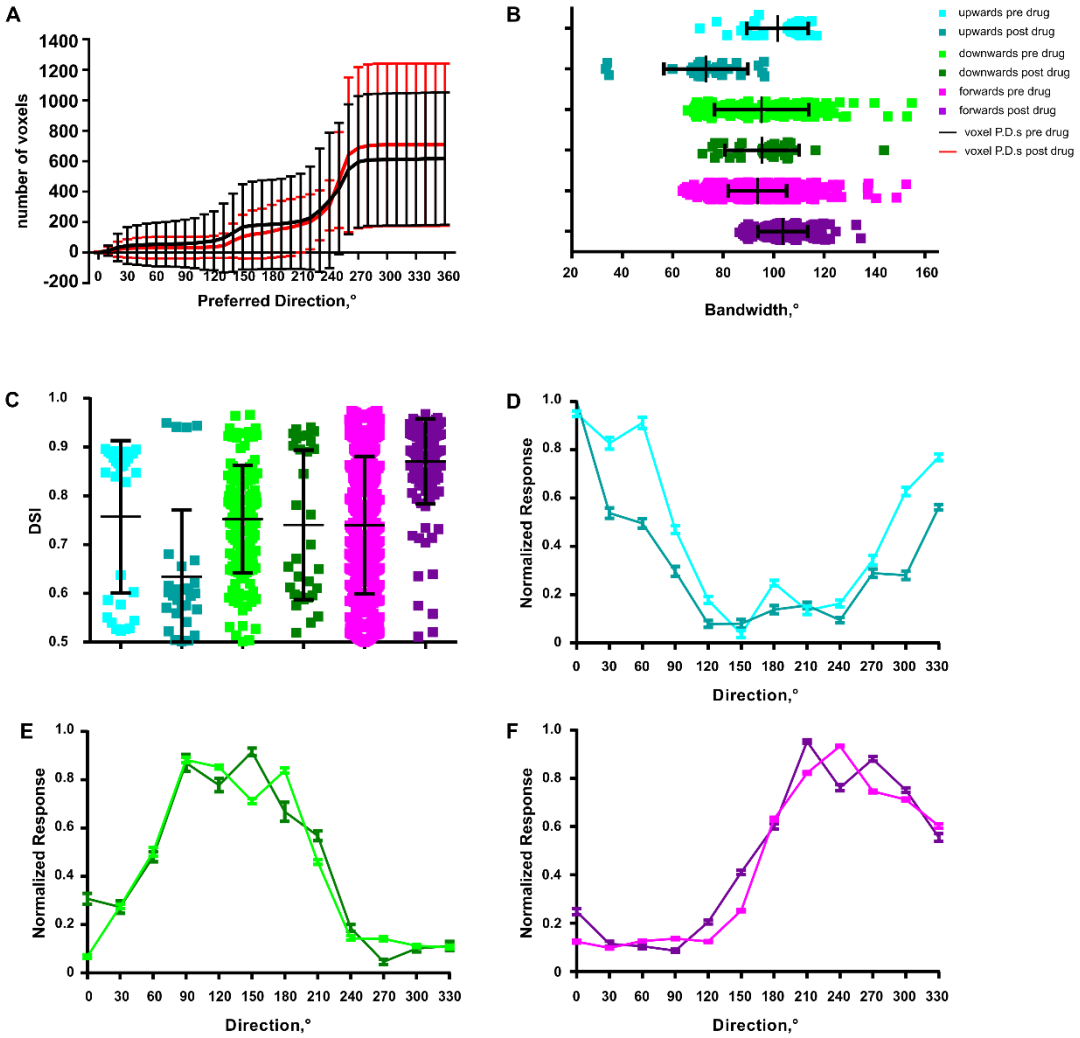

Figure 5-1 Responses of DSGC axons after injection of danieau into the tectum

A. Cumulative frequency histogram showing DSGC voxel preferred directions, pre injection in black, post injection in red, error bars indicate ±S.D. B. DSGC voxel bandwidths before and after danieau injection, bars indicate mean for each population and ± S.D. C. DSGC voxel DSI values, bars indicate mean and ±S.D. D. Plot of upward motion responsive DSGC mean normalized population responses before and after injection, error bars indicate ±S.E.M. E. Plot of downward motion responsive DSGC mean normalized population responses before and after injection, error bars indicate ±S.E.M. F. Plot of forward motion responsive DSGC mean normalized population responses before and after injection, error bars indicate ±S.E.M

As a further control APV/NBQX was injected, this combination of drugs blocks both NMDA and AMPA receptor activity, thus blocking the excitation of neurons in the tectum. Similar to danieau control injections no obvious changes to voxel preferred directions and numbers (Figure 5.2 A), as well as bandwidths (Figure 5.2 B), DSI values (Figure 5.2 C) and the mean normalized responses were found within each DS population (Figures 5.2 D-F). This preliminary control result is an interesting, as it is an indirect indication that GABA inhibition provided by the tectum is not necessary for producing DSGC voxel response properties, as any inhibition provided by the tectum is derived from excitatory RGC inputs into the tectal circuitry, which the APV/NBQX drug combination inhibits.

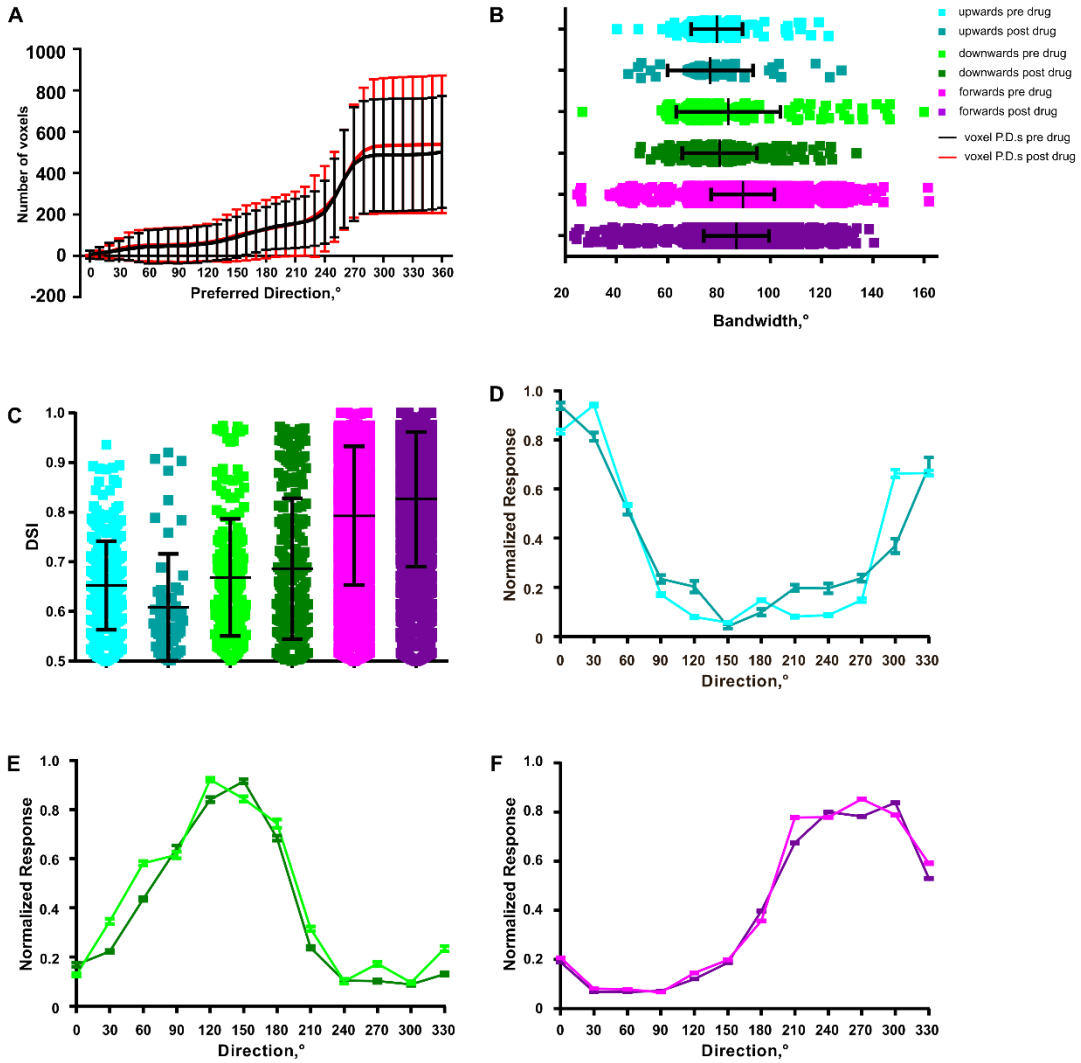

Figure 5-2 Responses of DSGC axons after injection of APV/NBQX into the tectum

A. Cumulative frequency histogram showing DSGC voxel preferred directions, pre injection in black, post injection in red, error bars indicate ±S.D. B. DSGC voxel bandwidths before and after danieau injection, bars indicate mean for each population and ± S.D. C. DSGC voxel DSI values, bars indicate mean and ±S.D. D. plot of upward motion responsive DSGC mean normalized population responses before and after injection, error bars indicate ±S.E.M. E. plot of downward motion responsive DSGC mean normalized population responses before and after injection, error bars indicate ±S.E.M. F. plot of forward motion responsive DSGC mean normalized population responses before and after injection, error bars indicate ±S.E.M.

Having found that both danieau and APV/NBQX injections didn't produce changes in DSGC properties Gabazine, a GABA-A receptor antagonist, was injected into the neuropil to identify the effects of GABA-A receptor mediated inhibition on DSGC axon responses. From the cumulative frequency plot of voxel preferred directions (Figure 5.3 A), there is a shift in the preferred directions of responsive voxels after gabazine injection, however there is also a large overlap of pre and post drug injection variability as indicated by the S.D., showing great variability in voxel numbers and preferred directions between larvae. As a result, it is not possible to rule out variation between larvae as a cause of this shift in preferred directions. The bandwidths of voxels in each DS population are not altered significantly (Figure 5.3 B), excluding the upward DS population voxels after injection of Gabazine, this is likely to be a result of the increased number of voxels with this preferred direction after injection of drug. This difference in upward responsive DS voxels post injection is also seen in the mean voxel DSI values (Figure 5.3 C), but again can be a result of increased voxel numbers. The normalized integral responses of voxels pre and post injection are also unchanged (Figure 5.3 D-F), so blocking GABA-A mediated inhibition has no effect on the normalized responses of DSGCs.

CGP45626, a GABA-B receptor antagonist, was also injected into the tectum. It was predicted that perturbing GABA-B receptor mediated inhibition should prevent presynaptic inhibition. When comparing changes in DSGC axonal responses in the absence of GABA-B receptor mediated inhibition, mean DS voxel preferred directions, and numbers, remain very similar after injection of drug (Figure 5.4 A), with changes well within the margin of error (error bars indicating S.D.). Not only this, but the mean voxel bandwidths (Figure 5.4 B) and DSI values (Figure 5.4 C) are unchanged. The normalised response properties of DS voxels within each population also do not change significantly after drug injection (Figures 5.4 D-F), indicating that these curves are not shaped by presynaptic inhibition. These results indicate that GABA-B receptor mediated presynaptic inhibition is not involves in shaping of DSGC responses in the tectal neuropil.

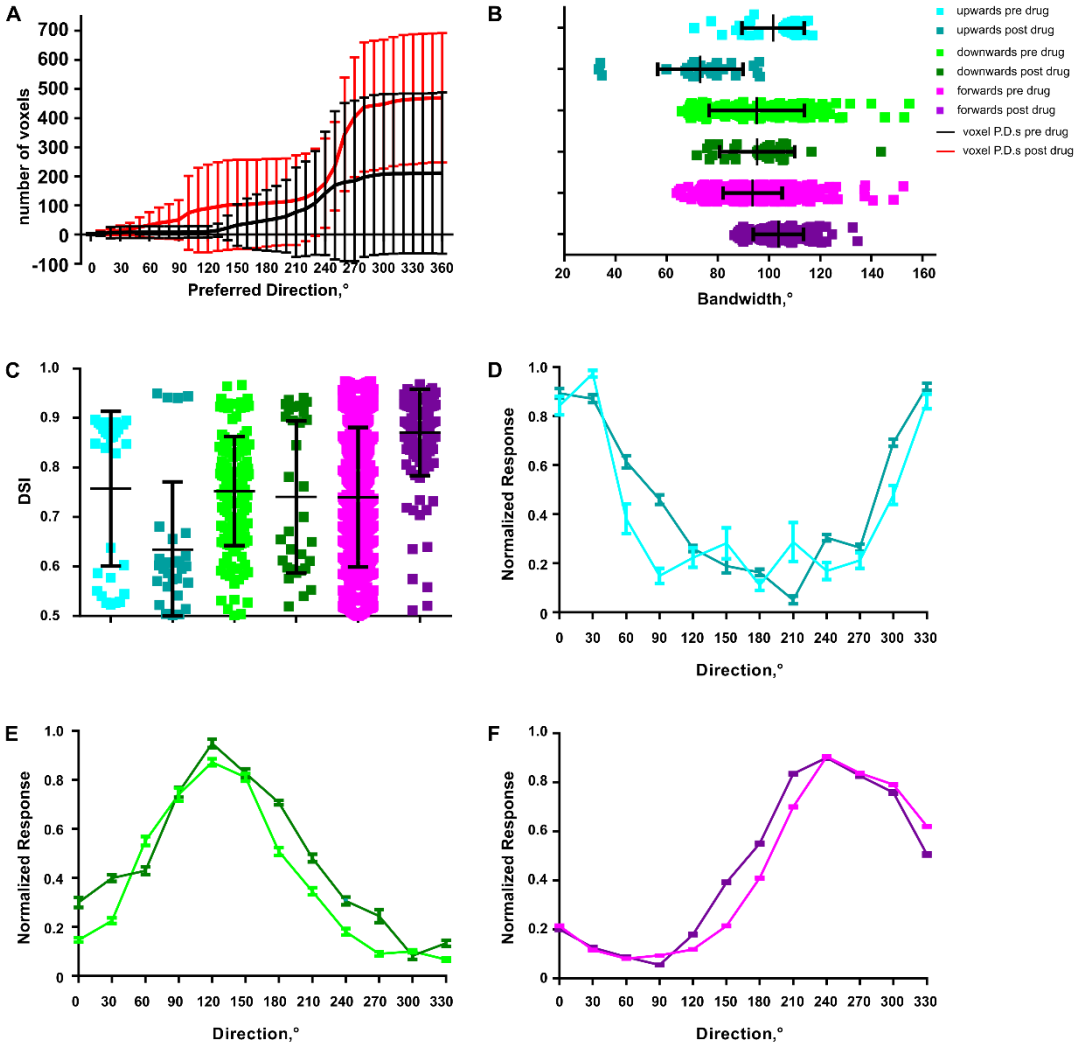

Figure 5-3 Responses of DSGC axons after injection of Gabazine into the tectum:

A. Cumulative frequency histogram showing DSGC voxel preferred directions, pre injection in black, post injection in red, error bars indicate ±S.D. B. DSGC voxel bandwidths before and after danieau injection, bars indicate mean for each population and ± S.D. C. DSGC voxel DSI values, bars indicate mean and ±S.D. D. Plot of upward motion responsive DSGC mean normalized population responses before and after injection, error bars indicate ±S.E.M. E. Plot of downward motion responsive DSGC mean normalized population responses before and after injection, error bars indicate ±S.E.M. F. Plot of forward motion responsive DSGC mean normalized population responses before and after injection, error bars indicate ±S.E.M.

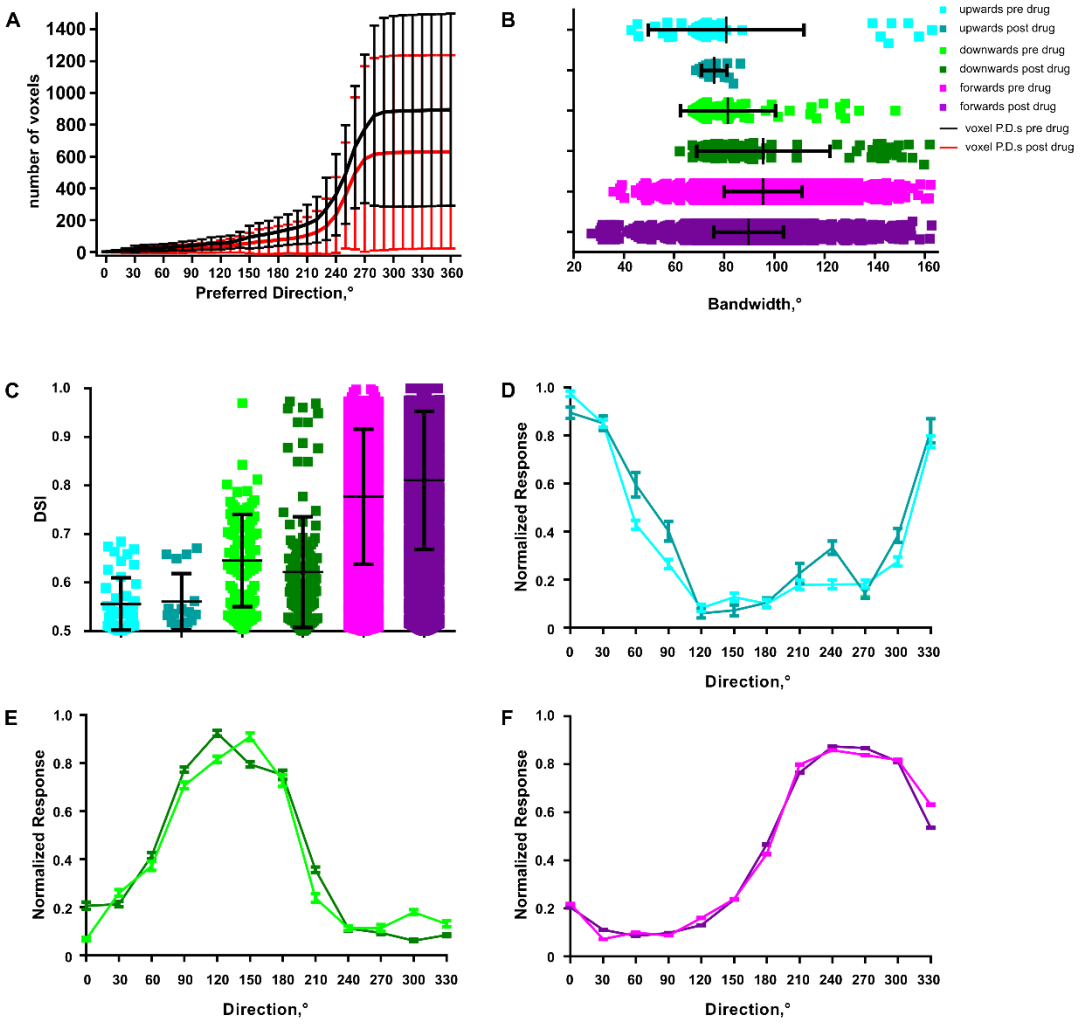

Figure 5-4 Responses of DSGC axons after injection of CGP54626 into the tectum

A. Cumulative frequency histogram showing DSGC voxel preferred directions, pre injection in black, post injection in red, error bars indicate ±S.D. B. DSGC voxel bandwidths before and after danieau injection, bars indicate mean for each population and ± S.D. C. DSGC voxel DSI values, bars indicate mean and ±S.D. D. Plot of upward motion responsive DSGC mean normalized population responses before and after injection, error bars indicate ±S.E.M. E. Plot of downward motion responsive DSGC mean normalized population responses before and after injection, error bars indicate ±S.E.M. F. Plot of forward motion responsive DSGC mean normalized population responses before and after injection, error bars indicate ±S.E.M.

Baclofen is a GABA-B receptor agonist, thus it was predicted that if GABA mediated presynaptic modulation of DSGC occurs in the tectal neuropil, injection of this drug would potentiate its effects on DSGC axonal outputs. Comparing the cumulative frequency histograms before and after injection, the responding DS voxel numbers increase after injection of drug, but this is accompanied by much larger error bars than seen before injection. This indicates that there is a lot of variability between larvae after injection. As mentioned previously, this is probably linked to the shortfalls of the drug injection protocol. Comparing pre and post drug DS voxel bandwidths, upward and downward motion sensitive voxels have different mean voxel bandwidths after injection. Again, this is probably linked to

differences in sampled voxels after injection of drug. This alteration in the mean DSI values of DSGC voxels also occurs after drug injection. The mean normalized responses of DS voxels in each population also do not change significantly after drug injection. The potentiation of GABA-B receptor signalling may introduce differences to DSGC voxel properties; however, the drug injection protocol may also provide explanations for the differences seen post injection.

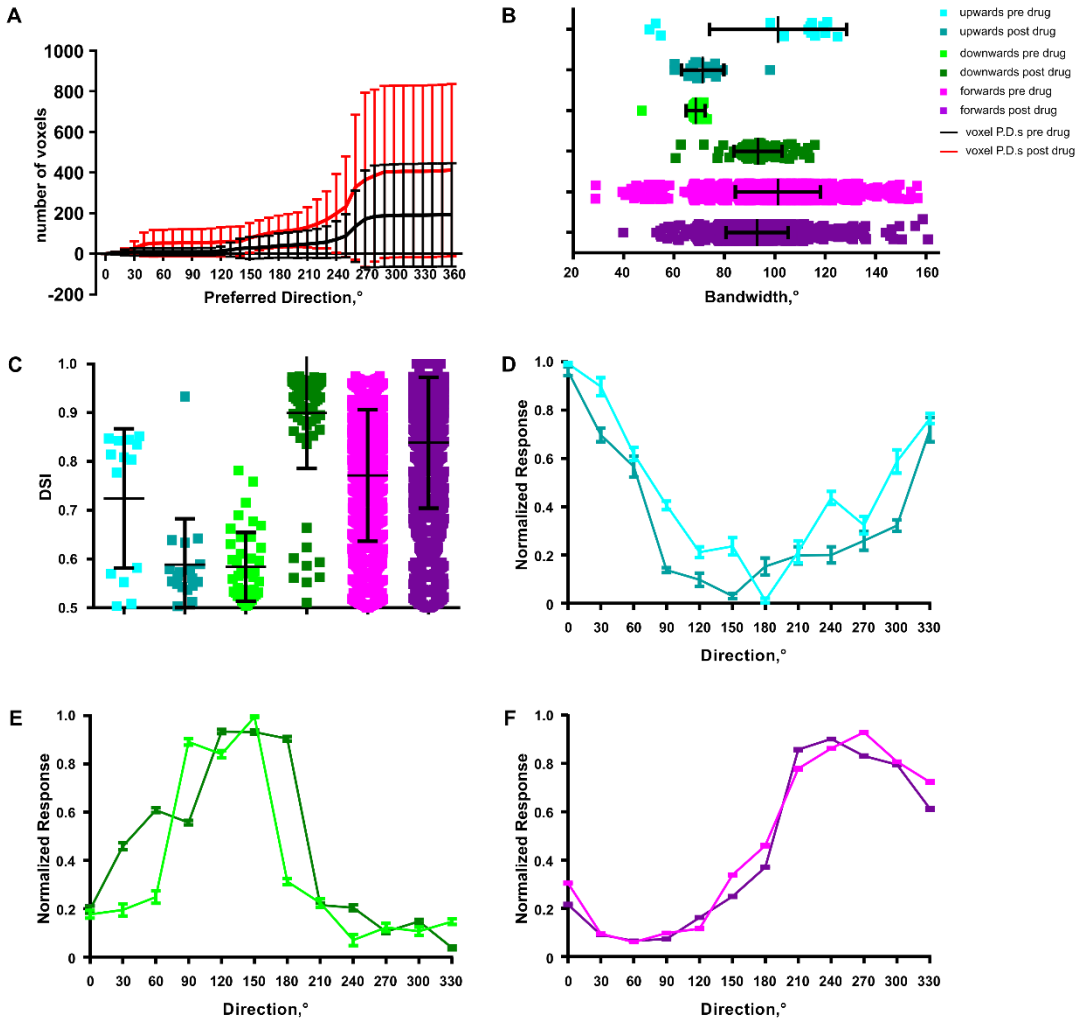

Figure 5-5 Responses of DSGC axons after injection of Baclofen into the tectum

A. Cumulative frequency histogram showing DSGC voxel preferred directions, pre injection in black, post injection in red, error bars indicate ±S.D. B. DSGC voxel bandwidths before and after danieau injection, bars indicate mean for each population and ± S.D. C. DSGC voxel DSI values, bars indicate mean and ±S.D. D. Plot of upward motion responsive DSGC mean normalized population responses before and after injection, error bars indicate ±S.E.M. E. Plot of downward motion responsive DSGC mean normalized population responses before and after injection, error bars indicate ±S.E.M. F. Plot of forward motion responsive DSGC mean normalized population responses before and after injection, error bars indicate ±S.E.M.

To determine the variability of voxel preferred directions between larvae, the mean pre-drug DS voxel preferred directions per fish for each pre-drug condition were plotted on cumulative frequency histograms. Histogram bins were set to 10°. The cumulative histogram (Figure 5.6) indicates that there is great variability in voxel numbers between fish in each pre-drug group, indicated by the large sizes of error bars, and their overlaps between drug conditions (error bars indicate ±S.D.). This variability between numbers of DS voxels between control fish means comparing differences in voxel numbers pre and post drug injection, and sizes of relative DSGC populations impossible to compare. It is likely that this variability is a result of experimental procedures. Possible factors introducing this variability includes the fact that only one plane through the tectal neuropil was imaged per fish, due to the short time scale available before drug activity was sufficient to induce and effect. Not only this, but slight differences in the depth through the neuropil, and slight alterations in the angle of mounted larvae, or levels of GCaMP expression could produce differences in levels of representation of each DSGC population, or the overall responding voxel number.

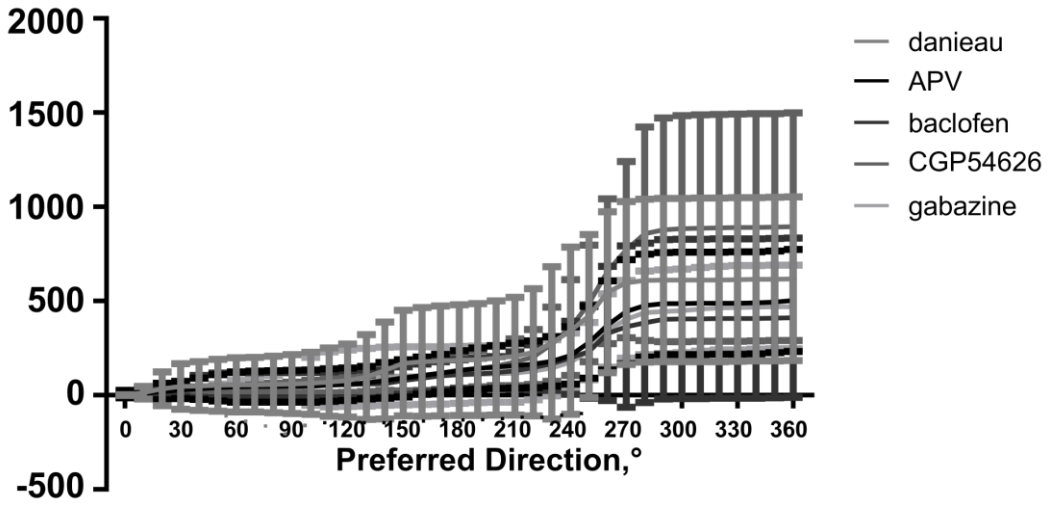

Figure 5-6 DSGC voxel numbers and preferred directions are variable between control larvae

Bars indicate ±S.D, data taken from control experiments before drug injection.

5.2.2 Role of inhibition on shaping DS tectal neuron populations:

Having determined that inhibition does not play a role in pre-synaptically shaping DSGC outputs in the neuropil, I then explored a role for inhibition in the shaping of DS tectal neuron responses. To test this the differences in DS tectal neuron responses before and after injection of GABA-receptor modulating drugs were compared in HuCGCaMP5 expressing larvae.

APV/NBQX is a drug combination that prevents NMDA/AMPA receptor activity, and should prevent excitation of neurons in the periventricular layer on injection of these drugs DS activity in the tectal neurons should cease. However, after injection, tectal cell voxels are still visually responsive (Figure 5.7 A). By plotting the average cumulative histograms of voxel preferred directions per larva, differences can be identified. The loss of voxels responding to upward motion and the slight decrease in overall responding voxel numbers post injection, but there were no significant differences between pre and post drug injection conditions (Figure 5.7A, multiple t tests with Holm-Sidak correction, $p > 0.05$ all points, total pre n = 271, post n =236 voxels, n = 7 larvae) indicates that the drug was still slightly active, pointing to the explanation that the drug was degraded in the neuropil before the post-drug experiment could be completed, or that concentrations of the drug were insufficient. DSI values were unchanged for the largest population, the forward motion direction selective voxels, but significantly higher after injection in the smaller backward motion population (Figure 5.7 B, Mann Whitney U test, upward population n = 12, backward population pre n =22, post n = 58, $p < 0.0001$, forward population pre n = 76, post n = 81, $p = 0.0750$, bars indicate mean ±S.D.), bandwidths did not change for the upward population, but lowered significantly in the forward population, (Figure 5.7 C, Mann Whitney U test, upward population n = 12, backward population pre n =22, post n = 58, $p = 0.410$, forward population pre n = 76, post n = 81, $p < 0.0001$, bars indicate mean ±S.D).

Comparing the pre and post drug injection normalized responses, there are no distinct changes to response size nor selectivity (Figures 5.8 A-C, error bars show ±S.E.M.) indicating that any responding voxels after injection of drug remained DS.

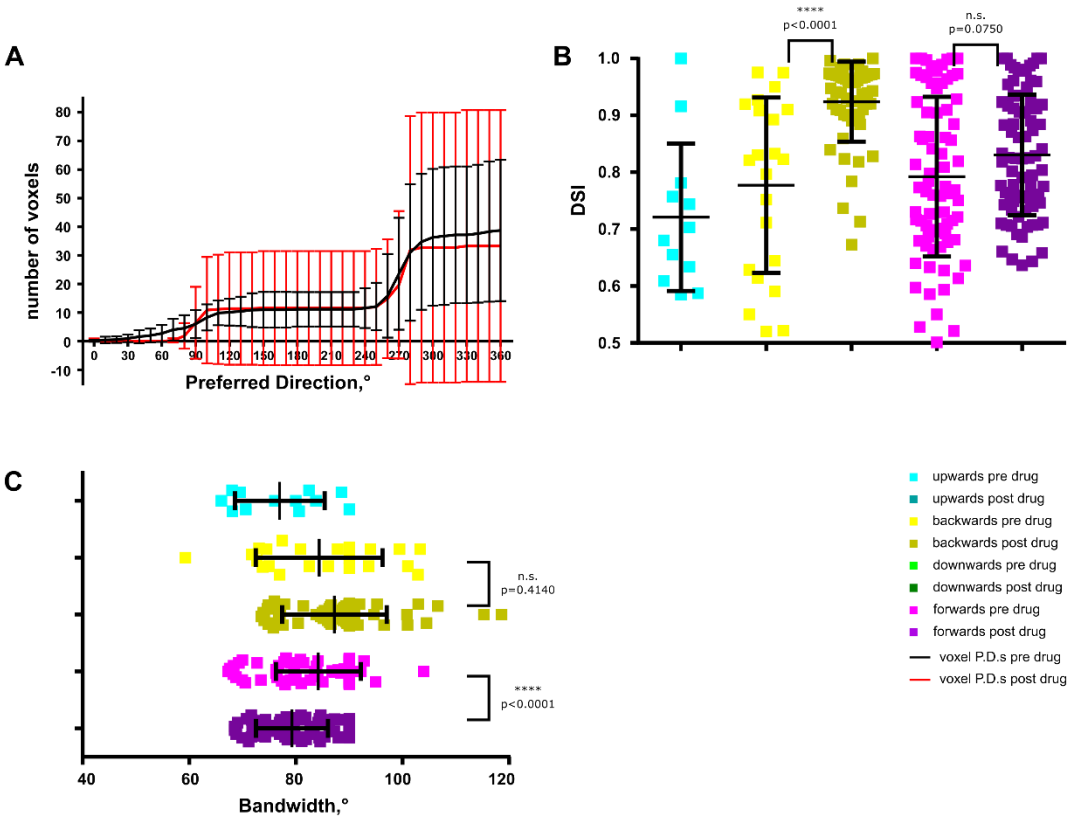

Figure 5-7 Responses of DS tectal neuron voxels after injection of APV/NBQX

A. Cumulative frequency histogram of average DS tectal cell voxel preferred directions per larva, pre injection in black, post injection in red, error bars indicate ±S.D., B. DS tectal cell voxel DSI values before and after danieau injection, bars indicate mean for each population ± S.D., comparisons using Mann Whitney U test, with significance indicated C. DS tectal cell voxel bandwidths before and after APV/NBQX injection, bars indicate mean for each population ± S.D, comparisons using Mann Whitney U test, with significance indicated.

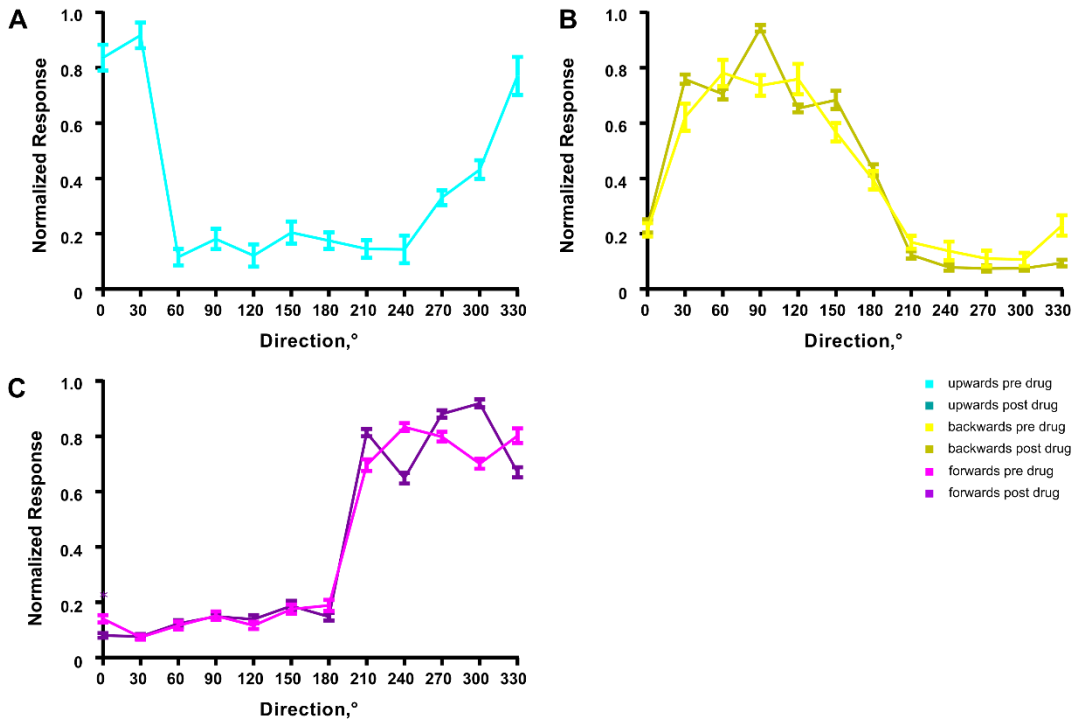

Figure 5-8 DS tectal neuron voxel responses after APV/NBQX injections

Plot of DS tectal cell mean normalized population responses before and after injection, A. Upward motion responsive B. Backward motion responsive C. Downward motion responsive, all error bars indicate ±S.E.M.

To perturb GABA-A receptor mediated inhibition Gabazine was injected into the tectum. Comparing pre and post injection DS tectal cell voxels preferred directions (Figure 5.9 A, multiple t tests with Holm-Sidak correction, all points p >0.05, total pre-injection n = 599 voxels, post injection n = 405 voxels, n = 13 larvae) there is an overall reduction in responding voxels, however, there is also variability in voxel numbers between larvae, indicated by the large S.D. . DS voxel bandwidths were not significantly different, except between pre and post drug injection in the forward motion sensitive population (Figure 5.9B, Mann-Whitney U test, upward responding population pre n = 8 voxels, post n = 12 voxels, p = 0.1147, downward responding population pre n =115 voxels, post n = 43 voxels p = 0.5436, forward responding population pre n = 243 voxels, post n = 173 voxels, p = 0.0003). This significant difference is likely to due to the larger number of voxels skewing statistical tests, as the mean bandwidths are very similar (mean bandwidth pre injection = 80.61°, post injection = 83.68°). DSI was significantly different after drug injection in the downward and forward motion sensitive populations (Figure 5.9 C, Mann-Whitney U test, upward responding population pre n = 8 voxels, post n = 12 voxels, p = 0.6716, downward responding population pre n = 115 voxels, post n = 43 voxels p = 0.0013, forward responding population pre n = 243 voxels, post n = 173 voxels, p = 0.0028), but again for forward motion sensitive voxels this significance is likely due to the large numbers.

Comparing population mean responses, there is no statistical difference in response sizes at each direction of motion presented (Figures 5.10 A-D, multiple t tests with Holm-Sidak correction, $p > 0.05$ for all points, error bars indicate ± S.E.M.). These results show that perturbing GABA-A receptor mediated inhibition produces no dramatic effects on DS tectal neuron responses, indicating that DS properties are largely inherited directly from RGC inputs. Interestingly, the backward motion sensitive population is still present after drug injection, indicating that this emergent DS population may not be reliant upon inhibition. However, these findings should be treated with caution, as the results obtained with APV/NBQX did not give the expected results suggesting that drug injections are not always reliable.

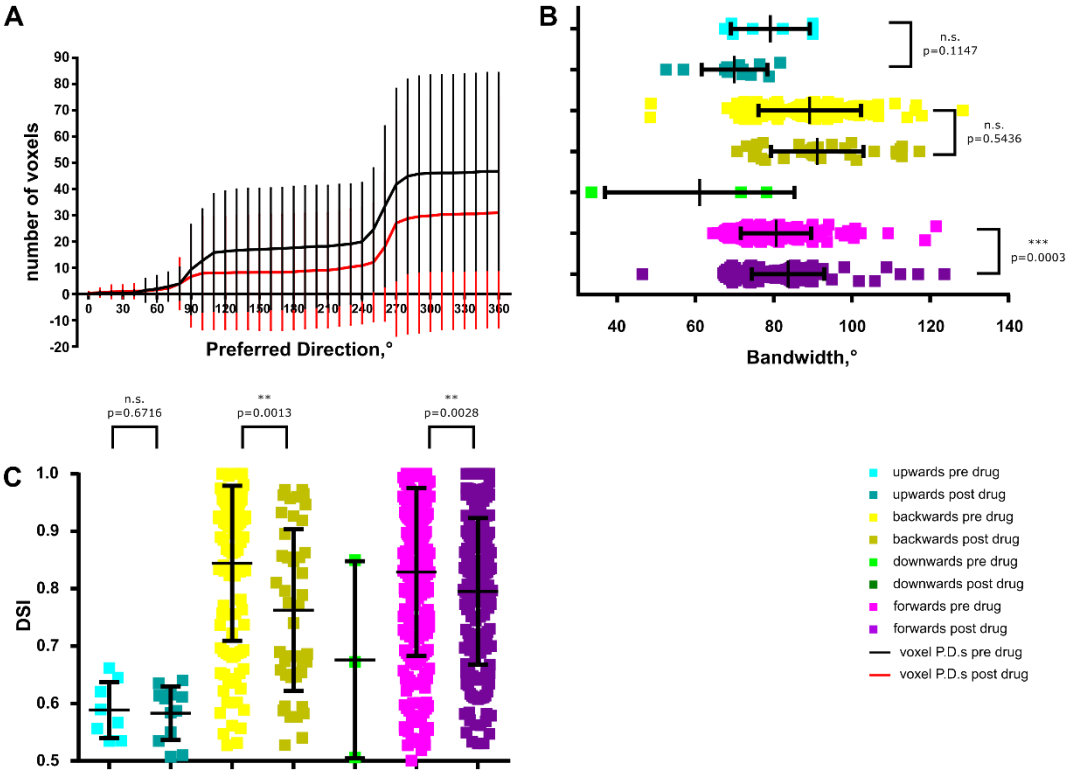

Figure 5-9 Responses of DS tectal cell voxels after injection of Gabazine

A. Cumulative frequency histogram showing DS tectal cell voxel preferred directions, pre injection in black, post injection in red, error bars indicate ±S.D. B. DS tectal cell voxel bandwidths before and after danieau injection, bars indicate mean for each population and ± S.D. C. DS tectal cell voxel DSI values, bars indicate mean and ±S.D.

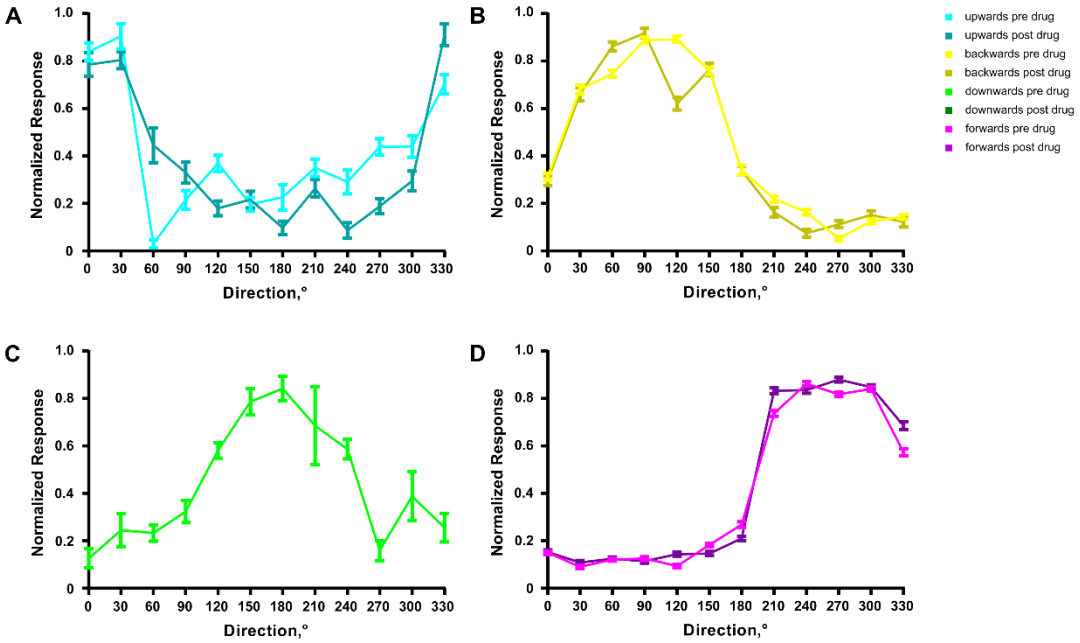

Figure 5-10 DS tectal voxel responses after Gabazine injection

Plot of DS tectal cell voxel mean normalized population responses before and after injection A. Upward motion responsive B. Backward motion responsive C. Downward motion responsive D. Forward motion responsive, all error bars indicate ±S.E.M

Baclofen is a GABA-B receptor agonist, injection of this drug into the tectum caused striking differences in DS voxel numbers, with a reduction in average number of direction selective voxels after injection (Figure 5.11 A, total pre injection voxel n = 653, post injection voxel n =228 , all points p >0.05, multiple t tests with Holm-Sidak correction, n = 9 larvae, error bars indicate ±S.D.). DS voxel DSI values remained unchanged in the two smaller tectal neuron populations (Figure 5.11 B, upward pre injection n =15 voxels, post injection n =6 voxels, p = 0.34, and downward pre injection n = 7 voxels, post injection n = 3 voxels, p = 0.3833, two tailed Mann-Whitney U test), but changed significantly in the two larger DS populations (Figure 5.11 B, backward pre injection n = 125 voxels, post injection n = 97 voxels, p = 0.0007 and forward pre injection n = 221 voxels, post injection n = 29 voxels, p = 0.0004, two tailed Mann-Whitney U). Whilst the means for these two populations are different, comparing these values per larva would be more appropriate to ensure statistical significance is real. Bandwidths remained the same after drug injection in all populations except the downward motion sensitive DS tectal neuron voxels (Figure 5.11 C, upward pre injection n =15 voxels, post injection n =6 voxels, p = 0.7883, and downward pre injection n = 7 voxels, post injection n = 3 voxels, p = 0.0.0167, backward pre injection n = 125 voxels, post injection n = 97 voxels, p = 0.1412 and forward pre injection n = 221 voxels, post injection n = 29 voxels, p = 0.3346, two tailed Mann-Whitney U test).

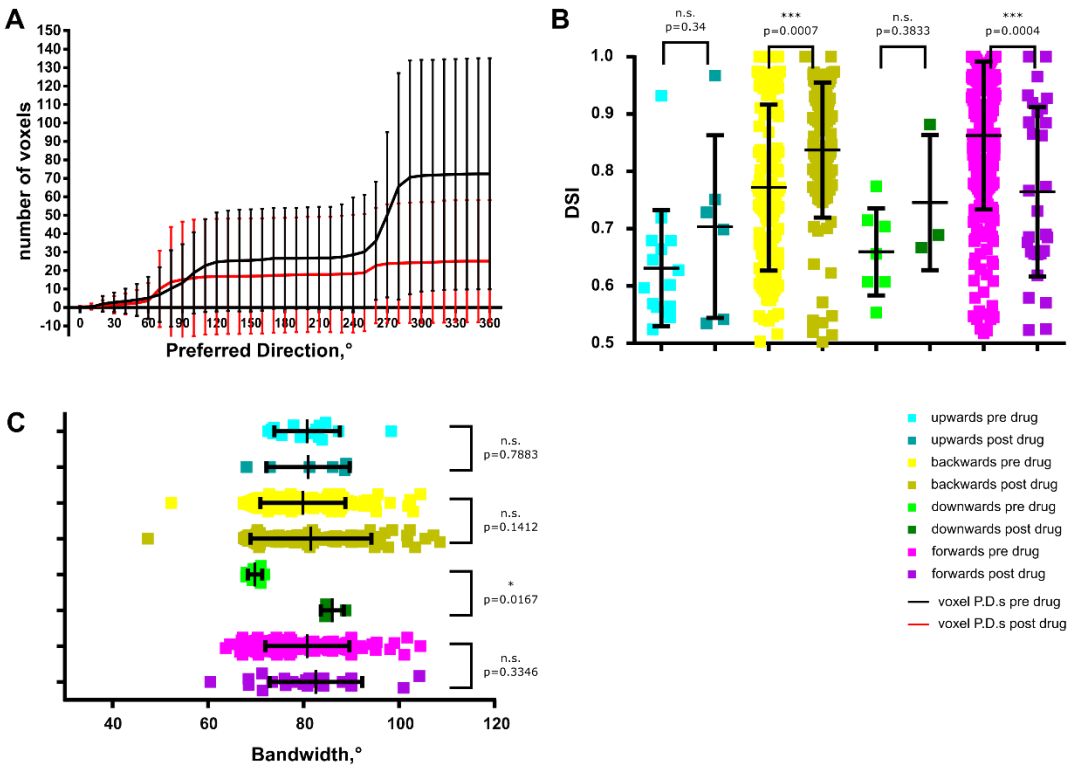

Figure 5-11 Responses of DS tectal voxels after injection of Baclofen

A. Cumulative frequency histogram showing DS tectal cell voxel preferred directions, pre injection in black, post injection in red, error bars indicate ±S.D. B. DS tectal cell voxel bandwidths before and after danieau injection, bars indicate mean for each population and ± S.D. C. DS tectal cell voxel DSI values, bars indicate mean and ±S.D

Comparing mean normalized population responses, DS tectal cell voxel responses remained largely similar, however, significant differences after drug injection were found for some directions of motion (Figures 5.12 A-D, $p < 0.05$ indicated by asterisks, multiple t tests with Holm-Sidak correction, error bars indicate ±SEM).

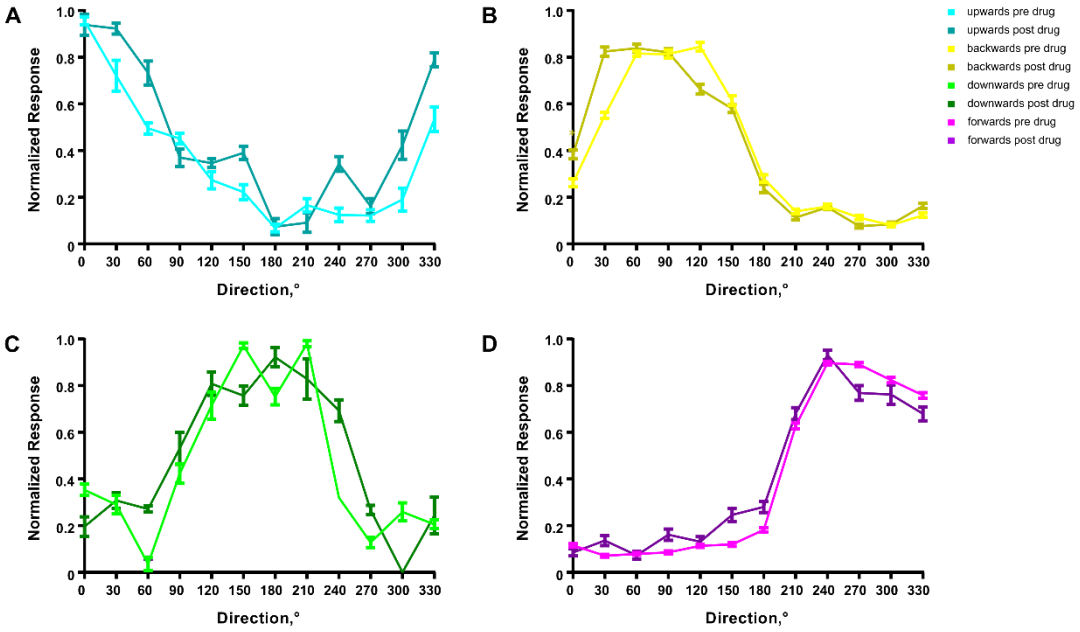

Figure 5-12 DS tectal voxel responses after Baclofen injection

Plot of DS tectal cell voxel mean normalized population responses before and after injection, A. Upward motion responsive B. Backward motion responsive C. Downward motion responsive D. Forward motion responsive, all error bars indicate ±S.E.M

CGP54626 is a GABA-A receptor agonist, when injected it produced a reduction in DS responsive voxels (Figure 5.13 A, total pre injection voxels n = 296, post injection voxel n = 90, all points p >0.05, multiple t tests with Holm-Sidak correction, n = 9 larvae, error bars indicate ±S.D.). Bandwidths were not significantly altered after injection except for backward responsive voxels (Figure 5.13 B upward pre injection n = 2 voxels, post injection n = 0 voxels, downward pre injection n = 3 voxels, post injection n = 1 voxels, backward pre injection n = 52 voxels, post injection n = 14 voxels, p = 0.0014 and forward pre injection n = 83 voxels, post injection n = 13 voxels, p = 0.7604, two tailed Mann-Whitney U test). DSI values were also not significantly different after injection of CGP54626 (Figure 5.13 C, upward pre injection n = 2 voxels, post injection n = 0 voxels, downward pre injection n = 3 voxels, post injection n = 1 voxels, backward pre injection n = 52 voxels, post injection n = 14 voxels, p = 0.1108 and forward pre injection n = 83 voxels, post injection n = 13 voxels, p = 0.0831, two tailed Mann-Whitney U test).

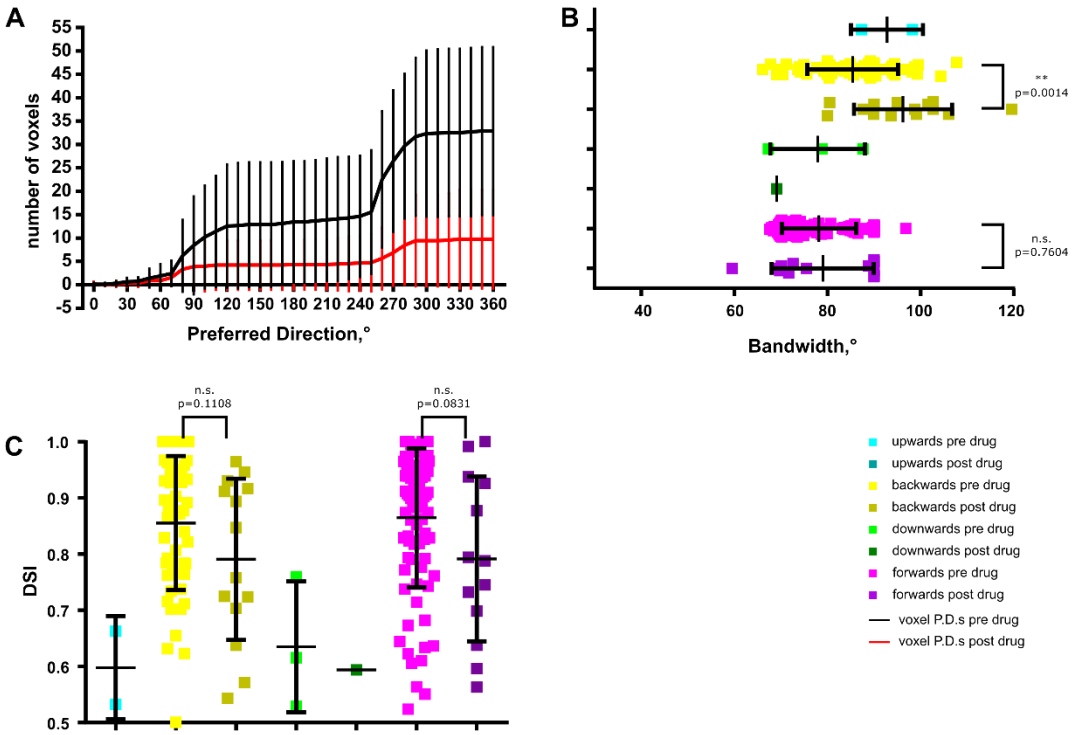

Figure 5-13 Responses of DS tectal voxels after injection of CGP54626

A. Cumulative frequency histogram showing DS tectal cell voxel preferred directions, pre injection in black, post injection in red, error bars indicate ±S.D. B. DS tectal cell voxel bandwidths before and after danieau injection, bars indicate mean for each population and ± S.D. C. DS tectal cell voxel DSI values, bars indicate mean and ±S.D.

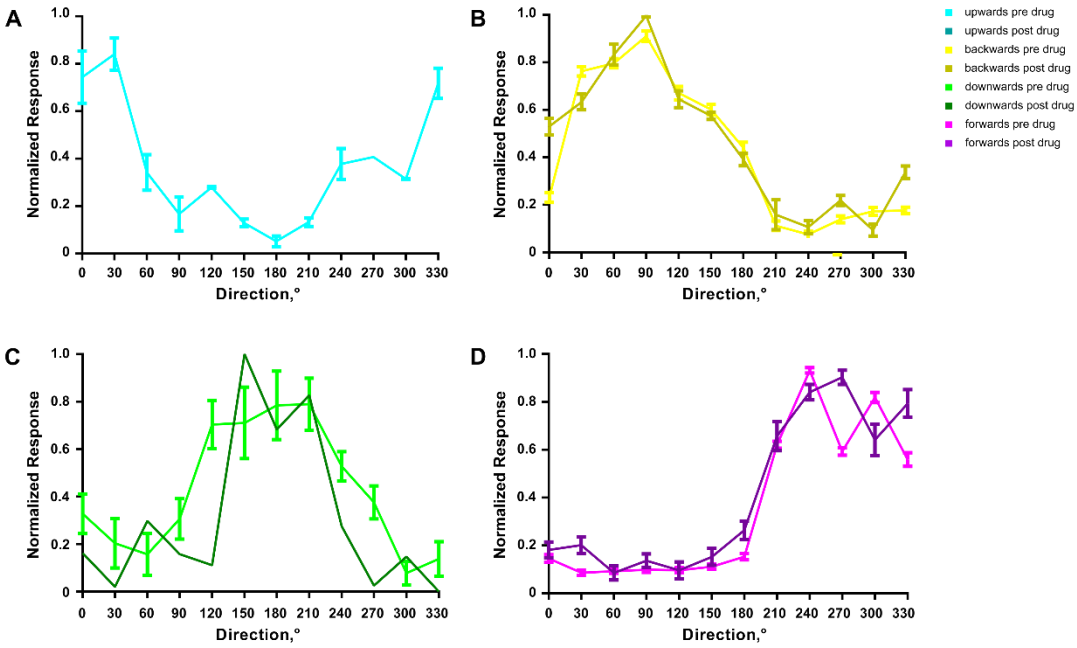

Figure 5-14 DS tectal neuron voxel responses after CGP54626 injection

Plot of DS tectal cell mean normalized population responses before and after injection, A. Upward motion responsive B. Backward motion responsive C. Downward motion responsive D. Forward motion responsive, all error bars indicate ±S.E.M

Comparing the DS voxel mean normalized responses for each DS population, there are no striking differences (Figures 5.14 A-D, error bars indicate ± SEM), indicating that the drug has no effect on the response properties of the DS neurons.

To demonstrate the variability in DS tectal cell populations between larvae, the mean cumulative frequency histograms for each pre drug injection condition were compared. These plots show that there is a great variability in numbers of responding DS voxels between larvae, and some variation in the preferred directions of these voxels (Figure 5.15, error bars indicate ±S.D.).

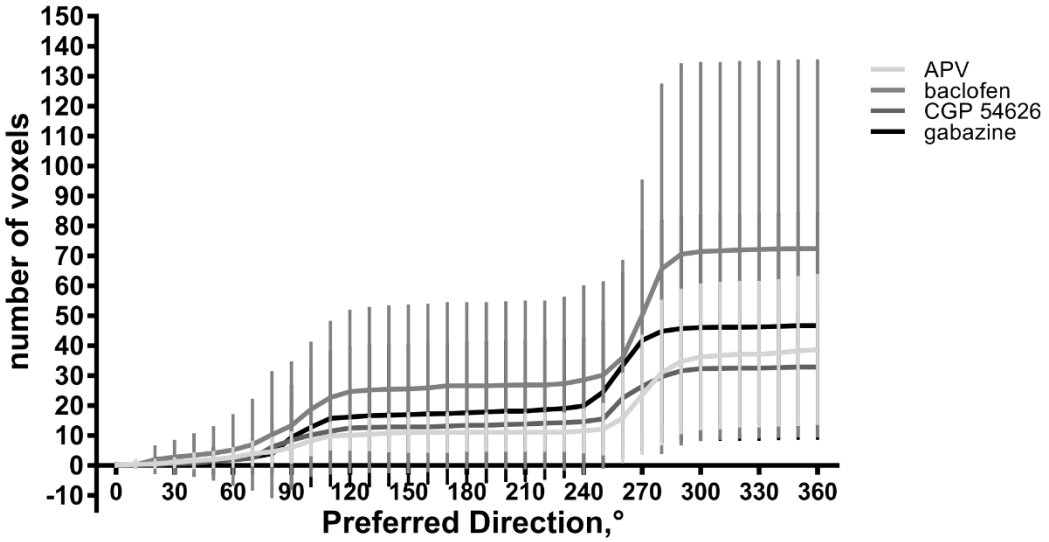

Figure 5-13 Larvae show great variability in numbers of DS tectal neuron voxels, and their preferred direction of motion

Mean cumulative frequency histograms per larvae for control larvae in each drug condition, error bars indicate ± S.D.

5.2.3 Genetically defined DS SIN ablation in the tectum

As a more specific experiment to determine the effects of DS SIN mediated inhibition in the tectal circuit, KillerRed was expressed under the control of the *s1156tGal4* line in a *HuCGCaMP5* background. This allowed the selective and temporally controlled ablation of SINs, and hence the removal of their activity from the tectal circuit. In order to determine if the expression of KillerRed in these neurons was not itself deleterious to the normal functioning of the tectal circuit, control experiments were carried out in which the triple transgenic larvae (*s1156t:Gal4; UAS:KillerRed; HuC:GCaMP5*) were not exposed to wide field fluorescence after initial direction selective experiments, and were imaged again at 7dpf. As there was not a limit on time for these experiments, it was possible to sample from three planes in the central tectum to achieve a greater representation of tectal neurons.

Comparing the cumulative frequencies of DS tectal cell voxels in each condition, the only differences found were between 6dpf populations for control and KR ablated larvae (Figure 5.16, multiple t tests with Holm-Sidak corrections, all comparisons $p > 0.05$ except for bins 260-360° between control 6dpf and 6dpf KR populations where $p<0.05$, 6dpf voxel n =218, 7dpf voxel n = 153). The curves of the cumulative histograms indicate the variability in DS tectal cell voxel numbers and preferred directions, even without the ablation, and between the 6dpf and 7dpf time points. This makes comparisons of voxel numbers and directions difficult.

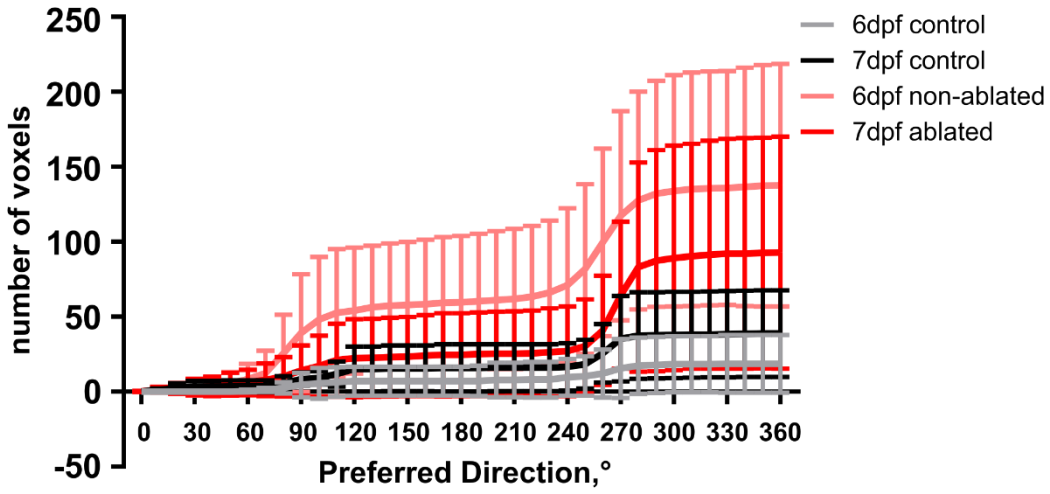

Figure 5-14 Numbers of DS tectal cell voxels change between 6 and 7dpf

Mean cumulative frequency histograms of DS tectal cell voxel preferred directions per larva from control experiments at 6 and 7dpf, and ablated conditions at 6 and 7dpf. Bars indicate ±S.D. Grey and Black plots indicate control siblings with no KillerRed ablation, Red and pale red plots indicate KillerRed ablated experiments.

Comparisons of DS tectal neuron properties in control experiments indicate that the time between imaging of tectum on 6dpf and 7dpf creates differences in response properties, specifically, it seems that forward motion sensitive voxels with lower DSI values at 6dpf are lost by 7dpf (Figure 5.17 A, backward DS population voxels at 6dpf n = 76, voxels at 7dpf n = 22, $p = 0.9008$, upward voxel 6dpf n = 89, 7dpf n = 87, $p < 0.0001$, Mann-Whitney U two tailed test, larvae n = 5). This could be due to the refinement of DS tectal neurons, or loss of GCaMP expression in these neurons over time. DS tectal neuron voxel bandwidths do not change significantly by 7dpf (Figure 5.17 B, backward DS population voxel 6dpf n = 76, 7dpf n = 22, $p = 0.4641$, upward voxel 6dpf n = 89, 7dpf n = 87, $p = 0.0324$, Mann-Whitney U two tailed test, larvae n = 5). Mean normalised response plots for each population indicates that between 6 and 7 dpf there is a slight change in normalized response sizes, but the specificity of which directions voxels respond to remains the same (Figure 5.17 C-F, multiple t tests with Holm Sidak correction, asterisks indicate where $p<0.05$, n = 15 larvae).

Ablation of SINs at 6dpf in KillerRed expressing larvae had no detectable effects on DS tectal neuron voxel properties. There was a reduction in responding DS voxels compared to control experiments at 6dpf (Figure 5.16, n = 15 larvae, 6dpf n =1633 voxels, 7dpf n = 1008 voxels), however this reduction was also found in non-ablated control larvae, and thus is most likely to be due to changes in DS voxel numbers during development or loss of GCaMP expression. Direction selective voxel DSI values did not change significantly after ablation,

except for the backward population (Figure 5.18 A upward DS population voxels 6dpf n =44, 7dpf n =35, p = 0.8692, backward voxel 6dpf n =520, 7dpf n =116, p = 0.0046, downward DS population voxel 6dpf n =22, 7dpf n =10, p = 0.9521, forward DS population voxel 6dpf n =646, 7dpf n =526, p =0.0507, Mann-Whitney U two tailed test, error bars indicate mean ±S.D., larvae n = 15). Comparing bandwidths, the bandwidth sizes remained largely the same, significant differences are likely just an artefact of large n numbers because the effect size is relatively small (Figure 5.18 B upward DS population voxels 6dpf n =44, 7dpf n =35, p = 0.2437, backward voxel 6dpf n =520, 7dpf n =116, p = p<0.0001, downward DS population voxels 6dpf n =22, 7dpf n =10, p = 0.3617, forward DS population voxels 6dpf n =646, 7dpf n =526, p <0.0001, Mann-Whitney U two tailed test, error bars indicate mean ± S.D., larvae n = 15). Comparing normalized population responses, there are very few significant differences in response sizes to direction presented, indicated with asterisks on the plots (Figure 5.18 C-F, n = 15 larvae). The response plots look strikingly similar before and after ablation indicating that there was no effect.

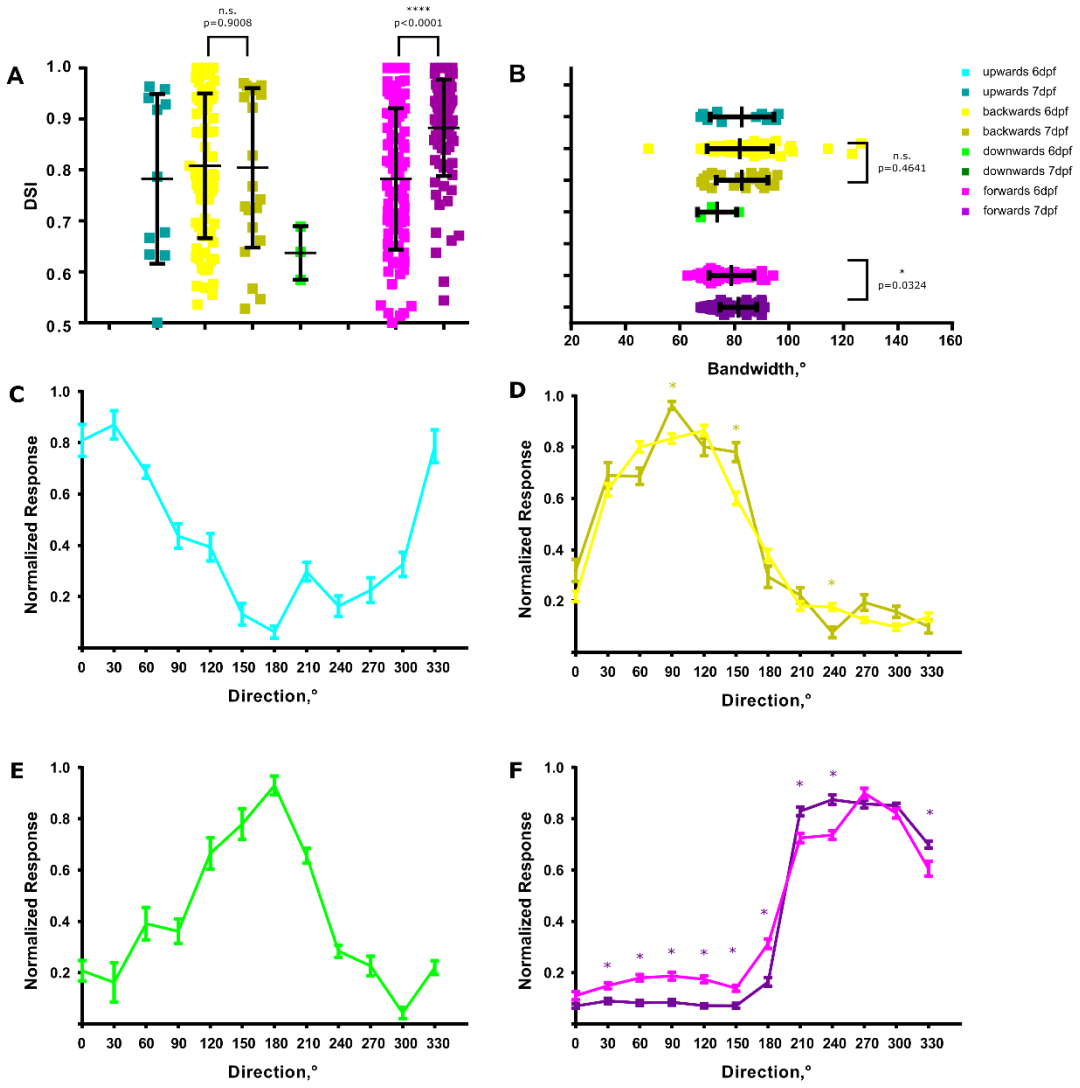

Figure 5-15 Comparisons of DS tectal cell voxel properties in 6 and 7dpf control larvae without killer red ablation

A. Changes in DSI values per population (Mann-Whitney U two tailed test, p values indicated, error bars indicate mean ±S.D.), B. Changes in bandwidths per population (Mann-Whitney U two tailed test, p values indicated, error bars indicate mean ±S.D.), C-F. Mean normalized responses to directions of motion by population (multiple t tests with Holm-Sidak correction, asterisks indicate p<0.05, error bars show ±SEM)

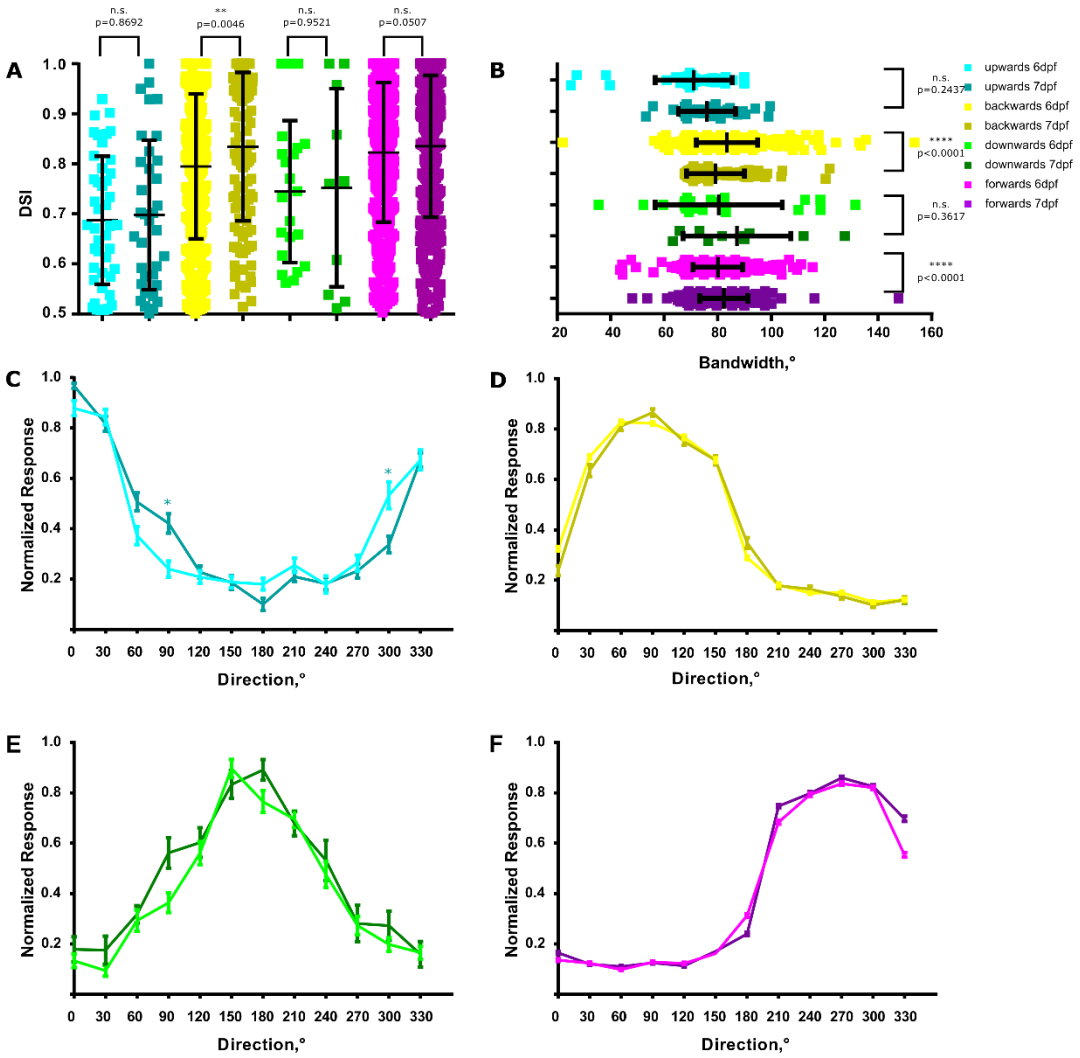

Figure 5-16 Comparisons of DS tectal cell voxel properties at 6dpf and 7dpf larvae after killer red ablation

A. Changes in DSI values per population (Mann-Whitney U two tailed test, p values indicated, error bars indicate mean ±S.D.), B. Changes in bandwidths per population (Mann-Whitney U two tailed test, p values indicated, error bars indicate mean ±S.D.), C-F. Mean normalized responses to directions of motion by population (multiple t tests with Holm-Sidak correction, asterisks indicate p<0.05, error bars show ±SEM).

5.3 Discussion

These experiments attempted to determine what effect GABA-mediated inhibition has on tectal DS circuitry by perturbing GABA receptor function. The superior location of SINs in the tectum provided cause to speculate that they might be involved in pre-synaptic inhibition of axonal outputs of RGCs. DSGC response properties did not change significantly after GABA receptor perturbation, including DSI, preferred direction or bandwidth. This indicates that RGC axonal outputs do not undergo presynaptic modulation via GABA-R mediated inhibition. DS tectal neurons also showed little difference in DS response properties after perturbation of GABA receptor mediated inhibition by injection of drugs.

One major problem with these experiments is inter-larval variability in DS voxel numbers and population representation. This variability after injection is problematic when analysing the effects of modulation with these drugs. There are several ways this variability could be introduced during experiments. For instance, only one plane through the tectum could be imaged whilst presenting visual stimuli, due to the short window of activity of these drugs, and the length of time each orientation experiment took (~6 minutes). As a result, there was no guarantee that the position in the tectum imaged post injection was identical to that imaged in control pre-drug conditions, despite all efforts to ensure otherwise. In an attempt to minimise these differences, imaging was restricted to the central plane of the tectum, however as mentioned previously, RGC synaptic boutons in the tectum are only 0.8µm in volume, and tectal cells are only 7µm in diameter, leaving a very small margin of error. Injection of volumes into the tectum also changed the volume of the area after drug was injected, contributing to a difficulty in locating the same tectal plane.

There was also no way of verifying the activity of the drugs, nor how quickly they were washed out or deactivated in tectal tissue. Ideally, this would be verified with the use of electrophysiological recording from neurons in the tissue to monitor changes in the signalling, however this was not possible. Whilst this is the case, the available tools were not sufficient to carry out a better experiment to identify the role of GABA signalling in tectum. Thus, multiple control experiments were carried out with the aim of using them as a baseline for variability introduced through experimental conditions. This in no way provides an indication that the drugs were active, however.

A second problem with these experiments is that all GABA-receptor mediated inhibition was blocked in the tectum after injection. This indiscriminate approach means that SIN mediated inhibition was not the only inhibition blocked, so effects seen after drug injection could not be attributed to the activity of SINs.

Thirdly, these experiments focussed only on the direction selective circuit. This is over-simplifying a potentially complex circuit. It is immediately clear that SINs are both DS and size selective, their role in the circuit could be linked to size discrimination of motion in a particular direction. A more appropriate experiment would probe both at once by presenting a sequence of directions at multiple spatial frequencies, thus determining if inhibition is necessary for size selective DS tectal neurons. Whilst the tools to carry such an experiment out were available, the time-sensitive nature of the activity of the drugs was a factor in not pursuing this. This experiment would be an ideal step towards discerning what inhibition does in the tectal circuit.

To address the problem of non-specific perturbation of inhibition in the circuit, KillerRed was used to ablate SIN neurons in the tectum. Using this technique, no detectable changes occurred in DS populations nor DS response properties beyond those seen in controls. Due to problems with potential photo-bleaching of photoreceptors in the eye, as well as the issues of bleaching GCaMP expression in the tectum, experiments had to be carried out over two days. Control larvae were also left overnight to allow recovery of GCaMP expression from the initial DS experiments, and it was found that despite no exposure to fluorescence, there was a difference in numbers of responsive voxels at 7dpf compared to 6dpf. This could be a result of several things, the larvae are still developing at 6dpf, and it is likely that within 24 hours there are still developmental changes occurring in DS tectal circuitry. Similarly, due to limits on time, it was not possible to generate triple transgenic larvae homozygous for HuCGCaMP5 expression. Thus, this lower GCaMP5 expression level meant that at 7dpf GCaMP5 expression was lower than 6dpf.

Finally, in a previous chapter I establish that the *s1156tGal4* line does not label all SINs, but very small subset (~10%), and of this subset, not all are visually responsive to drifting grating stimuli. By ablating SINs targeted by this line, it is possible that there are still DS SINs left in the tectum that are still providing inhibition to the DS tectal circuit. This could explain why no significant differences are identified in the DS populations after ablation.

6 DISCUSSION

6.1 Overview

Systems neuroscience aims to generate a comprehensive description of circuits in the brain, the roles of which are involved in a myriad of processes necessary for an organism's survival, ranging from olfaction, to somatosensation. Like a circuit board within a computer, the process of understanding this circuitry involves not only describing the individual components of the circuit (i.e. the neuronal subtypes), but also how they connect to each other (connectome), what inputs they receive and outputs they generate and what processing occurs between input and output (neuronal computations).

The visual system provides an experimentally tractable system to study. Inputs to the circuit can be simplified to patterns of light ranging from spots, changes in contrast, changes in shape and movement. Hubel and Wiesel, (1959) were one of the first to characterise the properties of neurons in the visual system with their work on cat striate cortex, first identifying the properties of simple cells, a class of neuron with a centre surround receptive field that responds well to bars or edges in a particular orientation. This was one of the first identifications of a more complex receptive field - a "feature detector" in the visual system. Lettvin et al., (1959) later added to this with their work on properties of frog ganglion cells. From their recordings, they proposed a bug perceiver, the 'convexity detector' with a receptive field detecting small (3°) objects moving within the receptive field of the particular neuronal subtype. This is one of the first links of neuron receptive field preferences to a behavioural/survival outcome.

Much work has focussed on the circuitry within the retina of multiple species, and great progress has been made in determining the connectivity as well as the functional properties of these neurons. Whilst this direction selective (DS) circuit has a partial description of connectivity and cell subtypes, there is still much that is unknown. A prime example of this is the mechanism of how direction selectivity is generated in the retina, it is generally agreed that this is produced at the synapses of starburst amacrine cells, bipolar cells and DSGCs, but the precise mechanism is still under debate (Vaney et al., 2012).

Due to lack of cell type specific labelling, progress on describing both morphological and functional neuronal subtypes within the visual system was slow until relatively recently, due to developments in genetic manipulation, and optogenetics. The availability and increasing sensitivity of genetically encoded probes of activity like GCaMP (Akerboom et al., 2012;

Dreosti et al., 2009; Mao et al., 2008; Tian et al., 2009) has led to an increase in functional descriptions of neurons within the visual system, allowing long-term recording of neuronal activity with little invasiveness as well as morphological characterisation. The experiments in this thesis utilise genetically encoded calcium indicators (GECIs) to carry out *in vivo* live imaging of a subtype of interneuron in zebrafish larvae. This thesis aims to add to this description of the visual system in zebrafish, by characterising the response properties of a specific neuron in the optic tectum, the primary retinorecipient area of the brain, using GECIs and in vivo live imaging. By comparing the responses of SINs to those of the ganglion cell inputs, the processing these neurons may carry out on inputs can be determined. Similarly, as Lettvin et al., (1959) did in their seminal paper on frog, we can use the feature selectivity of these neurons to speculate what behavioural functions these neurons may be involved in.

6.2 Thesis Findings:

6.2.1 Characterisation of SINs

This thesis aimed to generate a characterisation of response properties of a particular subtype of neuron within the optic tectum, the superficial inhibitory interneuron. Whilst there have been other studies which have looked at the response properties of these neurons (Del Bene et al., 2010; Preuss et al., 2014), the approach used in this thesis has two advantages. Firstly, the preferred direction of motion of the neurons was determined, before then probing spatial and temporal frequency properties. This is the first examination of multiple receptive field properties of this neuronal subtype using spatial frequency and directional tuning; this information provides information on what types of behaviours these cells may be involved in.

To carry out such a study, the *s1156tGal4* enhancer trap line was used, a line previously described as labelling SINs selectively (Scott and Baier, 2009). We determined that this line labels a subset of SINs, approximately 10% of the total number of neurons found in the tectal neuropil, whilst also labelling some tectal neurons and RGC axons. GCaMP5 was expressed in these neurons, and changes in fluorescence at the soma were used as a measure of the neuronal responses to visual stimuli, presented to larval zebrafish *in vivo*.

This genetically encoded calcium indicator (GECI) approach is a valuable methodology for understanding response properties for neurons within the visual system as it allows *in vivo* recording from intact organisms without the necessity of anaesthesia, which may affect

response properties of the visual system to stimuli. Using sinusoidal grating stimuli moving in 12 different directions we generated DS response profiles for each of our SINs, the culmination of which resulted in a finding that SINs labelled in the *s1156tGal4* line form 3 DS populations mirroring that of the DSGCs. We now know that there are three population of direction selective SINs with size selective receptive field properties. From other work on the direction (Nikolaou et al., 2012) and size selectivity (Preuss et al., 2014) of RGC axons in the tectal neuropil we can presume that this selectivity is probably inherited from DSGC inputs. What is not clear is if this is inherited directly, or via an intermediate tectal interneuron.

Whilst labelling in this line isn't sufficiently selective to be able to identify where SIN processes arborize in the tectal neuropil, the size tuning allows us to infer that these DS cells are thus the 'small' tuned SINs, with arborisations in the superficial SFGS layers (Preuss et al., 2014). Incidentally, DSGCs arborize primarily in the more superficial SFGS layer (Nikolaou et al., 2012).

The integral response plots indicate that these SINs are band-pass filters for spatial frequency, responding to movement of objects within a specific range sizes. This implies that these neurons respond to particular types of moving object within the visual field, perhaps of prey related size. There is debate on what absolute size of stimulus produces prey capture and predator avoidance. It is more likely that DS SINs respond to prey sized objects, rather than larger predator sized objects.

Sinusoidal grating stimuli were used to probe temporal frequency tuning properties of the SINs. The data collected from these experiments were not conclusive, temporal frequency (TF) responses were very variable between neurons and refinement of either the stimuli provided, or analysis may be required. However, we did see an increase in response size as stimulus size increased. Results from Bianco and Engert (2015) indicated that prey capture behaviour was elicited best at 30°/s this is approximately the highest temporal frequency presented in this thesis, 0.05 cycles/° at 1.5 cycle/second, to which DS SINs responded maximally. It is likely that the range of temporal frequencies used to probe TF selectivity of these neurons was insufficient to identify any bandpass tuning properties, expanding this range is probably necessary to generate appropriate tuning curves.

6.2.2 SIN DS tuning is narrower than that of DSGC input to the tectum, an inhibition independent property

Although the similarity between directional tuning in SINs and RGCs suggests that SINs receive input from RGCs, there were notable differences in tuning properties between these two cells types. The most notable of difference is the DSI values and population FWHM bandwidths. DS SINs are significantly more tuned when comparing DSI and population response bandwidth than their partners in RGCs, across all three populations. Similarly, comparing the DS tuning of DS SINs to their respective populations in DS tectal neurons, SINs have much narrower tuning. This narrow DS tuning is also seen in the more superficial layers of superior colliculus (SC) of mouse, compared to neurons in the deeper layers of the SC (Inayat et al., 2015).

Two different hypotheses could explain this narrowing of tuning. The first is that SINs have non-linear responses to stimuli through intrinsically lower excitability, thus narrowing their bandwidths and increasing DSI values, i.e. they respond maximally when their inputs are maximally active when motion in the preferred direction is presented. It is possible that only the largest changes in membrane potential results in spiking activity, which in this case is caused by visual stimuli closest to preferred direction, a so called “iceberg effect” (Rose and Blakemore, 1974). An ideal test of this hypothesis would involve electrophysiological recordings from SINs. This technique would allow us to examine whether excitatory inputs to SINs exhibit broader tuning which would be evident from SIN spike output.

An alternative hypothesis that might explain the narrower tuning is SINs receive inhibitory input tuned to non-preferred directions that narrows their tuning profile. As the majority of inhibition in the optic tectum is GABAergic, perturbation of GABA-A receptor signalling using pharmacology was carried out whilst imaging SIN responses. As this inhibition is indiscriminate, targeting any GABA-A receptors in the tectal neuropil, no assumptions were made on which neurons provided this inhibition. The inhibition could either have been SIN-SIN inhibition, or via inhibitory tectal neurons with somata located in the periventricular layer.

The use of the *s1156tGal4* line for this experiment was ideal, it labels predominantly DS SINs from three different populations, and this sparse labelling meant that individual SINs were imaged before and after drug injection with confidence. SINs do not lose sharp DS tuning when GABA-A signalling is blocked, this finding challenges the theory that their DS tuning is mediated through inhibition, and suggests that SINs have an intrinsic mechanism to generate narrower DS tuning properties compared to DSGC inputs to the tectum. This spike

thresholding has been found to sharpen selectivity of direction selective neurons in the visual cortex (Jagadeesh et al., 1993; Priebe and Ferster, 2005). This could be due to differences in Na^+/K^+ channel ratios at axon terminals when compared to axons. Blocking of a specific voltage gated K^+ channel family, Kv-1 (including Kv1.1, Kv1.2 and Kv1.3), with the drug OSK-1, results in dramatic changes in membrane conductance at axon terminals in Purkinje cells (Kawaguchi and Sakaba, 2015). A similar difference in voltage gated ion potassium and sodium channel numbers may be how SINs are less excitable; an increased number of K^+ ion channels and lower number of Na^+ channels means there is less Na^+ ion membrane conductance, the largest driver of membrane potential change.

Further, in these pharmacological perturbations, only DS response tuning was tested. Ideally, other aspects of the receptive field properties of SINs that were characterised would also have been tested. In Preuss et al., (2014) it was hypothesised that SINs are involved in a size discriminative circuit, in which two separate size discrimination circuits, one for large and one for small moving objects mutually inhibited each other. To test this hypothesis, perturbation of GABA signalling while probing size selectivity in the tectum is necessary. Unfortunately there was insufficient time to test receptive field properties such as size tuning, and the effect of perturbation of inhibition on these properties.

6.2.3 Perturbation of inhibition in the tectum does not alter DSRGC or DS tectal neuronal properties

In a more surprising result, the injection of pharmacological agents that altered GABA signalling did not have significant effects on the DS populations in the tectal neuropil, including DSGCs and DS tectal neurons. This has two implications. It implies that DS properties are inherited from DSGC inputs, as well as implying that these inputs do not undergo presynaptic modulation. Furthermore, the emergent DS population in tectal neurons, the 90° or backward motion, are not lost during the drug treatment, indicating that this population is likely to be generated from inputs without inhibitory influences.

6.3 A Putative role for SINs in the DS tectal circuit

The data described in this thesis indicates that the subset of SINs labelled by the *s1156tGal4* line is DS and size selective for stimuli of "prey" size. Two hypotheses on the role of the size selective circuit in the tectum have been proposed previously, either that the two circuits provides inhibition to the opposing size selective circuit via the SINs, i.e. neurons in the circuit responsive to small stimuli inhibit the large, and vice versa. These two circuits are hypothesises to exist at different laminar depths in the tectum. An alternative idea is that SIN-mediated inhibition is involved in providing lateral inhibition- inhibiting cells that are adjacent in the topographic axes of the tectum.

The lateral competitive inhibition theory is particularly attractive. The superior colliculus, the equivalent brain area in mammals to optic tectum, has been demonstrated to be vital in selecting amongst competing visual stimuli. If multiple stimuli of a prey-like size are presented to the larva at once, a decision regarding which particular stimulus to pursue needs to be made, to ensure successful prey capture. This thesis presents evidence that SINs are direction and size selective, indicating they may have a role in a deciding between multiple competitive stimuli. The stimulus producing the largest response in SINs provides the largest level of inhibition in the tectal neuropil which is directed towards neighbouring areas in the tectal neuropil. As the tectal neuropil is retinotopically mapped, these neighbouring areas represent neighbouring areas of the world around the larva. Thus, this inhibition prevents excitation of motor circuits caused by moving stimuli activating RGCs in these regions of the visual field (Figure 6.1).

In fact, in lamprey this type of inhibitory circuitry has been identified (Kardamakis et al., 2015), however, in this case the inhibitory circuit is involved in gaze control, determining which visual stimulus gaze is directed towards. This evidence from lamprey may still implicate SIN inhibition in prey capture. Larvae must be able to locate prey visually in order to pursue and determine the locomotor transformations required to capture these prey, for which gaze control is important.

Furthermore, a priority map was identified in rat SC, in which $GABA_A$ receptor activity was biased towards the rostral end of the visuosensory map than rostral (Bayguinov et al., 2015). This inhibition mediates the prioritisation of caudal activity over subsequent rostral sites of activity in the superior colliculus.

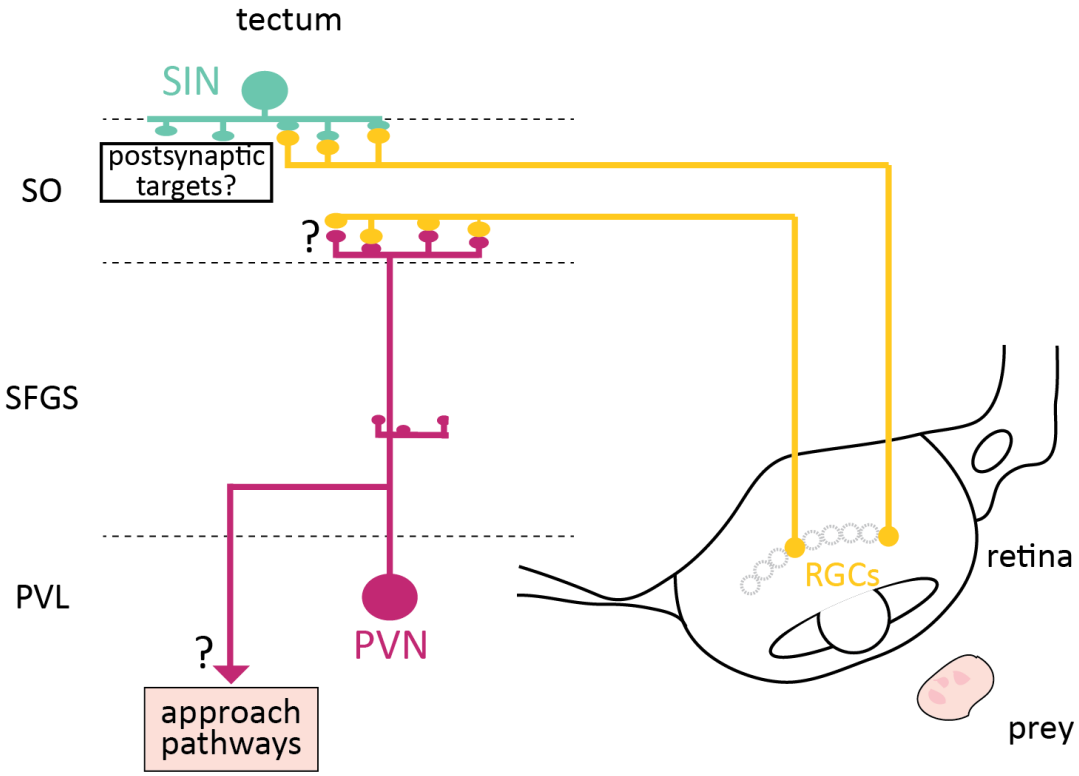

Figure 6-1 Schematic of a possible role for SINs in a "winner-takes-all" selective attention circuit

RGCs selective for prey-sized objects moving in the visual field excite two possible circuits, a SIN, which provides inhibition to surrounding areas of the tectal neuropil, which represent surrounding areas of the visual field. These RGCs simultaneously excite projection neurons responsible for locomotor movements involved in prey capture. The SIN mediated inhibition prevents the activation of similar neurons in the tectum by RGCs detecting subsequent, or less optimal, prey like objects in the visual field (not to scale).

6.4 Future work

This thesis attempted to determine the role of SINs within the visual system, but due to constraints on time, availability of techniques and the non-specificity of labelling seen with the transgenic lines used, it is by no means a complete description of these neurons. We have been left with several key unanswered questions can be addressed with further experiments. How do SINs contribute to size tuning in the tectum? What subtypes of SIN are present in the entire population? What behaviours do SINs contribute towards? How are SINs wired up within the tectum? What inputs do SINs receive?

How do SINs contribute to size tuning within the tectum? The contribution of SIN mediated inhibition to size tuning in the tectum was not explored. It has been established that there are size tuned RGC inputs to the tectum, as well as tectal neurons, with preferences for "small" or "large" sizes of stimuli (Preuss et al., 2014). A theory that these two size selective circuits mutually inhibit each other through size selective SINs was proposed. If this were the case, on perturbation of GABA signalling in the tectum, we would expect to see the two size selective circuits active simultaneously if both sizes of stimulus is present. Bulk injection of GABA receptor antagonists into the tectum, as used in the experiments in this thesis, could be suitable. More appropriate experiments would utilise targeted ablation of SINs through the use of genetically encoded proteins such as KillerRed (Bulina et al., 2006) under the control of a transgenic line in which all SINs are labelled.

What functional subtype exist in the whole SIN population? The *s1156tGal4* line does not label the entire SIN population, but a very small portion (~10%), one question that remains is what visual stimuli these remaining neurons are responsive to. Previous work using Oregon Green BAPTA bulk labelling in the tectum found SINs with both DS and OS receptive field properties (Hunter et al., 2013). It is possible that the *s1156tGal4* does not label these other SINs, but targets a DS sub population. Furthermore, the experiments in this thesis used stimuli designed only to probe motion sensitivity, specifically to whole field motion, using a greater variety of stimuli that probe more aspects of visual information would be a better description of the range of SIN subtypes in the tectum. To determine the properties of these neurons, use of a line such as Oh-Gal4 used in Preuss et al., (2014), to label a larger proportion of SINs is necessary.

What behaviours do the DS SINs control? Conditional ablation of SINs in the tectum could provide strong evidence towards their involvement in prey capture behaviours. Ablation using KillerRed under the control of a Gal4 transgenic line such as the Oh-Gal4 mentioned

previously would allow temporally controlled ablation of SINs in the tectum once the tectal circuit is developed and larvae have established prey capture behaviour. By recording the prey successful prey captures of larvae without ablated SINs to those with ablation, the effects of SIN inhibition on the prey capture can be determined. Previous work used whole tectal ablation to determine the tectum is necessary in prey capture (Del Bene et al., 2010; Gahtan et al., 2005). Prey capture behaviours in larval zebrafish are a complex series of different movements. (Budick and O'Malley, 2000). Information on motion in the visual field could be used in several ways during prey capture; to select optimally located prey to pursue, to control eye movements to maintain tracking of the movement of prey, to determine the angle of turning towards the prey required to maintain pursuit, and to determine velocity required to pursue. Discerning which aspect of prey capture SIN inhibition may be involved in would require specific experiments examining the effects of ablation on eye movements, as well as differences in any particular part of the characterised locomotor manoeuvres demonstrated to be part of prey capture.

This proposed role of SINs however neglects other important behaviours in zebrafish that are also visually guided, including obstacle avoidance, and general free flowing movement behaviour. Whilst the SINs are size selective and it is attractive to assign this property to an identifiable behaviour such as prey capture, it is likely that this visual information is also involved in multiple types of visually guided behaviours, probing how information from SINs is integrated with the rest of the visual circuit is an important factor to consider. Similar experiments using ablation and identifying the changes in behavioural responses to visual stimuli will also dissect out this role.

How are SINs embedded within tectal circuits? To determine this, the ideal method to use would be transsynaptic viral labelling, a technique used extensively in rodents but only very recently developed for use in zebrafish (Mundell et al., 2015). Injection of viral vector into our line would help identify direct synaptic partners with little doubt, and could be combined with the expression of GCaMP rather than a fluorescent marker of morphology, allowing functional characterisation of these connected neurons after identification of their connectivity. Electron microscopy (EM) could also provide us with data on connectivity of SINs, A prime example of the use of EM to trace synaptic partners in a circuit is the work carried out using serial block-face electron microscopy (SBEM) to determine how starburst amacrine cells (SACs) connect to DSGCs in the retina (Briggman et al., 2011). The location of the SINs, the tectal neuropil, is also an immensely dense area of synaptic connections thus complicating the process of identifying synapses. SBEM, combined with calcium imaging of tectum before immunolabeling may provide a solution to such problems, allowing the

determination of the functional properties of SINs, labelling them, before reconstruction using SBEM.

What are the inputs to SINs? Electrophysiological recording of the inputs to the SINs in presence of our visual stimulation would provide crucial details on the functional properties of the neurons. Using electrophysiology, both inhibitory and excitatory inputs can be recorded during visual stimulation. Equally, the contributions of inhibition can be dissected from excitatory currents through the use of voltage-clamp recordings. Whilst these techniques are not in use in our lab, they have been successfully carried out in SINs in other labs (for example Preuss et al., 2014) in larvae. Such recordings can also provide information on what mechanisms may cause the narrower DS tuning of SINs relative to their RGCs inputs. Recordings in the presence of drugs such as OSK-1 a K_v-1 receptor family antagonist, or AM 92016 hydrochloride as Na_v receptor antagonist, that perturb the activity of specific voltage gated ion channels may be particularly useful, providing insights on the ion channel contributions to this tuning.

The visual system of zebrafish is ideal for studying the processing required for goal driven behaviours due to the relatively simple structure of the circuitry as well as ease of imaging; however, this simplicity has not made understanding the circuitry any less challenging. The characterisation of cell types such as SINs contributes towards a description of how the brain processes channels of feature specific information from the retina to drive distinct behaviours. To progress further, a better understanding of the functional subtypes of neuron in the tectum is required, as well as the outputs of projection neurons from the tectum to motor neurons responsible for locomotion. The results in this thesis demonstrate that systematic probing of the responses of a subtype of neuron to visual stimuli can provide important insights into the functional role of that neuron. With a concerted effort to carry out similar studies on other genetically targeted neurons in the visual system, we may yet be able to describe a full sensory-motor circuit responsible for a particular behaviour, such as prey capture.

7 BIBLIOGRAPHY

Adesnik, H., Bruns, W., Taniguchi, H., Huang, Z.J., and Scanziani, M. (2012). A neural circuit for spatial summation in visual cortex. Nature *490*, 226–231.

Akerboom, J., Chen, T.-W., Wardill, T.J., Tian, L., Marvin, J.S., Mutlu, S., Calderón, N.C., Esposti, F., Borghuis, B.G., Sun, X.R., et al. (2012). Optimization of a GCaMP Calcium Indicator for Neural Activity Imaging. J. Neurosci. *32*, 13819–13840.

Albright, T.D., and Stoner, G.R. (2002). Contextual influences on visual processing. Annu. Rev. Neurosci. *25*, 339–379.

Amthor, F.R., Oyster, C.W., and Takahashi, E.S. (1984). Morphology of on-off direction-selective ganglion cells in the rabbit retina. Brain Res. *298*, 187–190.

Auferkorte, O.N., Baden, T., Kaushalya, S.K., Zabouri, N., Rudolph, U., Haverkamp, S., and Euler, T. (2012). GABA(A) receptors containing the α2 subunit are critical for direction-selective inhibition in the retina. PLoS One *7*, e35109.

Badea, T.C., and Nathans, J. (2004). Quantitative analysis of neuronal morphologies in the mouse retina visualized by using a genetically directed reporter. J. Comp. Neurol. *480*, 331–351.

Baden, T., Nikolaev, A., Esposti, F., Dreosti, E., Odermatt, B., and Lagnado, L. (2014). A synaptic mechanism for temporal filtering of visual signals. PLoS Biol. *12*, e1001972.

Baden, T., Berens, P., Franke, K., Roman-Roson, M., Bethge, M., and Euler, T. (2016). The functional diversity of mouse retinal ganglion cells. Nature 1–21.

Barker, A.J., and Baier, H. (2013). SINs and SOMs: neural microcircuits for size tuning in the zebrafish and mouse visual pathway. Front. Neural Circuits *7*, 1–4.

Barlow, H.B., and Levick, W.R. (1965). The mechanism of directionally selective units in rabbit's retina. J. Physiol. *178*, 477–504.

Bass, S.L.S., and Gerlai, R. (2008). Zebrafish (Danio rerio) responds differentially to stimulus fish: The effects of sympatric and allopatric predators and harmless fish. Behav. Brain Res. *186*, 107–117.

Batschelet, E.C. (1981). Circular statistics in biology (Academic Press, London.).

Bayguinov, P.O., Ghitani, N., Jackson, M.B., and Basso, M. a. (2015). A hard-wired priority map in the superior colliculus shaped by asymmetric inhibitory circuitry. J. Neurophysiol. *114*, 662–676.

Del Bene, F., Wyart, C., Robles, E., Tran, A., Looger, L.L., Scott, E.K., Isacoff, E.Y., and Baier, H. (2010). Filtering of Visual Information in the Tectum by an Identified Neural Circuit. Science (80-.). *330*, 669–673.

Berson, D.M., Pu, M., and Famiglietti, E. V (1998). The zeta cell: A new ganglion cell type in cat retina. J. Comp. Neurol. *399*, 269–288.

Bianco, I.H., and Engert, F. (2015). Visuomotor Transformations Underlying Hunting Behavior in Zebrafish. Curr. Biol. *25*, 1–16.

Bianco, I.H., Kampff, A.R., and Engert, F. (2011). Prey capture behavior evoked by simple visual stimuli in larval zebrafish. Front. Syst. Neurosci. *5*, 101.

Bonds, A.B. (1989). Role of Inhibition in the Specification of Orientation Selectivity of Cells in the Cat Striate Cortex. Vis. Neurosci. *2*, 41–55.

Boycott, B.B., Hopkins, J.M., and Sperling, H.G. (1987). Cone Connections of the Horizontal Cells of the Rhesus Monkey's Retina. Proc. R. Soc. London. Ser. B, Biol. Sci. *229*, 345–379.

Branchek, T. (1984). The development of photoreceptors in the zebrafish, Brachydanio rerio. II. Function. J. Comp. Neurol. *224*, 116–122.

Bredfeldt, C., and Ringach, D.L. (2010). Dynamics of spatial frequency tuning of macaque LGN. J. Vis. *2*, 219–219.

Briggman, K.L., Helmstaedter, M., and Denk, W. (2011). Wiring specificity in the direction-selectivity circuit of the retina. Nature *471*, 183–188.

Budick, S. a, and O'Malley, D.M. (2000). Locomotor repertoire of the larval zebrafish: swimming, turning and prey capture. J. Exp. Biol. *203*, 2565–2579.

Bulina, M.E., Lukyanov, K. a, Britanova, O. V, Onichtchouk, D., Lukyanov, S., and Chudakov, D.M. (2006). Chromophore-assisted light inactivation (CALI) using the phototoxic fluorescent protein KillerRed. Nat. Protoc. *1*, 947–953.

Burrill, J.D., and Easter, S.S. (1994). Development of the retinofugal projections in the embryonic and larval zebrafish (Brachydanio rerio). J. Comp. Neurol. *346*, 583–600.

Carello, C.D., and Krauzlis, R.J. (2004). Manipulating Intent: Evidence for a Causal Role of the Superior Colliculus in Target Selection. Neuron *43*, 575–583.

Chen, X., and Engert, F. (2014). Navigational strategies underlying phototaxis in larval zebrafish. Front. Syst. Neurosci. *8*, 39.

Connaughton, V.P., Graham, D., and Nelson, R. (2004). Identification and morphological

classification of horizontal, bipolar, and amacrine cells within the zebrafish retina. J. Comp. Neurol. *477*, 371–385.

Cottam, J.C.H., Smith, S.L., and Häusser, M. (2013). Target-specific effects of somatostatin-expressing interneurons on neocortical visual processing. J. Neurosci. *33*, 19567–19578.

Cynader, M., and Berman, N. (1972). Receptive-field organization of monkey superior colliculus. J. Neurophysiol. *35*, 187–201.

Deeg, K.E., Sears, I.B., and Aizenman, C.D. (2009). Development of multisensory convergence in the Xenopus optic tectum. J. Neurophysiol. *102*, 3392–3404.

DeVries, S.H. (2000). Bipolar cells use kainate and AMPA receptors to filter visual information into separate channels. Neuron *28*, 847–856.

DeVries, S.H., and Baylor, D.A. (1997). Mosaic arrangement of ganglion cell receptive fields in rabbit retina. J. Neurophysiol. *78*, 2048–2060.

Dhande, O.S., Estevez, M.E., Quattrochi, L.E., El-Danaf, R.N., Nguyen, P.L., Berson, D.M., and Huberman, A.D. (2013). Genetic dissection of retinal inputs to brainstem nuclei controlling image stabilization. J. Neurosci. *33*, 17797–17813.

Douglas, R.H., Eva, J., and Guttridge, N. (1988). Size constancy in goldfish (Carassius auratus). Behav. Brain Res. *30*, 37–42.

Douglass, A.D., Kraves, S., Deisseroth, K., Schier, A.F., and Engert, F. (2008). Escape behavior elicited by single, channelrhodopsin-2-evoked spikes in zebrafish somatosensory neurons. Curr. Biol. *18*, 1133–1137.

Dreosti, E., Odermatt, B., Dorostkar, M.M., and Lagnado, L. (2009). A genetically encoded reporter of synaptic activity in vivo. Nat. Methods *6*, 883–889.

Endo, T., Yanagawa, Y., Obata, K., and Isa, T. (2003). Characteristics of GABAergic neurons in the superficial superior colliculus in mice. Neurosci. Lett. *346*, 81–84.

Euler, T., Detwiler, P.B., and Denk, W. (2002). Directionally selective calcium signals in dendrites of starburst amacrine cells. Nature *418*, 845–852.

Famiglietti, E. V, and Kolb, H. (1976). Structural basis for ON-and OFF-center responses in retinal ganglion cells. Science *194*, 193–195.

Feierstein, C.E., Portugues, R., and Orger, M.B. (2014). Seeing the whole picture: A comprehensive imaging approach to functional mapping of circuits in behaving zebrafish. Neuroscience *296*, 26–38.

Field, G.D., and Chichilnisky, E.J. (2007). Information processing in the primate retina: circuitry and coding. Annu. Rev. Neurosci. *30*, 1–30.

Ben Fredj, N., Hammond, S., Otsuna, H., Chien, C.-B., Burrone, J., and Meyer, M.P. (2010). Synaptic Activity and Activity-Dependent Competition Regulates Axon Arbor Maturation, Growth Arrest, and Territory in the Retinotectal Projection. J. Neurosci. *30*, 10939–10951.

Fried, S.I., Münch, T. a, and Werblin, F.S. (2002). Mechanisms and circuitry underlying directional selectivity in the retina. Nature *420*, 411–414.

Gabbiani, F., Krapp, H.G., and Laurent, G. (1999). Computation of object approach by a wide-field, motion-sensitive neuron. J. Neurosci. *19*, 1122–1141.

Gabriel, J.P., Trivedi, C.A., Maurer, C.M., Ryu, S., and Bollmann, J.H. (2012). Layer-Specific Targeting of Direction-Selective Neurons in the Zebrafish Optic Tectum. Neuron *76*, 1147–1160.

Gahtan, E., Tanger, P., and Baier, H. (2005). Visual prey capture in larval zebrafish is controlled by identified reticulospinal neurons downstream of the tectum. J. Neurosci. *25*, 9294–9303.

Gerlai, R., Fernandes, Y., and Pereira, T. (2009). Zebrafish (Danio rerio) responds to the animated image of a predator: Towards the development of an automated aversive task. Behav. Brain Res. *201*, 318–324.

Ghosh, K.K., Bujan, S., Haverkamp, S., Feigenspan, A., and Wässle, H. (2004). Types of Bipolar Cells in the Mouse Retina. J. Comp. Neurol. *469*, 70–82.

Girman, S. V, and Lund, R.D. (2007). Most Superficial Sublamina of Rat Superior Colliculus: Neuronal Response Properties and Correlates With Perceptual Figure – Ground Segregation. J.Neurophysiol. *98*, 161–177.

Glickfeld, L.L., Histed, M.H., and Maunsell, J.H.R. (2013). Mouse primary visual cortex is used to detect both orientation and contrast changes. J. Neurosci. *33*, 19416–19422.

Gollisch, T., and Meister, M. (2010). Eye Smarter than Scientists Believed: Neural Computations in Circuits of the Retina. Neuron *65*, 150–164.

Gonchar, Y., Wang, Q., and Burkhalter, A. (2007). Multiple distinct subtypes of GABAergic neurons in mouse visual cortex identified by triple immunostaining. Front. Neuroanat. *1*, 3.

Grama, A., and Engert, F. (2012). Direction selectivity in the larval zebrafish tectum is mediated by asymmetric inhibition. Front. Neural Circuits *6*, 59.

Grubb, M.S., and Thompson, I.D. (2003). Quantitative characterization of visual response

properties in the mouse dorsal lateral geniculate nucleus. J. Neurophysiol. *90*, 3594–3607.

Grzywacz, N.M., Amthor, F.R., and Merwine, D.K. (1998). Necessity of acetylcholine for retinal directionally selective responses to drifting gratings in rabbit. J. Physiol. *512 (Pt 2*, 575–581.

Hamos, J.E., Van Horn, S.C., Raczkowski, D., Uhlrich, D.J., and Sherman, S.M. (1985). Synaptic connectivity of a local circuit neurone in lateral geniculate nucleus of the cat. Nature *317*, 618–621.

Hatsopoulos, N., Gabbiani, F., and Laurent, G. (1995). Elementary Computation of Object Approach by a Wide-Field Visual Neuron. Sci. *270* , 1000–1003.

Hiramoto, M., and Cline, H.T. (2009). Convergence of multisensory inputs in xenopus tadpole tectum. Dev. Neurobiol. *69*, 959–971.

Hisatomi, O., Satoh, T., Barthel, L.K., Stenkamp, D.L., Raymond, P.A., and Tokunaga, F. (1996). Molecular Cloning and characterization of the putative ultraviolet-sensitive visual pigment of goldfish. Vision Res. *36*, 933–939.

Hofbauer, A., and Dräger, U.C. (1985). Depth segregation of retinal ganglion cells projecting to mouse superior colliculus. J. Comp. Neurol. *234*, 465–474.

Hubel, D.H., and Wiesel, T.N. (1959). Receptive fields of single neurones in the cat's striate cortex. J. Physiol. *148*, 574–591.

Hubel, D.H., and Wiesel, T.N. (1962). Receptive fields, binocular interaction and functional architecture in the cat's visual cortex. J. Physiol. *160*, 106–154.

Huberman, A.D., Wei, W., Elstrott, J., Stafford, B.K., Feller, M.B., and Barres, B.A. (2009). Genetic Identification of an On-Off Direction- Selective Retinal Ganglion Cell Subtype Reveals a Layer-Specific Subcortical Map of Posterior Motion. Neuron *62*, 327–334.

Hunter, P.R., Lowe, A.S., Thompson, I.D., and Meyer, M.P. (2013). Emergent properties of the optic tectum revealed by population analysis of direction and orientation selectivity. J. Neurosci. *33*, 13940–13945.

Inayat, S., Barchini, J., Chen, H., Feng, L., Liu, X., and Cang, J. (2015). Neurons in the Most Superficial Lamina of the Mouse Superior Colliculus Are Highly Selective for Stimulus Direction. J. Neurosci. *35*, 7992–8003.

Isaacson, J.S., and Scanziani, M. (2011). How inhibition shapes cortical activity. Neuron *72*, 231–243.

Issa, N.P., Trepel, C., and Stryker, M.P. (2000). Spatial Frequency Maps in Cat Visual Cortex. J.

Neurosci. *20* , 8504–8514.

Jacobs, G.H. (2009). Evolution of colour vision in mammals. Philos. Trans. R. Soc. B Biol. Sci. *364*, 2957–2967.

Jagadeesh, B., Wheat, H., and Ferster, D. (1993). Linearity of summation of synaptic potentials underlying direction selectivity in simple cells of the cat visual cortex. Science (80-.). *262*, 1901–1904.

Kardamakis, A. a., Saitoh, K., and Grillner, S. (2015). Tectal microcircuit generating visual selection commands on gaze-controlling neurons. Proc. Natl. Acad. Sci. *112*, E1956–E1965.

Kassing, V., Engelmann, J., and Kurtz, R. (2013). Monitoring of Single-Cell Responses in the Optic Tectum of Adult Zebrafish with Dextran-Coupled Calcium Dyes Delivered via Local Electroporation. PLoS One *8*, e62846.

Kawaguchi, S., and Sakaba, T. (2015). Control of Inhibitory Synaptic Outputs by Low Excitability of Axon Terminals Revealed by Direct Recording. Neuron 1–16.

Kay, J.N., De la Huerta, I., Kim, I.-J., Zhang, Y., Yamagata, M., Chu, M.W., Meister, M., and Sanes, J.R. (2011). Retinal ganglion cells with distinct directional preferences differ in molecular identity, structure, and central projections. J. Neurosci. *31*, 7753–7762.

Kerlin, A.M., Andermann, M.L., Berezovskii, V.K., and Reid, R.C. (2010). Broadly Tuned Response Properties of Diverse Inhibitory Neuron Subtypes in Mouse Visual Cortex. Neuron *67*, 858–871.

Kim, I.-J., Zhang, Y., Yamagata, M., Meister, M., and Sanes, J.R. (2008). Molecular identification of a retinal cell type that responds to upward motion. Nature *452*, 478–482.

Kim, T., Soto, F., and Kerschensteiner, D. (2015). An excitatory amacrine cell detects object motion and provides feature-selective input to ganglion cells in the mouse retina. Elife *4*, 1–15.

Kinoshita, M., Ueda, R., Kojima, S., Sato, K., Watanabe, M., Urano, A., and Ito, E. (2002). Multiple-site optical recording for characterization of functional synaptic organization of the optic tectum of rainbow trout. Eur. J. Neurosci. *16*, 868–876.

Kolb, H., and Marshak, D. (2003). The midget pathways of the primate retina. Doc. Ophthalmol. *106*, 67–81.

Langer, T.P., and Lund, R.D. (1974). The upper layers of the superior colliculus of the rat: A Golgi study. J. Comp. Neurol. *158*, 405–435.

Lee, S., Chen, L., Chen, M.-G., Ye, M., Seal, R.P., and Zhou, Z.J. (2014). An Unconventional Glutamatergic Circuit in the Retina Formed by vGluT3 Amacrine Cells. Neuron *84*, 708–715.

Lettvin, J.Y., Maturana, H.R., McCulloch, W.S., and Pitts, W.H. (1959). What the Frog's Eye Tells the Frogs's Brain. Proc. Tha IRE *3*, 1940–1951.

Levick, W.R. (1967). Receptive fields and trigger features of ganglion cells in the visual streak of the rabbits retina. J. Physiol. *188*, 285–307.

Lindstrom, S.H., Ryan, D.G., Shi, J., and DeVries, S.H. (2014). Kainate receptor subunit diversity underlying response diversity in retinal off bipolar cells. J. Physiol. *592*, 1457–1477.

Ling, C., Schneider, G.E., and Jhaveri, S. (1998). Target-specific morphology of retinal axon arbors in the adult hamster. Vis. Neurosci. *15*, 559–579.

Lipetz, L.E., and Hill, R.M. (1970). Discrimination characteristics of the turtle's retinal ganglion cells. Experientia *26*, 373–374.

Lister, J. a, Robertson, C.P., Lepage, T., Johnson, S.L., and Raible, D.W. (1999). nacre encodes a zebrafish microphthalmia-related protein that regulates neural-crest-derived pigment cell fate. Development *126*, 3757–3767.

Lowe, A.S., Nikolaou, N., Hunter, P.R., Thompson, I.D., and Meyer, M.P. (2013). A systems-based dissection of retinal inputs to the zebrafish tectum reveals different rules for different functional classes during development. J. Neurosci. *33*, 13946–13956.

Macneil, M. a., Heussy, J.K., Dacheux, R.F., Raviola, E., and Masland, R.H. (1999). The shapes and numbers of amacrine cells: Matching of photofilled with Golgi-stained cells in the rabbit retina and comparison with other mammalian species. J. Comp. Neurol. *413*, 305–326.

Mangrum, W.I., Dowling, J.E., and Cohen, E.D. (2002). A morphological classification of ganglion cells in the zebrafish retina. Vis. Neurosci. *19*, 767–779.

Mao, T., O'Connor, D.H., Scheuss, V., Nakai, J., and Svoboda, K. (2008). Characterization and subcellular targeting of GCaMP-type genetically-encoded calcium indicators. PLoS One *3*, e1796.

Markram, H., Toledo-Rodriguez, M., Wang, Y., Gupta, A., Silberberg, G., and Wu, C. (2004). Interneurons of the neocortical inhibitory system. Nat. Rev. Neurosci. *5*, 793–807.

Marshel, J.H., Kaye, A.P., Nauhaus, I., and Callaway, E.M. (2012). Anterior-Posterior Direction Opponency in the Superficial Mouse Lateral Geniculate Nucleus. Neuron *76*, 713–720.

Masland, R.H. (2012). The tasks of amacrine cells. Vis. Neurosci. *29*, 3–9.

Maturana, H.R., Lettvin, J.Y., McCulloch, W.S., and Pitts, W.H. (1960). Anatomy and Physiology of Vision in the Frog (Rana pipiens). J. Gen. Physiol. *43*, 129–175.

Maximov, V., Maximova, E., and Maximov, P. (2005). Direction selectivity in the goldfish tectum revisited. Ann. N. Y. Acad. Sci. *1048*, 198–205.

Mazurek, M., Kager, M., and Van Hooser, S.D. (2014). Robust quantification of orientation selectivity and direction selectivity. Front. Neural Circuits *8*, 1–17.

Meek, J., and Schellart, N. a (1978). A Golgi study of goldfish optic tectum. J. Comp. Neurol. *182*, 89–122.

Meyer, M.P., Trimmer, J.S., Gilthorpe, J.D., and Smith, S.J. (2005). Characterization of zebrafish PSD-95 gene family members. J. Neurobiol. *63*, 91–105.

Mize, R.R. (1992). The organization of GABAergic neurons in the mammalian superior colliculus. Prog. Brain Res. *90*, 219–248.

Mooney, R.D., Klein, B.G., and Rhoades, R.W. (1985). Correlations between the structural and functional characteristics of neurons in the superficial laminae and the hamster's superior colliculus. J Neurosci *5*, 2989–3009.

Morgans, C.W., Zhang, J., Jeffrey, B.G., Nelson, S.M., Burke, N.S., Duvoisin, R.M., and Brown, R.L. (2009). TRPM1 is required for the depolarizing light response in retinal ON-bipolar cells. Proc. Natl. Acad. Sci. *106* , 19174–19178.

Münch, T. a, da Silveira, R.A., Siegert, S., Viney, T.J., Awatramani, G.B., and Roska, B. (2009). Approach sensitivity in the retina processed by a multifunctional neural circuit. Nat. Neurosci. *12*, 1308–1316.

Mundell, N.A., Beier, K.T., Pan, Y.A., Lapan, S.W., Göz Aytürk, D., Berezovskii, V.K., Wark, A.R., Drokhlyansky, E., Bielecki, J., Born, R.T., et al. (2015). Vesicular stomatitis virus enables gene transfer and transsynaptic tracing in a wide range of organisms. J. Comp. Neurol. *523*, 1639–1663.

Murphy-Baum, B.L., and Taylor, W.R. (2015). The Synaptic and Morphological Basis of Orientation Selectivity in a Polyaxonal Amacrine Cell of the Rabbit Retina. J. Neurosci. *35*, 13336–13350.

Muto, A., and Kawakami, K. (2013). Prey capture in zebrafish larvae serves as a model to study cognitive functions. Front. Neural Circuits *7*, 110.

Muto, A., Ohkura, M., Abe, G., Nakai, J., and Kawakami, K. (2013). Real-Time Visualization of

Neuronal Activity during Perception. Curr. Biol. *23*, 307–311.

Nawrocki, L., Bremiller, R., Streisinger, G., and Kaplan, M. (1985). Larval and adult visual pigments of the zebrafish, Brachydanio rerio. Vision Res. *25*, 1569–1576.

Nevin, L.M., Robles, E., Baier, H., and Scott, E.K. (2010). Focusing on optic tectum circuitry through the lens of genetics. BMC Biol. *8*, 126.

Niell, C.M. (2011). Exploring the next frontier of mouse vision. Neuron *72*, 889–892.

Niell, C.M., and Smith, S.J. (2005). Functional imaging reveals rapid development of visual response properties in the zebrafish tectum. Neuron *45*, 941–951.

Niell, C.M., and Stryker, M.P. (2008). Highly selective receptive fields in mouse visual cortex. J. Neurosci. *28*, 7520–7536.

Nikolaev, A., Leung, K.-M., Odermatt, B., and Lagnado, L. (2013). Synaptic mechanisms of adaptation and sensitization in the retina. Nat. Neurosci. *16*, 934–941.

Nikolaou, N., Lowe, A.S., Walker, A.S., Abbas, F., Hunter, P.R., Thompson, I.D., and Meyer, M.P. (2012). Parametric functional maps of visual inputs to the tectum. Neuron *76*, 317–324.

O'Malley, D.M., and Masland, R.H. (1989). Co-release of acetylcholine and gamma-aminobutyric acid by a retinal neuron. Proc. Natl. Acad. Sci. U. S. A. *86*, 3414–3418.

Olsen, S.R., Bortone, D.S., Adesnik, H., and Scanziani, M. (2012). Gain control by layer six in cortical circuits of vision. Nature *483*, 47–52.

Orger, M.B., Kampff, A.R., Severi, K.E., Bollmann, J.H., and Engert, F. (2008). Control of visually guided behavior by distinct populations of spinal projection neurons. Nat. Neurosci. *11*, 327–333.

Ott, M., Walz, B.C., Paulsen, U.J., Mack, A.F., and Wagner, H.-J. (2007). Retinotectal ganglion cells in the zebrafish, Danio rerio. J. Comp. Neurol. *501*, 647–658.

Oyster, C.W., and Barlow, H.B. (1967). Direction-Selective Units in Rabbit Retina: Distribution of Preferred Directions. Science (80-.). *155*, 841–842.

Passaglia, C.L., Troy, J.B., Rüttiger, L., and Lee, B.B. (2002). Orientation sensitivity of ganglion cells in primate retina. Vision Res. *42*, 683–694.

Patterson, B.W., Abraham, A.O., Maciver, M. a, and McLean, D.L. (2013). Visually guided gradation of prey capture movements in larval zebrafish. J. Exp. Biol. *216*, 3071–3083.

Pearson, J.T., and Kerschensteiner, D. (2015). Ambient illumination switches contrast

preference of specific retinal processing streams. J. Neurophysiol. *114*, 540–550.

Pei, Z., Chen, Q., Koren, D., Giammarinaro, B., Acaron Ledesma, H., and Wei, W. (2015). Conditional Knock-Out of Vesicular GABA Transporter Gene from Starburst Amacrine Cells Reveals the Contributions of Multiple Synaptic Mechanisms Underlying Direction Selectivity in the Retina. J. Neurosci. *35*, 13219–13232.

Peichl, L., and González-Soriano, J. (1994). Morphological types of horizontal cell in rodent retinae: a comparison of rat, mouse, gerbil, and guinea pig. Vis. Neurosci. *11*, 501–517.

Perry, V.H., Oehler, R., and Cowey, A. (1984). Retinal ganglion cells that project to the dorsal lateral geniculate nucleus in the macaque monkey. Neuroscience *12*, 1101–1123.

Pfleger, B., and Bonds, A.B. (1995). Dynamic differentiation of GABAA-sensitive influences on orientation selectivity of complex cells in the cat striate cortex. Exp. Brain Res. *104*, 81–88.

Piscopo, D.M., El-Danaf, R.N., Huberman, A.D., and Niell, C.M. (2013). Diverse visual features encoded in mouse lateral geniculate nucleus. J. Neurosci. *33*, 4642–4656.

Portugues, R., and Engert, F. (2009). The neural basis of visual behaviors in the larval zebrafish. Curr. Opin. Neurobiol. *19*, 644–647.

Preuss, S.J., Trivedi, C.A., Vom Berg-Maurer, C.M., Ryu, S., and Bollmann, J.H. (2014). Classification of Object Size in Retinotectal Microcircuits. Curr. Biol. *24*, 2376–2385.

Prévost, F., Lepore, F., and Guillemot, J.-P. (2007). Spatio-temporal receptive field properties of cells in the rat superior colliculus. Brain Res. *1142*, 80–91.

Priebe, N.J., and Ferster, D. (2005). Direction selectivity of excitation and inhibition in simple cells of the cat primary visual cortex. Neuron *45*, 133–145.

Puller, C., Ivanova, E., Euler, T., Haverkamp, S., and Schubert, T. (2013). OFF bipolar cells express distinct types of dendritic glutamate receptors in the mouse retina. Neuroscience *243*, 136–148.

Ramdya, P., and Engert, F. (2008). Emergence of binocular functional properties in a monocular neural circuit. Nat. Neurosci. *11*, 1083–1090.

Ramón y Cajal, S. (1898). Estructura del kiasma óptico y teoría general de los entrecruzamientos de las vías nerviosas. Rev. Trim. Micrográfica 3.

Ringach, D.L., Hawken, M.J., and Shapley, R.M. (2002). Receptive field structure of neurons in monkey primary visual cortex revealed by stimulation with natural image sequences. J. Vis. *2*, 12–24.

Rivlin-Etzion, M., Zhou, K., Wei, W., Elstrott, J., Nguyen, P.L., Barres, B.A., Huberman, A.D., and Feller, M.B. (2011). Transgenic Mice Reveal Unexpected Diversity of On-Off Direction-Selective Retinal Ganglion Cell Subtypes and Brain Structures Involved in Motion Processing. J. Neurosci. *31* , 8760–8769.

Robles, E., Filosa, a., and Baier, H. (2013). Precise Lamination of Retinal Axons Generates Multiple Parallel Input Pathways in the Tectum. J. Neurosci. *33*, 5027–5039.

Robles, E., Laurell, E., and Baier, H. (2014). The Retinal Projectome Reveals Brain-Area-Specific Visual Representations Generated by Ganglion Cell Diversity. Curr. Biol. *24*, 2085–2096.

Rodieck, R.W., and Watanabe, M. (1993). Survey of the morphology of macaque retinal ganglion cells that project to the pretectum, superior colliculus, and parvicellular laminae of the lateral geniculate nucleus. J. Comp. Neurol. *338*, 289–303.

Röhrenbeck, J., Wässle, H., and Boycott, B.B. (1989). Horizontal Cells in the Monkey Retina: Immunocytochemical staining with antibodies against calcium binding proteins. Eur. J. Neurosci. *1*, 407–420.

Rose, D., and Blakemore, C. (1974). Effects of bicuculline on functions of inhibition in visual cortex. Nature *249*, 375–377.

Sajovic, P., and Levinthal, C. (1982a). Visual cells of zebrafish optic tectum: mapping with small spots. Neuroscience *7*, 2407–2426.

Sajovic, P., and Levinthal, C. (1982b). Visual response properties of zebrafish tectal cells. Neuroscience *7*, 2427–2440.

Sajovic, P., and Levinthal, C. (1983). Inhibitory mechanism in zebrafish optic tectum: Visual response properties of tectal cells altered by picrotoxin and bicuculline. Brain Res. *271*, 227–240.

Sanes, J.R., and Masland, R.H. (2014). The Types of Retinal Ganglion Cells: Current Status and Implications for Neuronal Classification. Annu. Rev. Neurosci. *38*, 150421150146009.

Schuett, S., Bonhoeffer, T., and Hübener, M. (2002). Mapping Retinotopic Structure in Mouse Visual Cortex with Optical Imaging. J. Neurosci. *22* , 6549–6559.

Scott, E.K., and Baier, H. (2009). The cellular architecture of the larval zebrafish tectum, as revealed by gal4 enhancer trap lines. Front. Neural Circuits *3*, 13.

Semmelhack, J.L., Donovan, J.C., Thiele, T.R., Kuehn, E., Francisco, S., Laurell, E., and Baier, H. (2014). A dedicated visual pathway for prey detection in larval zebrafish. Elife *3*, 1–19.

Shapley, R.M., Hawken, M.J., and Ringach, D.L. (2003). Dynamics of orientation selectivity in the primary visual cortex and the importance of cortical inhibition. Neuron *38*, 689–699.

Sherman, S.M. (2004). Interneurons and triadic circuitry of the thalamus. Trends Neurosci. *27*, 670–675.

Sherman, S.M., and Guillery, R.W. (2001). Exploring the thalamus (Oxford Univ Press).

Smear, M.C., Tao, H.W., Staub, W., Orger, M.B., Gosse, N.J., Liu, Y., Takahashi, K., Poo, M.-M., and Baier, H. (2007). Vesicular glutamate transport at a central synapse limits the acuity of visual perception in zebrafish. Neuron *53*, 65–77.

Soiza-Reilly, M., Anderson, W.B., Vaughan, C.W., and Commons, K.G. (2013). Presynaptic gating of excitation in the dorsal raphe nucleus by GABA. Proc. Natl. Acad. Sci. U. S. A. *110*.

Somers, D.C., Nelson, S.B., and Sur, M. (1995). An emergent model of orientation selectivity in cat visual cortical simple cells. J. Neurosci. *15*, 5448–5465.

Strettoi, E., Dacheux, R.F., and Raviola, E. (1994). Cone bipolar cells as interneurons in the rod pathway of the rabbit retina. J. Comp. Neurol. *347*, 139–149.

Stuermer, C. (1988). Retinotopic organization of the developing retinotectal projection in the zebrafish embryo. J. Neurosci. *8*, 4513–4530.

Swindale, N. V (1998). Orientation tuning curves: empirical description and estimation of parameters. Biol. Cybern. *78*, 45–56.

Tabor, R., Yaksi, E., and Friedrich, R.W. (2008). Multiple functions of GABA A and GABA B receptors during pattern processing in the zebrafish olfactory bulb. Eur. J. Neurosci. *28*, 117–127.

Teh, C., Chudakov, D.M., Poon, K.-L., Mamedov, I.Z., Sek, J.-Y., Shidlovsky, K., Lukyanov, S., and Korzh, V. (2010). Optogenetic in vivo cell manipulation in KillerRed-expressing zebrafish transgenics. BMC Dev. Biol. *10*, 110.

Thiele, T.R., Donovan, J.C., and Baier, H. (2014). Descending Control of Swim Posture by a Midbrain Nucleus in Zebrafish. Neuron *83*, 679–691.

Tian, L., Hires, S.A., Mao, T., Huber, D., Chiappe, M.E., Chalasani, S.H., Petreanu, L., Akerboom, J., McKinney, S. a, Schreiter, E.R., et al. (2009). Imaging neural activity in worms, flies and mice with improved GCaMP calcium indicators. Nat. Methods *6*, 875–881.

Tikidji-Hamburyan, A., Reinhard, K., Seitter, H., Hovhannisyan, A., Procyk, C.A., Allen, A.E., Schenk, M., Lucas, R.J., and Munch, T.A. (2015). Retinal output changes qualitatively with

every change in ambient illuminance. Nat. Neurosci. *18*, 66–74.

De Valois, R.L., William Yund, E., and Hepler, N. (1982). The orientation and direction selectivity of cells in macaque visual cortex. Vision Res. *22*, 531–544.

Vanegas, H., Amat, J., and Essayag-Millán, E. (1974). Postsynaptic phenomena in optic tectum neurons following optic nerve stimulation in fish. Brain Res. *77*, 25–38.

Vaney, D.I., Sivyer, B., and Taylor, W.R. (2012). Direction selectivity in the retina: symmetry and asymmetry in structure and function. Nat. Rev. Neurosci. *13*.

Venkataramani, S., and Taylor, W.R. (2010). Orientation selectivity in rabbit retinal ganglion cells is mediated by presynaptic inhibition. J. Neurosci. *30*, 15664–15676.

Wagor, E., Mangini, N.J., and Pearlman, A.L. (1980). Retinotopic organization of striate and extrastriate visual cortex in the mouse. J. Comp. Neurol. *193*, 187–202.

Wang, L., Sarnaik, R., Rangarajan, K., Liu, X., and Cang, J. (2010). Visual receptive field properties of neurons in the superficial superior colliculus of the mouse. J. Neurosci. *30*, 16573–16584.

Wang, Y., Toledo-Rodriguez, M., Gupta, A., Wu, C., Silberberg, G., Luo, J., and Markram, H. (2004). Anatomical, physiological and molecular properties of Martinotti cells in the somatosensory cortex of the juvenile rat. J. Physiol. *561*, 65–90.

Wässle, H., Puller, C., Müller, F., and Haverkamp, S. (2009). Cone contacts, mosaics, and territories of bipolar cells in the mouse retina. J. Neurosci. *29*, 106–117.

Wurtz, R.H., and Albano, J.E. (1980). Visual-motor function of the primate superior colliculus. Annu. Rev. Neurosci. *3*, 189–226.

Wyatt, H., and Day, N. (1976). Specific effects of neurotransmitter antagonists on ganglion cells in rabbit retina. Science (80-.). *191*, 204–205.

van Wyk, M., Taylor, W.R., and Vaney, D.I. (2006). Local edge detectors: a substrate for fine spatial vision at low temporal frequencies in rabbit retina. J. Neurosci. *26*, 13250–13263.

Xu, X., Roby, K.D., and Callaway, E.M. (2010). Immunochemical characterization of inhibitory mouse cortical neurons: Three chemically distinct classes of inhibitory cells. J. Comp. Neurol. *518*, 389–404.

Xu, Y., Dhingra, N.K., Smith, R.G., and Sterling, P. (2005). Sluggish and Brisk Ganglion Cells Detect Contrast With Similar Sensitivity. J. Neurophysiol. *93*, 2388–2395.

Yilmaz, M., and Meister, M. (2013). Rapid innate defensive responses of mice to looming

visual stimuli. Curr. Biol. *23*, 2011–2015.

Yonehara, K., Ishikane, H., Sakuta, H., Shintani, T., Nakamura-Yonehara, K., Kamiji, N.L., Usui, S., and Noda, M. (2009). Identification of retinal ganglion cells and their projections involved in central transmission of information about upward and downward image motion. PLoS One *4*, e4320.

Yoshida, K., Watanabe, D., Ishikane, H., Tachibana, M., Pastan, I., and Nakanishi, S. (2001). A key role of starburst amacrine cells in originating retinal directional selectivity and optokinetic eye movement. Neuron *30*, 771–780.

Zeck, G.M., Xiao, Q., and Masland, R.H. (2005). The spatial filtering properties of local edge detectors and brisk–sustained retinal ganglion cells. Eur. J. Neurosci. *22*, 2016–2026.

Zhang, Y., Kim, I.-J., Sanes, J.R., and Meister, M. (2012). PNAS Plus: The most numerous ganglion cell type of the mouse retina is a selective feature detector. Proc. Natl. Acad. Sci. *109*, E2391–E2398.

Zhao, X., Chen, H., Liu, X., and Cang, J. (2013). Orientation-selective Responses in the Mouse Lateral Geniculate Nucleus. J. Neurosci. *33*, 12751–12763.